Inaugural dissertation

for

obtaining the doctoral degree

of the

Combined Faculty of Mathematics, Engineering and Natural Sciences

of the

Ruprecht - Karls - University

Heidelberg

Presented by M.Sc. Elena Muñoz Perez-Vico

Born in: Heidelberg

Oral examination: March 9th, 2023

Implications of the Val66Met polymorphism of the *BDNF* gene on neuronal morphology and function using human iPSC-derived neuronal cultures

Referees: Prof. Dr. Christoph Schuster

Prof. Dr. med. Philipp Koch

¡… células de formas delicadas y elegantes, las misteriosas mariposas del alma, cuyo batir de alas quién sabe si esclarecerá algún día el secreto de la vida mental!

- Santiago Ramón y Cajal -

… cells with delicate and elegant forms, the mysterious butterflies of the soul, the beating of whose wings may some day, who knows, clarify the secret of mental life

Table of Content

List of Figures

List of Tables

List of Abbreviations

%	percent
Ø	diameter
#	number
(v/v)	volume percent
(w/v)	weight percent
°C	degree Celsius
1X	single concentrated
2D	two dimensional
3D	three dimensional
α	anti-
A	adenine
AA	ascorbic acid
ACSF	artificial cerebrospinal fluid
AMPA	α-amino-3-hydroxy-5-methyl-4-isoxazolepropionic acid
AP	action potential
ASCL	acheate-scute like
BDNF	brain-derived neurotrophic factor
BMP	bone morphogenic protein
BSA	bovine serum albumin
bp	base pair
Cas9	CRISPR-associated protein 9
cDNA	complementary DNA
CDS	coding sequence
CNS	central nervous system
CPE	carboxypeptidase E
CREB	cAMP response element-binding protein
CRISPR	clustered regulatory interspaced palindromic repeats
CTIP2	coup-TFI interacting protein 2
DAPI	4,6-diamidino-2-phenylindole
DAPT	N-[N-(3,5.Difluorophenacetyl)- L-alanyl]-S-phenylglycine t-butyl ester
ddH_2O	double-distilled water
DEPC	diethyl pyrocarbonate
DLG4	discs Large MAGUK Scaffold Protein 4
DLX2	distal-Less Homeobox 2
DMSO	dimethyl sulfoxide
DNA	Desoxyribonucleic acid
dNTPs	deoxynucleotide triphosphate
EDTA	ethylenediaminetetraacetic acid
EGF	epidermal growth factor
ER	endoplasmic reticulum
ERK	extracellular signal-regulated kinases
et al.	et alia (and others)
FBS	fetal bovine serum
FGF	fibroblast growth factor
FOX	forkhead box
g	gram
G	guanine
GABA	γ-Aminobutyric acid

gDNA	genomic DNA
GO	gene ontology
GFAP	glial fibrillary protein
GRIA	glutamate Ionotropic Receptor AMPA Type Subunit
GRIN	glutamate Ionotropic Receptor NMDA Type Subunit
gRNA	guide RNA
h	hour
HA	hemagglutinin
HEK	human embryonic kidney cells
HOX	homeobox
ICC	immunocytochemistry
iPSCs	induced pluripotent stem cells
JNK	c-Jun-N-terminale Kinase
kDa	kilodalton
KOSR	KnockOut™ Serum Replacement
LAAP	L-ascorbic acid 2-phosphate
LB	lysogeny broth
LTD	long-term depression
m	milli-
M	molar (mol/l)
MAP2	microtubule-associated protein 2
MAPK	mitogen-activated protein kinase
mBDNF	mature BDNF
Met	methionine
mEPSC	miniature excitatory postsynaptic current
min	minute
MMP	matrix metalloproteinases
mRNA	messenger RNA
MW	molecular weight
µ	micro-
n	nano-
N/A	not applicable
ns	not significant
NEAA	non-essential amino acid
NECs	neuroepithelial cells
NES	neuroepithelial stem cell protein
NeuN	neuronal nuclei
NFKB	nuclear factor 'kappa-light-chain-enhancer' of activated B-cells
NGF	nerve growth factor
NMDA	N-methyl-D-aspartate
NPC	neural progenitor cell
NT	neurotrophin
NTRK2	neurotrophic receptor tyrosine kinase 2
OCT3/4	octamer-binding transcription factor 3/4
ON	overnight
OTX2	orthodenticle homeobox 2
p	significance level
PAGE	polyacrylamide gel electrophoresis
PAM	protospacer adjacent motif
PAX	paired box protein

PBS	phosphate-buffered saline
PCs	protein convertases
PCR	polymerase chain reaction
PEI	polyethyleneimine
Pen/Strep	penicillin/streptomycin
PFA	paraformaldehyde
PI3K	phosphatidylinositol 3-kinase
PKC	protein kinase C
PLCγ	phospholipase Cγ
PSD95	postsynaptic density-95
qPCR	quantitative PCR
RBFOX	RNA binding fox-1 homolog
RIN	RNA integrity number
RNA	ribonucleic acid
RhoA	Ras homolog family member A
ROI	region of interest
rpm	revolutions per minute
RT	room temperature
SEM	standard error of the mean
sEPSC	spontaneous excitatory postynaptic current
SCG2	secretogranin II
SD	standard deviation
SDS	sodium dodecyl sulfate
SLC	solute carrier family
SNP	single nucleotide polymorphism
ssoligo	single-stranded oligonucleotide
SOX2	sex-determining region Y-box 2
SSEA4	stage-specific embryonic antigen 4
SV2	synaptic vesicle protein 2
SYN	synapsin
TBR1	T-box brain 1
TBS-T	tris-buffered saline with Tween®20
TEMED	N, N, N‘, N‘ - tetramethylethylenediamine
TGF-β	transforming growth factor
TGN	trans-Golgi network
TRK	tropomyosin receptor kinase
TTX	Tetrodotoxin
TUBB3	βIII-tubulin
UTR	untranslated region
Val	valine
vs	versus
x g	times gravity

1 Abstract

Psychiatric disorders such as schizophrenia or major depression are often associated with specific congenital genetic variants. One of these variants, which has been associated with that kind of disorder, is the human-specific single nucleotide polymorphism (SNP, rs6265) in the *brain-derived neurotrophic factor (BDNF)* gene. About 30 to 60% of the worldwide population is either homo- or heterozygous for this SNP which is located at codon 66 in the pro-domain of the protein (Val66Met). It results in a substitution of valine (Val) to methionine (Met) that impairs the intracellular trafficking as well as the activity-dependent release of the protein. BDNF, a member of the neurotrophin family, is known to be important in brain development being involved in neuronal survival, neurite outgrowth and synaptic plasticity.

The aim of this thesis was to investigate the effects of the Val66Met polymorphism on BDNF trafficking, neuronal morphology and function on an endogenous expression level in human-induced pluripotent stem cell (iPSC)-derived neuronal cultures generated from healthy donors homozygous for either the $BDNF^{Val}$ or $BDNF^{Met}$ variant. To account for the given genetic heterogeneity of humans, I additionally generated isogenic cell lines using CRISPR/Cas9 gene editing. Analysis of BDNF localization revealed a decreased number of $BDNF^{+}$ vesicles on neurites of $BDNF^{Met/Met}$ neurons compared to $BDNF^{Val/Val}$ neurons. Interestingly, the BDNF signal was accumulated at the soma of $BDNF^{Met/Met}$ neurons, indicating impaired trafficking of $BDNF^{Met}$. Furthermore, a significant reduction in neurite length and complexity in neurons derived from $BDNF^{Met/Met}$ carriers at early developmental stages was observed. This was persistent up to later stages of development and could be rescued by external application of recombinant BDNF. The morphological alterations were accompanied by a reduced synaptic density in $BDNF^{Met/Met}$ neurons analyzed by immunocytochemistry. These results were confirmed by functional characterization including calcium imaging and electrophysiological measurements that showed an altered synaptic function in neurons carrying $BDNF^{Met/Met}$.

Taken together, my data provide first experimental evidence identifying morphological and neurophysiological differences in human neurons carrying the BDNF Val66Met polymorphism. My work demonstrates that human iPSC-derived cortical neurons can be used as a cellular model to recapitulate previous results gained with animal studies, but also to highlight human-specific aspects, which might help to strengthen our understanding of BDNF signaling.

2 Zusammenfassung

Psychiatrische Erkrankungen wie Schizophrenie oder Bipolare Störung werden oft mit spezifischen Risikogenen in Zusammenhang gebracht. Eine Variation, die immer wieder mit diesen Krankheiten assoziiert wird, ist der humanspezifische SNP (rs6265) im *BDNF* Gen, der bei 30 bis 60 % der Bevölkerung auftritt. Dabei handelt es sich um eine Aminosäure-substitution von einem Valin zu einem Methionin (Val66Met) in der Prodomäne des Proteins. Diese Veränderung führt zur Beeinträchtigung des intrazellulären Transports sowie der aktivitätsabhängigen Sekretion von BDNF. Der Wachstumsfaktor BDNF, welcher im Gehirn weit verbreitet ist, spielt eine zentrale Rolle bei der Entwicklung, der Differenzierung sowie dem Überleben von verschiedenen neuronalen Populationen.

Im Rahmen dieser Arbeit wurde die endogene Auswirkung dieses Polymorphismus auf den Transport von BDNF, die Morphologie und neuronale Funktion in humanen iPSC-abgeleiteten neuronalen Kulturen untersucht. Dabei waren die Neuronen entweder homozygot für die $BDNF^{Val}$ oder die $BDNF^{Met}$ Variante. Außerdem wurden isogene Linien mittels CRISPR/Cas9-Geneditierung generiert, um die gegebene genetische Heterogenität des Menschen zu berücksichtigen. BDNF ist in den Neuronen axonal und somatodendritisch vorhanden und co-lokalisiert mit dem „dense-core“ Vesikel Marker secretogranin II (SCG2), wodurch von einer regulierten Sekretion ausgegangen werden kann. Des Weiteren wurde die Menge an BDNF in den Neuriten quantifiziert. Dabei sind mehr $BDNF^{+}$ Partikel in $BDNF^{Val/Val}$ Neuronen als in $BDNF^{Met/Met}$ Neuronen vorhanden. Stattdessen scheint $BDNF^{Met}$ im Soma zu akkumulieren, was auf einen beeinträchtigten Transport von $BDNF^{Met}$ hinweist. Die anschließende Analyse des Neuritenwachstum zeigte auf, dass endogenes $BDNF^{Met}$ zu einer signifikanten Reduktion der Neuritenlänge, sowie der Verzweigungen in Neuronen führt. Diese hält bis zu späteren Entwicklungsstadien an und konnte durch externe Anwendung von rekombinantem BDNF behoben werden. Die morphologischen Veränderungen wurden von einer verringerten synaptischen Dichte sowie neuronalen Aktivität in $BDNF^{Met/Met}$ Neuronen begleitet.

Zusammenfassend ist zu sagen, dass die hier untersuchten Zelllinien ein geeignetes *in vitro*-Modell zur Untersuchung der Funktion von BDNF und des Val66Met Polymorphismus in humanen Neuronen darstellen. Sie sind in der Lage bisherige Ergebnisse aus der Tierforschung zum Großteil zu rekapitulieren, identifizieren jedoch auch humanspezifische Aspekte, die dazu beitragen könnten, unser Verständnis der BDNF-Signalübertragung zu stärken.

3 Introduction

3.1 The neurotrophin BDNF

In 1982, Yves-Alain Barde and Hans Thoenen reported on an approximately 14 kDa basic protein that promoted the survival and neurite growth of sensory neurons *in vitro* (1). This was the first description of BDNF, a member of the neurotrophin family. Besides BDNF, this group includes three more highly conserved neuronal growth factors: the nerve growth factor (NGF) as well as neurotrophin 3 (NT-3) and neurotrophin 4/5 (NT-4/5). Since they all are derived from a common ancestral gene, they have similarities in sequence and protein structure (~50% identity in primary structure) leading to proteins of similar molecular weights (13.2–15.9 kDa) (2,3).

BDNF expression in the brain begins during embryonic development, continues postnatally and is present also in the adult brain (3,4). In contrast to other neurotrophins, expression levels of BDNF increase over the lifespan. During the development of the central nervous system (CNS), the expression is low and gradually increases as it matures, both structurally and functionally (1). Specifically, during infancy, the levels are relatively low and increase then approximately one-third to adulthood where the level is maintained throughout adulthood and aging (5).

This neurotrophin is present in large parts of the CNS, being especially abundant in the hippocampus, cortex and structures of the limbic system, but it can also be detected in the thalamus, the basal ganglia, the cerebellum and areas of the brain stem (6). Outside the CNS, BDNF can be found in other areas such as the prostate, retina and saliva (7–9).

The distribution of messenger ribonucleic acid (mRNA) and protein is not always consistent. For example, in the striatum, only the protein but not the mRNA can be found which is attributed to an anterograde transport of the BDNF into this region (10,11). In raphe neurons, the *BDNF* mRNA and the protein occur together (9). Overall, the amount of BDNF in the brain is very low (1). The intracellular BDNF expression is found predominantly in glutamatergic neurons (12) but it is expressed also in rodent astrocytes (13), microglia (14) and oligodendrocytes (15), both *in vivo* and *in vitro*.

3.1.1 The *BDNF* gene

The human *BDNF* gene is located on chromosome 11p14.1 and extends over 70 kB (16). It consists of 11 exons (I –IX, Vh and VIIIh) and at least nine functional alternative tissue-specific promotors. Interestingly, only one single exon (IX) encodes for the complete or most of the coding sequence of the BDNF protein depending on the 5' exon used. This exon also contains two separate polyadenylation signals (17).

In general, the human gene has a more complex regulation than the rodent one, having two additional exons, more translation initiation sites and more transcription start sites. The result of alternative promoters, splicing and polyadenylation sites is a higher amount of transcripts which can lead to more human BDNF pre-pro-proteins isoforms with an alternative or longer N-termini. The expression of the different transcripts depends on various factors like the developmental stages or the specific tissues where they are express. Specifically, transcripts containing exons II–V or VII are mostly brain-specific, whereas others containing exons VI and IXabcd are also expressed at variable levels in several non-neural tissues like the heart, lung, skeletal muscle, testis, prostate and placenta (17). Further, as previously mentioned, *BDNF* transcripts can be polyadenylated at different alternative sites. This leads to mRNAs with either a short 3'UTR or a long 3'UTR (18). Depending on the type, *BDNF* distribution differs in the neurons. Short 3'UTR *BDNF* mRNA is restricted to the soma while long 3'UTR *BDNF* mRNA is enriched in dendrites of cortical neurons (19).

Additionally, in neuronal cells the splicing is dependent on electrical activity-induced by Ca^{2+} elevation due to the binding of specific Ca^{2+} response elements (20). Environmental factors like exercise, hypoxia, stress and ischemia can also regulate and increase the expression of *BDNF* (20).

Besides, the human *BDNF* locus has an *antiBDNF* gene consisting of ten exons and one functional promoter. Hundreds of endogenous noncoding antisense RNAs, which are present in neuronal and nonneuronal tissues, can be transcribed. These *antiBDNF* transcripts form *in vivo* dsRNA duplexes with *BDNF* transcripts suggesting a regulation of the *BDNF* expression in humans also by the *antiBDNF* transcripts (17).

In general, the complex transcriptional organization starting with alternative promoter usage, to differential mRNA stability or differential subcellular localization of either mRNA or protein provides multiple layers and high flexibility of control and regulation of the *BDNF* expression,

which may be important to secure a developmental stage-specific and cell-type-specific expression of this important gene.

3.1.2 Synthesis and transport of BDNF

Like other neurotrophins, BDNF is translated as a pre-pro-protein at the rough endoplasmic reticulum (ER). The pre-region is split off immediately and the obtained 32 kDa proBDNF reaches via a vesicle-mediated transport to the Golgi apparatus, where it is post-translationally modified (i.e., glycosylation, amidation, etc.). Subsequently, it accumulates through vesicle transport in the trans-Golgi network (TGN) (21,22). Finally, proBDNF/mature BDNF (mBDNF)-containing vesicles are transported to the plasma membrane to the secretion sites.

BDNF represents one clear example of the coexistence of multiple mechanisms for dendritic trafficking. Based on information in the pro-domain, the proBDNF/mBDNF sorting is controlled (23,24). Sortilin, a trans-membrane protein and the receptor carboxypeptidase E (CPE) seem to play a role in the trafficking of proBDNF/mBDNF. Sortilin binds to the pro-domain between amino acid 44 and 102, whereby BDNF is packed in large dense-core vesicles, transported to the vicinity of active synapses and their regulatory secreted (21). The interaction of the CPE takes place with a tetrad of amino acids (I16, E18, I105, D106) in the mBDNF region, forming a specific recognition motif (22). On the one hand, the secretion of proBDNF/mBDNF can occur spontaneously, the so-called constitutive pathway. On the other hand, protein secretion can result in response to neuronal activity, the regulatory pathway (25). Unlike other growth factors that are primarily constitutively secreted, BDNF is secreted in response to neuronal activity, critically depending on intracellular Ca^{2+} concentration (23,26). For many years, it was not clear if BDNF-containing vesicles were secreted pre- or post-synaptic, but nowadays it is no longer doubted that the protein can be transported to either axon terminals or dendrites (27,28). The secreted BDNF can be present either as a monomer or as a non-covalently bound homodimer (29). In cultured neurons, proBDNF is the main form of secreted neurotrophin (30).

The cleavage of the pro-neurotrophins into mature 14 kDa neurotrophin can occur at numerous locations along both pathways. Intracellularly, for example in TGN or the immature secretion vesicles, it is mediated by the serine protease furin and pro-protein convertases (31).

After the release of the proproteins extracellularly, it is cleaved by proteases such as plasmin or matrix metalloproteinases (MMP) (32) (Figure 1). Here about 100 amino acids of the N-terminal pro-domain (pro-peptide) are split off, resulting in a circa 119 amino acids mature protein (31).

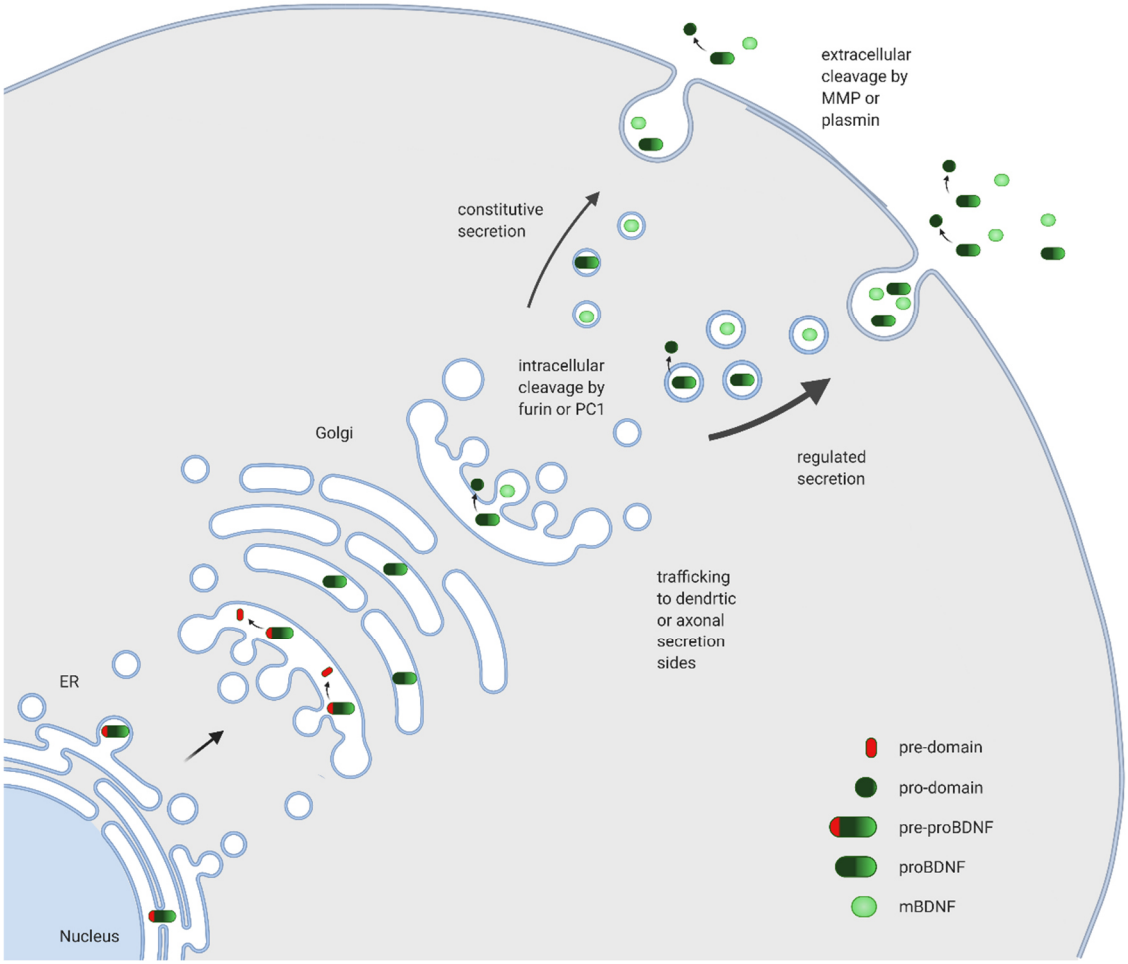

Figure 1: BDNF synthesis and secretion

BDNF is translated as a pre-pro-protein at the rough endoplasmic reticulum (ER), where the pre-region is cleaved immediately. Then proBDNF reaches the Golgi apparatus where it is post-translationally modified. Next, proBDNF/BDNF-containing vesicles are transported to dendritic and axonal secretion sites mainly through the regulated pathway, although BDNF can also be secreted constitutively. The cleavage of the proBDNF into mBDNF either takes place intracellularly in TGN or the immature secretion vesicles by the serine protease furin and PCs or extracellularly by proteases such as plasmin or MMP.

3.1.3 BDNF Signaling

Neurotrophins can activate two types of membrane-bound receptors. On the one hand, all neurotrophins can bind with a low affinity to the p75 neurotrophin receptor (p75NTR), a member of the tumor necrosis receptors. On the other hand, they specifically bind receptors of the tyrosine receptor kinase (Trk) family. Specifically, NGF binds TrkA, NT-4 can bind the TrkB and NT-3 binds TrkC and with low affinity to each of the other Trk receptors (33).

The effect of mBDNF is firstly in pre- or post-synaptic neurons by high-affinity extracellular binding to TrkB (33). This binding causes its autophosphorylation and dimerization of the kinase domain in the cytosolic region, resulting in a phosphorylated tyrosine kinase receptors (pTrkB). This receptor leads to the activation of different signaling pathways, like the phosphatidylinositol 3-kinase (PI3K), the mitogen-activated protein kinase/extracellular signal-regulated kinase (MAPK/ERK) and the phospholipase Cγ (PLCγ) (34,35) (Figure 2).

The TrkB phosphorylation site on Tyr515 leads to the recruitment and activation of different proteins, which in the end leads to the activation of Ras and activates the downstream kinases Raf, MEK and MAPK/ERK. MAPK/ERK signaling is involved in transcription events, like the activation of the cAMP response element-binding protein (CREB) transcription factor (34,35). Furthermore, PI3K also is activated by Ras that leads to the translocation to the plasma membrane and thus the activation of Akt/protein kinase B (34,36). The activated Akt is involved in protein translation (37).

The TrkB phosphorylation site on Tyr785 recruits and activates PLCγ, leading to the production of diacylglycerol (DAG) and inositol 1, 4, 5-trisphosphate (IP3). The protein kinase C (PKC) is then activated and Ca^{2+} from intracellular stores is released (34,35).

The activation of TrkB regulates different complex biological processes in the brain, promoting positive long- and short-term effects. In general, like all the others neurotrophins, mBDNF has effects on cell differentiation, neuronal survival and nerve growth (33). As results of its chemotropic properties, it plays an important role in migration and axon targeting (38).

In addition, BDNF is crucial in the development, maturation and control of synapses in the adult brain and leads to structural and functional effects (39,40). Here, the activity-dependent neurotrophin is essential for synaptic plasticity, especially in the hippocampus which is important for cognitive functions such as learning and memory (41,42). BDNF is particularly involved in the induction and maintenance of long-term potentiation (LTP) (43,44) as well as

the activity-dependent regulation of the structure and function of glutamatergic synapses (45). Presynaptically, mBDNF leads to the rapid release of glutamate (46,47). Postsynaptically, it affects the activity of the glutamate receptors either by inducing the phosphorylation of the receptor subunits or by increasing the amount of membrane-bound α-amino-3-hydroxy-5-methyl-4-isoxazolepropionic acid (AMPA) receptor subunits and N-methyl-D-aspartate (NMDA) receptor subunits (48–50).

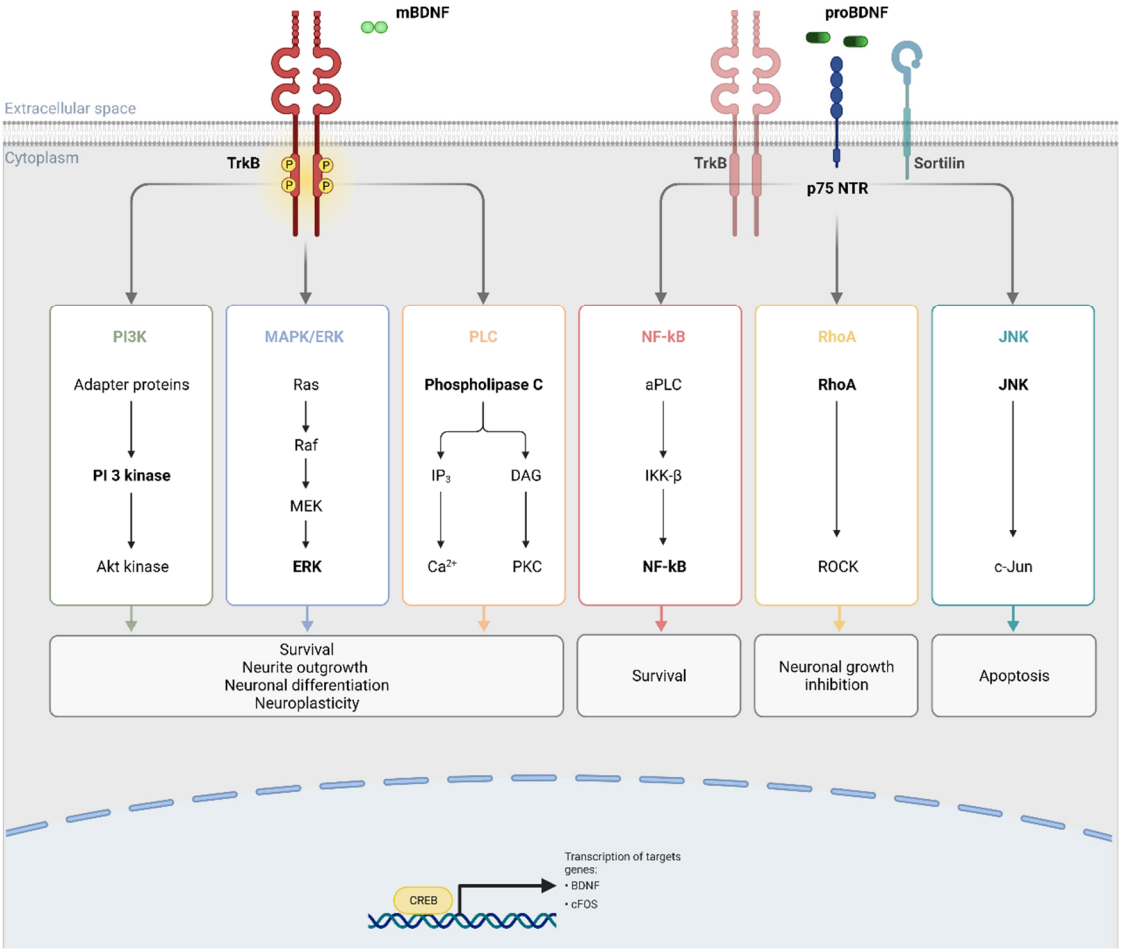

Figure 2: proBDNF/BDNF signaling

Secreted mBDNF dimers bind with high affinity to TrkB leading to its autophosphorylation and activation of different signaling cascades like PI3K, MAPK/ERK and PLC. The activation of these pathways leads to survival, neurite outgrowth, neural differentiation and neuroplasticity in the cells. In the nucleus, the transcription factor CREB is activated and it starts the transcription of specific genes like e.g. BDNF and cFOS. When proBDNF is secreted, it binds to the p75NTR. This receptor leads, depending on the co-receptor (e.g. TrkB or sortilin), to the activation of NF-kB, RhoA, or JNK pathway which can have positive effects like survival or negative effects like growth inhibition and apoptosis in the cell.

BDNF not only acts on glutamatergic but also on GABAergic neurons, having numerous pre- and post-synaptic effects on excitatory and inhibitory synaptic transmission (51,52). When uncleaved proBDNF is secreted, it binds with high affinity to p75NTR. This receptor lacks catalytic activity. Instead, it contains in the cytoplasmic region a motif similar to the death domains of tumor necrosis receptors (53). This receptor can interact extra- and intracellularly with many different proteins and form multimeric receptor complexes, leading to several cellular responses through the nuclear factor 'kappa-light-chain-enhancer' of activated B-cells (NFkB), Ras homolog family member A (RhoA) and c-Jun-N-terminale kinase (JNK) pathways (54,55). Depending on the co-receptor like sortilin or TrkB, it can generate either negative effects through its induction of apoptosis, myelination, neuronal growth inhibition and long-term depression (LTD) or positive effects like neuronal survival and neurite outgrowth (56,57) (Figure 2).

3.1.4 Psychiatric disorders associated with BDNF

As mentioned above, the neurotrophin BDNF is critical for many neural processes like differentiation, survival and growth, but is also involved in the maintenance and plasticity of the neural circuit. Due to the wide spectrum of BDNF activity, impairment of BDNF has been associated with a variety of mental disorders such as major depression, schizophrenia, or bipolar disorder (58,59). In fact, patients suffering from these neuropsychiatric disorders show a decreased BDNF expression and neuronal atrophy and exhibit a reduced volume of different brain regions. For instance, patients with major depression show a lower volume of the hippocampus and amygdala (60). Furthermore, postmortem hippocampal tissue and serum from patients with bipolar disorder or major depression show reduced levels of BDNF and his receptor TrkB (61,62). Several studies have been investigating the possible effect of BDNF on antidepressant mechanisms. Treatment with the antidepressant imipramine, for example, leads to a potentiate BDNF-induced glutamate release in cultured cortical neurons (63). Furthermore, rats chronically treated with antidepressants increase *BDNF* mRNA expression levels in the hippocampus (64). Not only a genetic predisposition but also stressful life events like early life trauma can be related to the onset of mental illnesses (65). Intriguingly, several studies show a reduction in BDNF levels in the brain of stressed animals (66). This stress-

induced reduction in BDNF expression may be a part of the pathophysiology of mental disorders.

Taking all these findings together, it is clear that BDNF has a crucial role in the pathophysiology associated with mental disorders such as major depression, schizophrenia and bipolar disorder. However, future work will be required to determine the actual involvement of BDNF in these disorders in order to identify effective and applicable BDNF-based therapies.

3.2 Val66Met polymorphism

Nowadays, neurotrophins have been implicated in the pathophysiology of many diseases, but the first alteration in a neurotrophin gene linked to clinical pathology was the SNP rs6265 in the *BDNF* gene. This non-synonymous polymorphism seems to be human-specific, not been identified in any other vertebrate (67). It causes a single base mutation with an A instead of a G at position 196 (G196A) which leads on protein level to an amino acid substitution of Val to Met at codon 66 (Val66Met) (67) (Figure 3).

An estimated 30 to 60% of the worldwide population is either homozygous (Met/Met) or heterozygous (Val/Met) for this common SNP. The percentage of Met carriers varies a lot between regions and ethnicity (68). The highest amount of Met carriers is of Indo-European descent. For example, in Japan, about 65% of the population carries this SNP (69). In comparison to that, only approximately 30% of the U.S. population carries the $BDNF^{Met}$ variant and even less are homozygous for the $BDNF^{Met}$ variant (5%) (67). In Italy, about 10% and 50% of the population are homozygous for the $BDNF^{Met}$ and $BDNF^{Val}$ variant, respectively (70). These differences in allele frequency between Caucasian and Asian populations may be due to a compensatory mechanism that supports or eliminates the negative effects of the $BDNF^{Met}$ mutation in the populations where it is more frequent. Most of the studies have been done on subjects of European descent since the most robust cognitive and behavioral effects associated with the Met genotype have been found in the Caucasian population (71).

Considering the important role of BDNF in the brain, more than 1300 genetic studies have investigated this polymorphism on brain function and behavior in health, as well as in diseases, particularly neuropsychiatric disorders (72,73) since its discovery in 2002 (74).

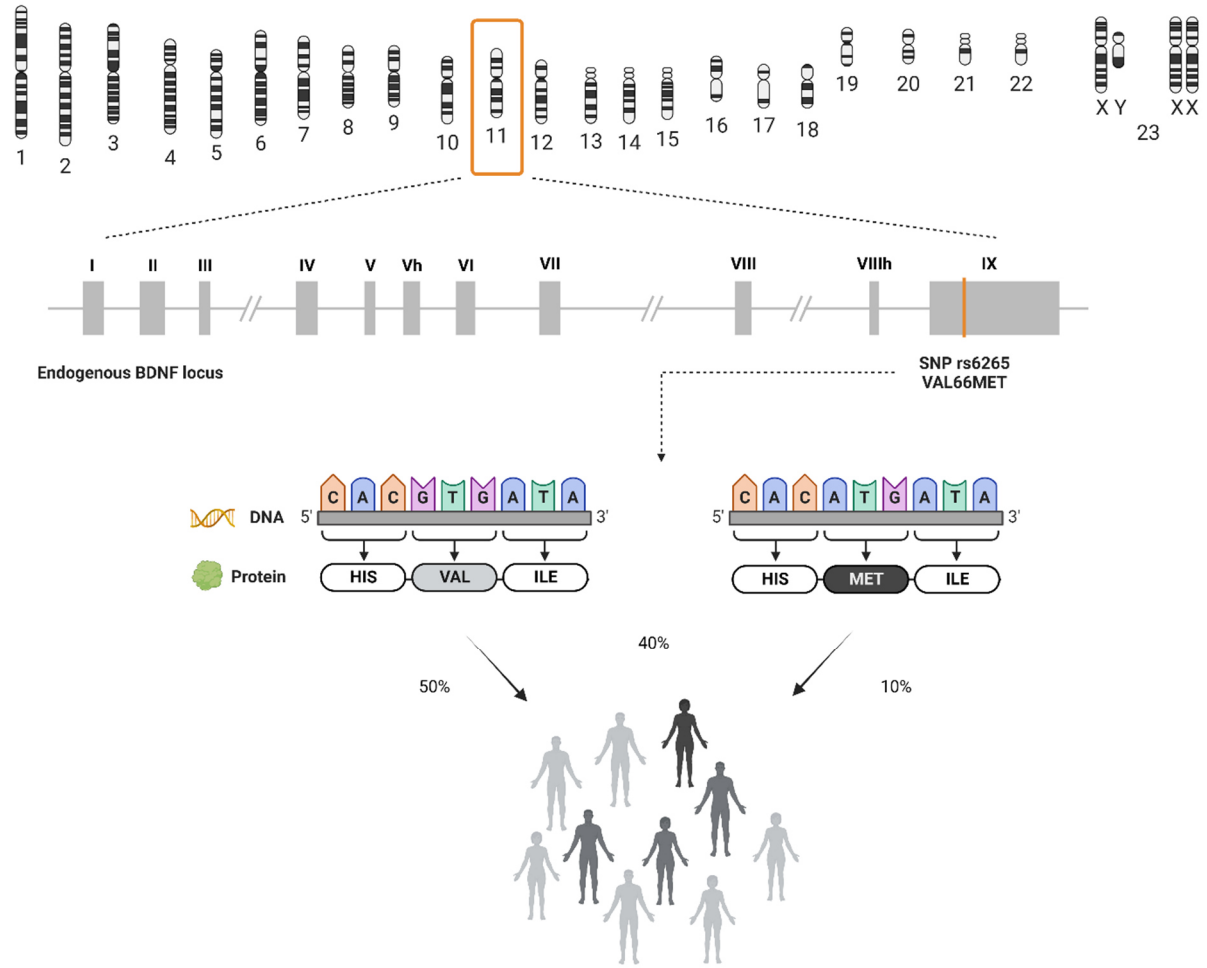

Figure 3: Val66Met polymorphism

BDNF gene is localized at chromosome 11p14.1 and consists of 11 exons (I–IX, Vh and VIIIh). The Val66Met polymorphism (SNP: rs6265) is localized in the last exon (IX) of the protein. The polymorphism leads to a substitution from G to an A which leads to an amino acid exchange at codon66 from a Val to Met located in the pro-domain. In the Caucasian population, about 50% are homozygous for the $BDNF^{Val}$ variant, 30% heterozygous and 10% homozygous for the $BDNF^{Met}$ variant.

3.2.1 Effects of Val66Met

In the last 20 years, several effects have been associated with the Val66Met polymorphism. Not only detrimental molecular, cellular and brain structural modifications but also social and cognitive dysfunction have been associated with this SNP (75) (Figure 4).

The non-synonymous polymorphism is located in the pro-domain of BDNF, the part of the protein, which is important for the sorting and intracellular transport (25).

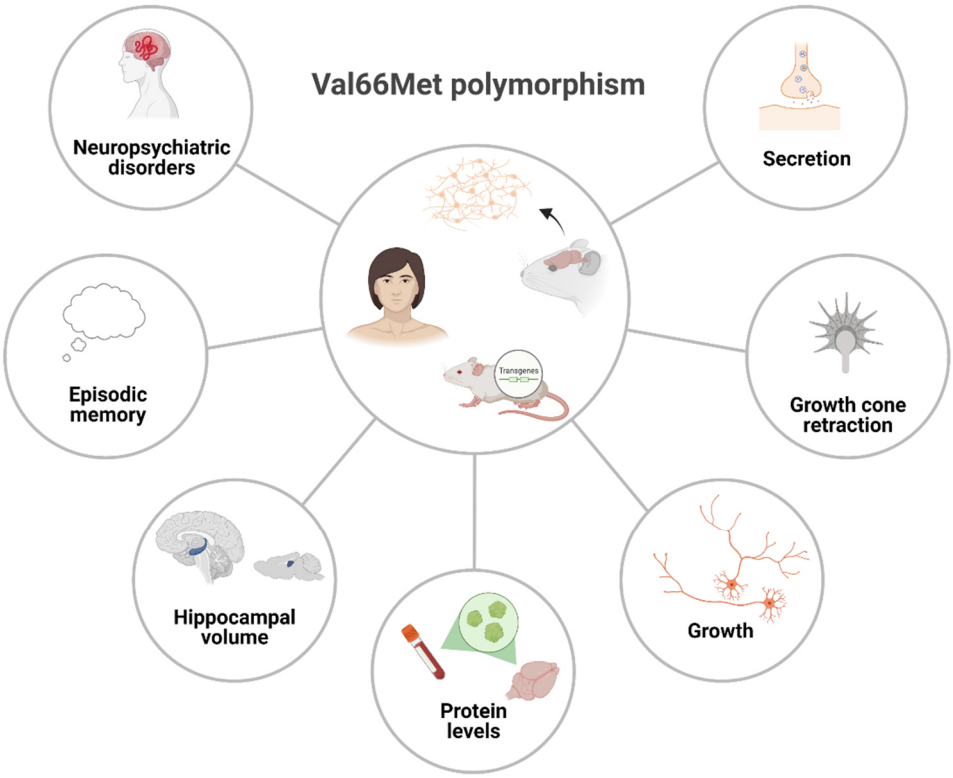

Figure 4: Effects of Val66Met

Studies in mice models as well as in human post-mortem tissues have shown that the Val66Met polymorphism impairs the regulated BDNF secretion, growth and growth cone retraction in neurons. It has an impact on BDNF protein levels in blood samples as well as in different brain regions. Hippocampal volume is reduced in $BDNF^{Met/Met}$ mice and humans. Furthermore, BDNF affects episodic memory and is associated with many neuropsychiatric disorders.

Several studies have shown an abnormal subcellular localization of BDNF upon Met substitution both on mRNA and protein levels. In transfected hippocampal neurons, $BDNF^{Val}$ appears more punctate and extends into secondary and tertiary dendrites, whereas $BDNF^{Met}$ is more diffuse, accumulates in the perinuclear region and is only partially transported in the proximal area of the primary dendrites (67,76). In addition, intracellular trafficking of *BDNF*^{Met} mRNA into dendrites is reduced (77). This impaired intracellular trafficking caused by the Val66Met, leads to a reduced regulated secretion (30% decrease) of $BDNF^{Met}$ compared to $BDNF^{Val}$ in hippocampal neurons, whereas the constitutive secretion first seemed not to be affected (67). A reason for that might be the inability of $BDNF^{Met}$ to be sorted from Golgi in the right vesicles. This could be due to the less efficient interaction of $BDNF^{Met}$ with sortilin, which then leads to a decreased targeting of $BDNF^{Met}$ to the regulated secretory pathway. This

hypothesis is supported by experiments in which $BDNF^{Met}$ was able to impair the trafficking of $BDNF^{Val}$ following the formation of BDNF heterodimers (76).

Furthermore, $BDNF^{Val}$ particles but not $BDNF^{Met}$ are colocalizing with $SCG2^{+}$ secretory vesicles and synaptophysin, a marker for synapses (67). In addition, $BDNF^{Met}$ is accumulated in $giantin^{+}$ Golgi vesicles, but no difference between both variants was found in $calnexin^{+}$ vesicles. Regarding the total number of vesicles, the ones containing $BDNF^{Met}$ were strongly reduced in comparison to $BDNF^{Val}$ by about 30% (78). In addition, in the hippocampus of *BDNF*$^{Met/Met}$ mice, also decreased basal BDNF protein levels were found (79). In contrast, significantly increased blood *BDNF* mRNA and protein levels (80) were found in *BDNF*^{Met} carriers. Overall, contradictory associations have been found regarding the circulating BDNF concentration and the Val66Met polymorphism.

An altered cortical and hippocampal morphology is one of the most reliable effects associated with this polymorphism. Magnetic resonance imaging (MRI) scans show that carriers of the *BDNF*^{Met} allele have reduced hippocampal volume in comparison to homozygous *BDNF*^{Val} carriers (81,82). Transgenic knock-in mouse (*BDNF*$^{Met/Met}$) studies show also a reduced hippocampal volume in comparison to wild-type mice (83). Since BDNF and its receptor play an important role in the developing and adult brain (33), the difference in volume could arise for example from a reduced dendritic complexity and/or fewer neuronal or supporting cells. Indeed, primary cultures of hippocampal neurons transfected with human $BDNF^{Met}$, lead to a reduced dendritic length and branching as well as reduced dendritic complexity in comparison to neurons transfected with $BDNF^{Val}$ (84). Another study found that $BDNF^{Met}$ could induce acute growth cone retraction, suggesting that the Met pro-peptide is a new active ligand that can modulate neuronal morphology (85).

In addition, $BDNF^{Val}$ increases dendritic spine density and volume in transfected neurons, where $BDNF^{Met}$ fails. Moreover, the number of excitatory synapses is reduced with $BDNF^{Met}$ (84) and in addition to that, studies have shown that *BDNF*$^{Met/Met}$ mice have in the dentate gyrus an impaired survival of newly generated cells and LTP (79).

Furthermore, the polymorphism is associated with cognitive dysfunction. Humans that are carriers of the *BDNF*^{Met} allele have subclinical memory deficits and impaired hippocampal activation (83,86). Transgenic mice also showed impaired learning of cues (87).

While much is known about the effects of mBDNF and proBDNF, the role of the pro-peptide alone is still not fully known. One role, which has been reported, is that the pro-peptide can

bind with high affinity to mBDNF. This complex is more stable with $BDNF^{Val}$ pro-peptide in comparison to $BDNF^{Met}$ pro-peptide which leads to the conclusion that

Val66Met polymorphism affects the stability of the complex formed between BDNF and its pro-peptide (88). Finally, the pro-peptide functions also as a modulator of synaptic plasticity being involved in the enhancement of hippocampal LTD. Here, $BDNF^{Met}$ pro-peptide in contrast to $BDNF^{Val}$ pro-peptide attenuates low-frequency stimulation-induced hippocampal LTD (89).

3.2.2 Disorders associated with Val66Met

Given the diverse functions of BDNF, it is not surprising that psychiatric disorders including bipolar disorder, schizophrenia, major depression, anxiety and eating disorders (72,90) are associated with the Val66Met polymorphism.

The first associations between Val66Met and a clinical phenotype were reported in 2002. Several studies showed an association between this polymorphism and the pathogenesis of bipolar disorder (91,92). In particular, lower hippocampal volume in patients with bipolar disorder has been correlated to Val66Met (93,94). However, this association seems only to be significant in Caucasians, but not in Asians (95).

Shortly after, a study on schizophrenic patients, their relatives and healthy controls on cognitive functions showed that the *BDNF*^{Met} allele reduces the delayed recall of episodic memory in all three groups but had no influence on other cognitive domains or intelligence quotient (IQ) (67).

There is also a correlation between the Val66Met polymorphism and depression, indicating that carriers of the *BDNF*^{Met} allele have a higher risk for this disorder (96). Furthermore, an interaction between the rs1475157 polymorphism of *NRN1* (a neurotrophic factor involved in synaptic plasticity) and the BDNF Val66Met polymorphism seems to modulate depressive symptoms (97).

A genetic predisposition was also found regarding suicidal behaviors (98). These results could not be confirmed in a meta-analysis study. However, in a subgroup analysis by ethnicity, evidence of an association between this polymorphism and suicidal behaviors was found in Asian and Caucasian populations (99).

In a large part of the positive association studies, the *BDNF*^{Met} allele is seen as the risk allele for psychiatric disorders. The reason for that could be the reduced activity-dependent secretion of BDNF and the association with its lower activity. Some studies although state that there are also disorderlike bipolar disorder or substance abuse associated with the *BDNF*^{Val} allele and its higher activity (91,100).

Even if many studies analyze the Val66Met polymorphism and the associations between it and some diseases have been found, there are still a lot of contradictory results and studies that could not be replicated. The Val66Met polymorphism seems to have pleiotropic effects on multiple phenotypes. It can have benefits and disadvantages in the same organism. The varying could be due to the differential expression of BDNF and its receptor in different regions of the brain, resulting in variable effects on for example amygdala-related behaviors (e.g., fear/anxiety) compared to hippocampal-dependent cognition (101). Furthermore, many factors such as age, sex, environmental factors and ethnicity also have been shown to lead to inconsistencies (102).

3.3 Generation of human neuronal cultures

In the last decade, the development of iPSCs has revolutionized the human disease modeling in a dish. They have provided an enormous potential to generate and study any type of human tissue contributing to our understanding of development as well as the pathogenesis of different diseases.

In general, stem cells are characterized by their ability to self-renew via extensive proliferation and their pluripotent capabilities, so the potency to differentiate into cell types of all three germ layers (103). After the identification in 1998 of the first stable human embryonic stem cell line (hESCs) from blastocysts, numerous possibilities to investigate human development and cells appeared, but their embryonic origin makes them not easily available due to strict legal constraints. Furthermore, their research is ethically and politically controversial discussed (104).

In contrast, iPSCs can be obtained from almost any cell type, avoiding ethical concerns associated with the use of embryos and may reduce the need for animal research. Over the years, not only fibroblast obtained by skin biopsy (105) but also less invasive to acquire,

available cell types like peripheral blood mononuclear cells or renal cells from urine can be used for efficiently reprogramming (106,107).

Originally, reprogramming was performed via retroviral ectopic expression of the pluripotency-related transcription factors octamer-binding transcription factor 4 (OCT4), sex-determining region Y-box 2 (SOX2), Kruppel-like factor 4 (KLF4) and MYC (108). In parallel, also a lentiviral approach with a slightly different combination of factors, namely OCT4, SOX2, NANOG and LIN28, was capable of reprogramming human iPSCs from somatic cells (109). The problem with these approaches is that they involve stable integration of the viral transgenes into the host genome which can lead to tumorigenic potential in therapeutic approaches. Nowadays, reprogramming can be performed without permanent transgene integration via nonintegrative delivery systems such as Sendai virus or adenoviral vectors, which leads to a transient expression of the reprogramming factors and counteracts the risk of mutations (110).

IPSCs can be differentiated into several cell types by treating them with specific factors. More and more, also increasingly complex human cell types can be generated such as distinct neuronal subtypes, cardiomyocytes and insulin-secreting pancreatic β cells (111–113). Besides, nowadays not only 2D but also 3D iPSC cultures, so-called organoids, can be generated. They are miniature models of whole tissue niches that facilitate insights into developmental processes. IPSCs technology offers a novel platform for disease modeling and drug screening and may better recapitulate the actual efficacy of lead drug candidates in the human system for which standard immortalized cell lines and animal models are less suitable (114,115). Another advantage is the use of iPSC-derived grafts for autologous transplantation within the scope of cell replacement therapy since this technology eliminates the risk of immune rejection even without the need to administer immunosuppressive drugs (116).

A disadvantage of the generation of iPSCs is the loss of the genomic and epigenetic traits of aging. That is why more recently a new technology has been studied to directly convert the cell fate through transdifferentiation. Here, somatic cells like fibroblasts or peripheral blood cells can be used to generate cells of choice skipping the pluripotent intermediary (117,118). During the process, the molecular aging signature of the respective donor individual is retained which opened up new possibilities to study age-related degenerative diseases overcoming the iPSCs challenges.

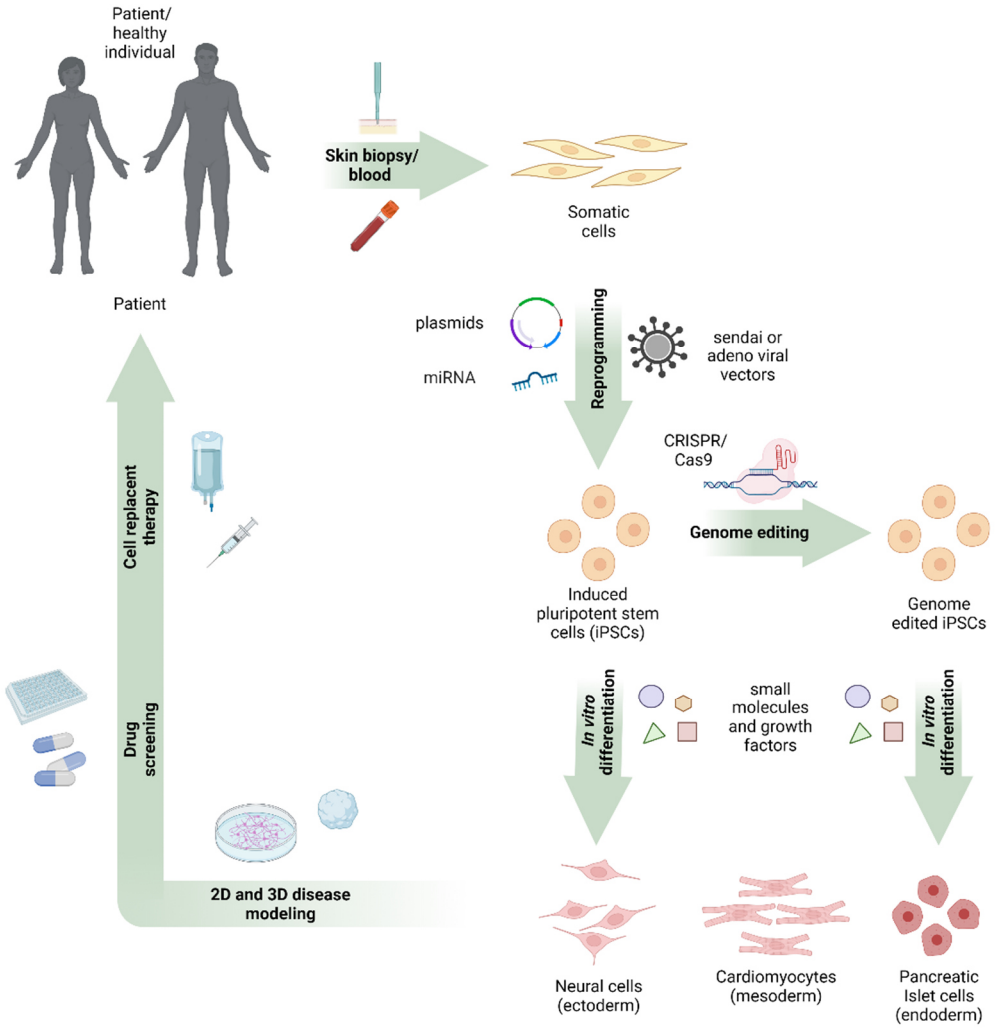

Figure 5: Human iPSC technology

Somatic cells from patients or healthy probands can be isolated from e.g. a skin biopsy or blood and be reprogrammed to human iPSCs. This is achieved by forced expression of specific transcription factors through viruses, plasmids, or miRNAs. If necessary human iPSCs can be genome-edited via CRISPR/Cas9. Protocols are available to differentiate iPSCs into different cell types. The obtained cells can be grown in 2D or 3D for disease modeling and drug screenings or they even may be transplanted back into the patient for cell replacement therapy.

IPSCs offer a novel platform to generate previously inaccessible tissue such as human neurons *in vitro.* By treating iPSCs with recombinant proteins and/or small molecules to mimic *in vivo* developmental morphogen signaling pathways, the cells can be directed into distinct neuronal subtypes as region-specific neuroepithelial cells (NECs) with the inherent tendency to differentiate into related types of neurons like excitatory and inhibitory cortical neurons,

dopaminergic neurons, serotonergic neurons, Purkinje cells, peripheral motor neurons or hippocampal granule neurons (119,120). Inhibition of SMAD-mediated bone morphogenic protein (BMP) and transforming growth factor beta (TGF-β) signaling and the WNT pathway leads to the generation of forebrain NECs (121). To generate neural progenitor cells (NPCs) with midbrain or hindbrain identity WNT signaling has to be fine-tuned to control the degree of caudalization (122). Moreover, the generation of 3D neuronal cultures, known as cerebral or brain organoids, recapitulate many aspects of embryonic brain development, such as the generation of various NPC subtypes at specific stereotypical stem cell niches of the developing brain and the migration of neurons away from these proliferative niches. Importantly, outer subventricular zone radial glia (oRG), a recently identified class of progenitors that is greatly expanded in humans, is also present in human cerebral organoids (123).

This groundbreaking technology is a remarkable benefit to the better understanding of the neurobiology behind psychiatric disorders and is changing the way we study human mental diseases, mainly due to their faithful recapitulation of hereditary and aging effects. It provides an alternative to primary human brain tissue which can be difficult to obtain and may lack cell types that can be critical for disease pathology.

3.4 Aims of this study

BDNF is involved in a multitude of processes that are important for brain development including neuronal survival, neurite outgrowth and synaptic plasticity. An estimated 30 to 60% of the population is homozygous or heterozygous for the human-specific BDNF Val66Met polymorphism located in the pro-domain of the protein. So far, most of the research regarding BDNF and this polymorphism has been done in the murine system. Animal overexpression models indicate that the modification of the BDNF protein impairs the intracellular trafficking, as well as the activity-dependent release of BDNF (67). However, these effects have not yet been investigated in human cell lines.

Therefore, the first aim of this thesis was to generate a human iPSC-based model to quantitative analyze the BDNF Val66Met polymorphism on an endogenous expression level in neuronal cultures. Additionally, isogenic iPSC lines should be created using CRISPR/Cas9-based gene editing to analyze the SNP on an identical background eliminating secondary genetic variations. Next, I set out to compare the intracellular localization and trafficking of $BDNF^{Val}$ and $BDNF^{Met}$ in human iPSC-derived neuronal cultures.

Besides, I addressed to investigate morphological alterations affecting neurite outgrowth and complexity at different time points of differentiation caused by the Val66Met polymorphism. Moreover, I aimed to evaluate the effects of BDNF variants on synaptic plasticity as well as neuronal network formation and function using inter alia calcium imaging and electrophysiological measurements.

Finally, I tried to identify if the external application of recombinant BDNF could rescue alterations caused by $BDNF^{Met}$ and thereby be considered a potential candidate for disease therapy.

4 Materials

4.1 Cell culture

4.1.1 Cell lines

Most of the cell lines listed in Table 1 were previously reprogrammed via Sendai virus from dermal fibroblast and further characterized in our group. Only the generation of Met/Met^{Iso} via CRISPR/Cas9 was part of this thesis. To identify and verify the genetic variant regarding the Val66Met polymorphism of the used cell lines, all lines were sequenced.

Table 1: Human iPSC lines used in this study

Name / genetic variant	**Cell line and clone**	**Donor / genetic background**	**Cell type and method of reprogramming**
Val/Val 1	028#1	healthy / female / age 44	Dermal fibroblast / Sendai virus
Val/Val 2	068#3	healthy / female / age 25	Dermal fibroblast / Sendai virus
Val/Val 2	068#4	healthy / female / age 25	Dermal fibroblast / Sendai virus
Met/Met 1	035#2	healthy / male / age 23	Dermal fibroblast / Sendai virus
Met/Met 2	069#2	healthy / female / age 23	Dermal fibroblast / Sendai virus
Met/Met 3	100#5	healthy / female / age 25	Dermal fibroblast / Sendai virus
Met/Met^{Iso} 1	028#17	028#1	N/A
Met/Met^{Iso} 2	028#45	028#1	N/A

4.1.2 Cell culture reagents, solutions and media

All reagents used for cell culture were either prepared under sterile conditions or sterile-filtered afterward. All cell culture base and ready-to-use media were stored at 4 °C.

Table 2: Commercial ready-to-use solutions

Compound	**Concentration**	**Cat. number**	**Manufacturer**
B-27 supplement	50X	17504044	Thermo Fisher Scientific (Waltham, USA)
BSA solution	7.5%	15260037	Thermo Fisher Scientific (Waltham, USA)
DPBS	1X	14190144	Thermo Fisher Scientific (Waltham, USA)

EDTA pH 8.0 UltraPure™	0.5 M	15575020	Thermo Fisher Scientific (Waltham, USA)
Geltrex™	15 mg/ml	A1413302	Thermo Fisher Scientific (Waltham, USA)
GlutaMAX supplement	100X	35050038	Thermo Fisher Scientific (Waltham, USA)
KnockOut™ Serum Replacement	100%	10828028	Thermo Fisher Scientific (Waltham, USA)
MEM NEAA	100X	11140035	Thermo Fisher Scientific (Waltham, USA)
PBS	1X	D8537-500ml	Sigma-Aldrich (St. Louis, USA)
Penicillin/Streptomycin	100X	15140122	Thermo Fisher Scientific (Waltham, USA)
Sodium pyruvate	100X	11360039	Thermo Fisher Scientific (Waltham, USA)
TrypLE™ Express	1X	12605028	Thermo Fisher Scientific (Waltham, USA)

Table 3: Cell culture base media

Medium	**Cat. number**	**Manufacturer**
Advanced DMEM/F-12	12634028	Thermo Fisher Scientific (Waltham, USA)
Advanced MEM	12492013	Thermo Fisher Scientific (Waltham, USA)
DMEM, GlutaMAX™	61965026	Thermo Fisher Scientific (Waltham, USA)
DMEM/F-12 (1:1)	11320074	Thermo Fisher Scientific (Waltham, USA)
DMEM/F-12, HEPES (1:1)	11330032	Thermo Fisher Scientific (Waltham, USA)
Neurobasal™	21103049	Thermo Fisher Scientific (Waltham, USA)

Table 4: Small molecules, growth factors and other chemicals used in cell culture

Compound	**Solvent**	**Cat. number**	**Manufacturer**
BDNF	H_2O	GFH1	R&D Systems (Minneapolis, USA)
BMP4	H_2O	120-05ET	Peprotech (Hamburg, Germany)
Boric acid	H_2O	15583	Thermo Fisher Scientific (Waltham, USA)
Bryostatin 1	Ethanol	203811	EMD Millipore (Burlington, USA)
Calcium chloride	H_2O	31307	Sigma-Aldrich (St. Louis, USA)
CHIR99021	DMSO	SM13	Cell Guidance Systems (Cambridge, UK)
DAPT	DMSO	SM15	Cell Guidance Systems (Cambridge, UK)
DMSO	N/A	D5879	Sigma-Aldrich (St. Louis, USA)
EGF	H_2O	GFH26	Cell Guidance Systems (Cambridge, UK)
Ethanol	N/A	32205	Sigma-Aldrich (St. Louis, USA)

FGF-2 (147)	H_2O	GFH28	Cell Guidance Systems (Cambridge, UK)
FGF-2 (154)	0.1% BSA	GFH146	Cell Guidance Systems (Cambridge, UK)
Forskolin	DMSO	SM18	Cell Guidance Systems (Cambridge, UK)
GABA	H_2O	A5835	Sigma-Aldrich (St. Louis, USA)
Glucose	H_2O	HN06.3	Carl Roth (Karlsruhe, Germany)
HEPES	H_2O	9105.4	Carl Roth (Karlsruhe, Germany)
Insulin	10 mM NaOH	91077C	Sigma-Aldrich (St. Louis, USA)
L-Ascorbic acid	H_2O	A4544	Sigma-Aldrich (St. Louis, USA)
L-Ascorbic acid 2-phosphate	H_2O	A8960	Sigma-Aldrich (St. Louis, USA)
Laminin	N/A	23017015	Thermo Fisher Scientific (Waltham, USA)
LDN193189	DMSO	72148	Stemcell Technologies (Vancouver, Canada)
Myo-Inositol	H_2O	I5125	Sigma-Aldrich (St. Louis, USA)
PD-0332991	DMSO	1116	Selleck Chemicals (Houston, USA)
Poly-L-Lysine hydrobromide	H_2O	P2636	Sigma-Aldrich (St. Louis, USA)
Pluronic F-127	DPBS	P2443	Sigma-Aldrich (St. Louis, USA)
Polyethyleneimine	H_2O	P3143	Sigma-Aldrich (St. Louis, USA)
Polyvinylalcohol	DPBS	P8136	Sigma-Aldrich (St. Louis, USA)
Progesterone	Ethanol	P8783	Sigma-Aldrich (St. Louis, USA)
Puromycin	H_2O	540222	EMD Millipore (Burlington, USA)
Putrescine	H_2O	51799	Sigma-Aldrich (St. Louis, USA)
SB431542	H_2O	SM33	Cell Guidance Systems (Cambridge, UK)
Sodium selenite	H_2O	S5261	Sigma-Aldrich (St. Louis, USA)
TGF-β1	H_2O	GFH39	Cell Guidance Systems (Cambridge, UK)
TTX	H_2O	BN0518	Biotrend (Köln, Germany)
Transferrin	H_2O	T3705	Sigma-Aldrich (St. Louis, USA)
XAV939	DMSO	SM38	Cell Guidance Systems (Cambridge, UK)
Y-27632	H_2O	SM02	Cell Guidance Systems (Cambridge, UK)

Table 5: Composition of ready-to-use cell culture media

Medium	**Component**	**Concentration**
Astrocyte medium	DMEM/F-12 Pen/Strep N-2 Glucose B-27 EGF FGF-2 (147)	 1% (v/v) 1% (v/v) 0.4% (v/v) 0.1% (v/v) 100 ng/µl 10 ng/ml
Astrocyte differentiation medium	DMEM/F-12 Pen/Strep	 1% (v/v)

	N-2 Glucose B-27 BMP4	1% (v/v) 0.4% (v/v) 0.1% (v/v) 10 ng/ml
Fibroblast medium	DMEM/F-12 Pen/Strep FBS Pen/Strep NEAA Sodium pyruvate GlutaMAX™	 1% (v/v) 10% (v/v) 1% (v/v) 1% (v/v) 1% (v/v) 1% (v/v)
Stem cell medium	DMEM/F-12, HEPES Pen/Strep L-Ascorbic acid 2-phosphate Sodium selenite FGF-2 (154) Insulin TGF-β1 Transferrin	 1% (v/v) 64 µg/ml 14 ng/ml 100 ng/ml 20 µg/ml 2 ng/ml 11 µg/ml
Stem cell freezing medium	KOSR Stem cell medium wout FGF-2, Insulin, TGF- β1, Transferrin DMSO Y-27632	50% (v/v) 40% (v/v) 10% (v/v) 10 µM
Neural progenitor induction medium I (NI-I)	Advanced DMEM/F-12 Pen/Strep GlutaMAX™ B-27 SB431542 LDN193189 XAV939	 1% (v/v) 1% (v/v) 1% (v/v) 10 µM 1 µM 2 µM
Neural progenitor induction medium II (NI-II)	Advanced DMEM/F-12 Pen/Strep GlutaMAX™ B-27 LDN193189 XAV939	 1% (v/v) 1% (v/v) 1% (v/v) 200 nM 2 µM
Neural progenitor propagation medium (NP)	Advanced DMEM Pen/Strep GlutaMAX™ B-27 FGF (147)	 1% (v/v) 1% (v/v) 1% (v/v) 20 ng/ml

Neuronal differentiation medium I (ND-I)	Neurobasal™ Pen/Strep GlutaMAX™ B-27 Ascorbic acid PD-0332991 DAPT	 1% (v/v) 1% (v/v) 0.5% (v/v) 200 µM 2 µM 5 µM
Neuronal differentiation medium II (ND-II)	Neuronal differentiation medium I CHIR99021 Forskolin GABA	 3 µM 10 µM 300 µM
Neuronal differentiation medium III (ND-III)	Neurobasal™ Pen/Strep GlutaMAX™ B-27 Ascorbic acid PD-0332991 CHIR99021	 1% (v/v) 1% (v/v) 0.5% (v/v) 200 µM 2 µM 3 µM
Neuronal differentiation medium IV (ND-IV)	Neurobasal™ Pen/Strep GlutaMAX™ B-27 Ascorbic acid PD-0332991	 1% (v/v) 1% (v/v) 0.5% (v/v) 200 µM 2 µM
Neuronal differentiation medium V (ND-V)	Advanced MEM Pen/Strep GlutaMAX™ B-27 Ascorbic acid PD-0332991 Bryostatin	 1% (v/v) 1% (v/v) 0.5% (v/v) 200 µM 2 µM 0.27 nM
Wash medium	DMEM, GlutaMax™ Pen/Strep	 1% (v/v)

Table 6: Composition of self-made media, buffers and supplements

Name	**Component**	**Concentration**
ACSF	NaCl $MgCl_2$ $CaCl_2$ KCl Glucose	125 mM 1 mM 2 mM 2.5 mM 10 mM

	$NaHCO_3$ NaH_2PO_4 adjust pH to 7.3 osmolarity 300 mOsm	25 mM 1.25 mM
Borate buffer	Boric acid adjust pH to 8.4 with NaOH	25 mM
Cytobuffer	Myo-Inositol Polyvinylalcohol PBS	240 mM 5 mg/ml (w/v) 0.2X
Imaging buffer	HEPES pH 7.4 NaCl KCl $CaCl_2$ $MgCl_2$ Glucose	20 mM 140 mM 2.5 mM 1.8 mM 1 mM 10 mM
Intracellular solution	K-gluconate KCl Na-phosphocreatine Mg-ATP GTP EGTA HEPES adjust pH to 7.3 osmolarity 300 mOsm	115 mM 20 mM 10 mM 4 mM 0.3 mM 0.2 mM 10 mM
N-2 supplement	DMEM / F12 Pen/Strep Insulin Progesterone Putrescine Sodium selenite Transferrin	70% (v/v) 1% (v/v) 500 µg/ml 630 ng/ml 1.611 mg/ml 520 ng/ml 10 mg/ml
Stimulation buffer	HEPES pH 7.4 NaCl KCl $CaCl_2$ $MgCl_2$ Glucose	20 mM 140 mM 8 mM 4 mM 1 mM 10 mM

4.2 Molecular biology

4.2.1 Enzymes

Table 7: Enzymes used in molecular biology

Enzyme	Cat. number	Manufacturer
DNase I, amplification grade	AMPD1-1KT	Sigma-Aldrich (Darmstadt, Germany)
DNase I, cell culture	10104159001	Sigma-Aldrich (Darmstadt, Germany)
GoTaq® G2 Flexi DNA polymerase	M780B	Promega (Madison, USA)
LongAmp *Taq* DNA polymerase	M0323S	New England Biolabs (Ipswich, USA)
Proteinase K	405-001	GeneON Bioscience (Ludwigshafen, Germany)
T4 DNA ligase	M0202L	New England Biolabs (Ipswich, USA)
T4 PNK	M0201	New England Biolabs (Ipswich, USA)
Taq DNA polymerase	331610	Biozym (Hessisch Oldendorf, Germany)

Table 8: Restriction enzymes used for cloning

Enzyme	Cat. number	Manufacturer
BbsI	R0539S	New England Biolabs (Ipswich, USA)

4.2.2 Plasmids

Table 9: Plasmid used for CRISPR/Cas9 genome editing

Name	Backbone	Insert (promotor-transgene)	Application	Source	Cat. number
pSpCas9(BB)-2A-Puro	px459	U6-empty CMV-Cas9-T2A-Puromycin	cloning	Addgene (Watertown, USA)	62988
$BDNF^{Met}$ RNA-plasmid	px459	U6-Met-BDNF gRNA CMV-Cas9-T2A-Puromycin	nucleofection	this thesis	N/A

4.2.3 Primers and Oligonucleotides

All primers and oligonucleotides were ordered from Integrated DNA Technologies, Inc. (Coralville, USA). The primers were reconstituted at 100 µM in nuclease-free H_2O for 30 min at 37 °C and 400 rpm.

Table 10: Primers used for PCR and qPCR

Primer name (Gene)	**forward/reverse**	**Sequence (5' → 3')**
18S	forward reverse	AAACGGCTACCACATCCAAG CCTCCAATGGATCCTCGTTA
ASCL1	forward reverse	CGCGGCCAACAAGAAGATG CGACGAGTAGGATGAGACCG
BDNF	forward reverse	TTTGGTTGCATGAAGGCTGC TGAGGACCAGAAAGTTCGGC
DLG4	forward reverse	AGCCCCAGGATATGAGTTGC CCCAGACCTGAGTTACCCCT
DLX2	forward reverse	CTCACCCAGACTCAGGTCAAAA CTCCGAGGGGATCTCACCA
FOXG1	forward reverse	CCCTCCCATTTCTGTACGTTT CTGGCGGCTCTTAGAGAT
hU6	forward	GAGGGCCTATTTCCCATGATT
GRIA2	forward reverse	GGATCCTCATTAAGAACCCCAGT TGAGGGCACTGGTCTTTTCC
GRIA4	forward reverse	CTCACCCCCTTTCCGCTTT AAGGCATCCAGTTTCCCTGTT
GRIN1	forward reverse	GGCAACACCAACATCTGGAA CCATCCGCATACTTGGAAGAC
GRIN2B	forward reverse	CTCACCCCCTTTCCGCTTT AAGGCATCCAGTTTCCCTGTT
HOXB2	forward reverse	TTTAGCCGTTCGCTTAGAGG CGGATAGCTGGAGACAGGAG
Mycoplasma	forward reverse	GGGAGCAAACAGGATTAGATACCCT TGCACCATCTGTCACTCTGTTAACCTC
RBFOX3	forward reverse	GCGCTGAGCCCGTTGAAAT CTCCTTCTGGACCGTCCTTG
NES	forward reverse	GGCGCACCTCAAGATGTCC CTTGGGGTCCTGAAAGCTG
NTRK2	forward reverse	TGGATGCATATCGTGCTCCG GTGCTTGGTTCAGCTCTTGC
OTX2	forward reverse	TGCAGGGGTTCTTCTGTGAT AGGGTCAGAGCAATTGACCA
PAX6	forward reverse	CCCCACATATGCAGACACACA GAACTGACACACCAGGGGAAA
SLC17A6	forward	TCAGATTCCGGGAGGCTACA

	reverse	TGGGTAGGTCACACCCTCAA
SLC17A7	forward reverse	AGCTGGGATCCAGAGACTGT CCGAAAACTCTGTTGGCTGC
SV2	forward reverse	AACCTAGACCAGGCACTCAT ACCCCTCCCCACAGTTACTTA
SYN	forward reverse	CAGCTCAACAAATCCCAGTCTC GGTCTCAGCTTTCACCTCGT
TUBB3	forward reverse	ATGGACAGTGTCCGCTCAGG TCACACTCCTTCCGCACCA

Table 11: Oligonucleotides used for CRISPR/Cas9 genome editing

Name	**Sequence (5' → 3')**
BDNF gRNA sense	CACCGACACGTGATAGAAGAGCTGT
BDNF gRNA antisense	AAACACACGTGATAGAAGAGCTGTC
BDNF G196A ssOligo	TCTGGAGAGCGTGAATGGGCCCAAGGCAGGTTCTAGAGGCTTGACAT CATTGGCTGACACTTTCGAACAC**A**TGATAGAAGAGCTGTTAGATGAG GACCAGAAAGTTCGGCCCAATGAAGAAAACAATAAGGACGCAGACTT

4.3 Antibodies

Table 12: Primary antibodies used for ICC

Antigen	**Host**	**Dilution**	**Cat. number**	**Manufacturer**
BDNF	rabbit	1:350	E-AB-18244	Elabscience (Houston, USA)
CTIP2	rat	1:500	ab18465	Abcam (Cambridge, US)
FOXG1	rabbit	1:100	NCFAB	Tebu-Bio (Offenbach am Main, Gerrmany)
GFAP	mouse	1:500	173011	Synaptic Systems (Göttingen, Germany)
HA -Tag	mouse	1:200	2367	Cell Signaling Technologies (Danvers, USA)
HOMER	guinea pig	1:500	160 004	Synaptic Systems (Göttingen, Germany)
MAP2	chicken	1:7000	822501	Biolegend (San Diego, USA)
mCherry	rabbit	1:100	43590S	Cell Signaling Technologies (Danvers, USA)
NES	mouse	1:600	MAB1259	R&D Systems (Minneapolis, USA)
NeuN	rabbit	1:200	MAB377	EMD Millipore (Burlington, USA)
NMDAR2B	mouse	1:200	818701	Biolegend (San Diego, USA)
OCT3/4	mouse	1:500	sc-5279	Santa Cruz Biotech (Dallas, USA)
PAX6	rabbit	1:500	901301	Biolegend (San Diego, USA)

proBDNF	mouse	1:100	sc-65513	Santa Cruz Biotech (Dallas, USA)
PSD95	rabbit	1:200	2507S	Cell Signaling Technologies (Danvers, USA)
PSD95	mouse	1:200	810401	Biolegend (San Diego, USA)
pTRKB	rabbit	1:100	sc-135645	Santa Cruz Biotech (Dallas, USA)
S100B	mouse	1:200	S2532	Sigma-Aldrich (St. Louis, USA)
SOX2	rabbit	1:200	3579	Cell Signaling Technology (Danvers, USA)
SSEA4	mouse	1:100	MC-813-70	Hybridoma Bank (Iowa City, USA)
SYN	mouse	1:500	853701	Biolegend (San Diego, USA)
TAU	guinea pig	1:750	314004	Synaptic Systems (Göttingen, Germany)
TBR1	rabbit	1:500	20932-1-ap	Proteintech (Rosemont, USA)
TUBB3	guinea pig	1:750	302 304	Synaptic Systems (Göttingen, Germany)

Table 13: Primary antibodies used for Western Blot

Antigen	**Host**	**Dilution**	**Cat. number**	**Manufacturer**
ACTIN	mouse	1:10000	3700S	Cell Signaling Technology (Danvers, USA)
ACTIN	rabbit	1:10000	4970S	Cell Signaling Technology (Danvers, USA)
BDNF	rabbit	1:2000	E-AB-18244	Elabscience (Houston, USA)
pTRKB	mouse	1:1000	sc-8058	Santa Cruz Biotech (Dallas, USA)
SYN	mouse	1:3000	853701	Biolegend (San Diego, USA)
TRKB	rabbit	1:1000	sc-8316	Santa Cruz Biotech (Dallas, USA)

Table 14: Secondary antibodies used for ICC and Western Blot

Antigen (clone)	**Host**	**Dilution**	**Cat. number**	**Manufacturer**
anti-chicken IgY Alexa Fluor-488	goat	1:1000	A11039	Thermo Fisher Scientific (Waltham, USA)
anti-guinea pig IgG Alexa Fluor-647	donkey	1:1000	A21450	Thermo Fisher Scientific (Waltham, USA)
anti-goat IgG Alexa Fluor-488	donkey	1:1000	A11055	Thermo Fisher Scientific (Waltham, USA)
anti-mouse IgG Alexa Fluor-488	goat	1:1000	A11001	Thermo Fisher Scientific (Waltham, USA)
anti-mouse IgG Alexa Fluor-568	goat	1:1000	A11004	Thermo Fisher Scientific (Waltham, USA)
anti-mouse IgG Alexa Fluor-647	goat	1:1000	A21236	Thermo Fisher Scientific (Waltham, USA)

anti-rabbit IgG Alexa Fluor-488	goat	1:1000	A11008	Thermo Fisher Scientific (Waltham, USA)
anti-rabbit IgG Alexa Fluor-555	goat	1:1000	A21428	Thermo Fisher Scientific (Waltham, USA)
Anti-mouse DyLight™ 680	goat	1:15000	5470S	Cell Signaling Technologies (Danvers, USA)
Anti-mouse DyLight™ 800	goat	1:15000	5257S	Cell Signaling Technologies (Danvers, USA)
Anti-rabbit DyLight™ 680	goat	1:15000	5366S	Cell Signaling Technologies (Danvers, USA)
Anti-rabbit DyLight™ 800	goat	1:15000	5151S	Cell Signaling Technologies (Danvers, USA)

Table 15: Fluorescent probes

Reagent	Dilution / Concentration	Cat. number	Manufacturer
DAPI	300 nM	422801	Biolegend (San Diego, USA)
Fluo-4 AM	1 µM	20552	AAT Bioquest (Sunnyvale, USA)

4.4 Kits

Table 16: Commercial kits

Kit	Cat. number	Manufacturer
BCA Protein-Assay	23228	Thermo Fisher Scientific (Waltham, USA)
Cell Line Nucleofector Kit V	VCA-1003	Lonza (Basel, Switzerland)
EXTRACTME® GENOMIC DNA Kit	EM13-050	BLIRT S.A. (Gdańsk, Poland)
Gel extraction, peqGOLD	12-2501-01	VWR (Radnor, USA)
iScript™ cDNA synthesis Kit	17088991BUN	Bio-Rad Laboratories (Hercules, USA)
Plasmid Maxiprep Kit, PureLink™ HiPure	K210015	Thermo Fisher Scientific (Waltham, USA)
Plasmid miniprep Kit, peqGOLD	732-2780	VWR (Radnor, USA)
RNA 6000 Nano Kit	5067-1511	Agilent Technologies (Santa Clara, USA)

4.5 Buffers and solutions

Table 17: Media used for bacterial cultures

Medium	Substance	Concentration
SOC medium	Bacto-Tryptone	2% (w/v)
	Yeast Extract	0.5% (w/v)
	NaCl	10 mM
	KCl	2.5 mM
	$MgCl_2$	10 mM
	$MgSO_4$	10 mM
	Glucose	200 mM
LB medium	LB medium powder	20% (w/v)
	Ampicillin	100 µg/ml
LB agar	LB medium powder	20% (w/v)
	Agar (Bacto™)	15% (w/v)
	Ampicillin	100 µg/ml

Table 18: Self-made buffers and solutions for protein biochemistry

Buffer / Solution	Component	Concentration
Protein lysis buffer	Tris-HCl, pH 7.4	50 mM
	NaCl	150 mM
	SDS	0.2% (w/v)
	EDTA	25 mM
	Phosphatase inhibitor tablet	1 tablet / 10 ml
	Protease inhibitor tablet	1 tablet / 10 ml
SDS-PAGE anode buffer (1X)	Tris-HCl, pH 8.8	200 mM
SDS-PAGE sample buffer (6X)	Tris-HCl, pH 6.8	93.75 mM
	SDS	6%
	Glycerol	6%
	2-Mercaptoethanol	9%
	Bromphenol blue	0.25%
SDS-PAGE gel buffer	Tris-HCl pH 8.45	3 M
	SDS	0.3% (w/v)
SDS-Polyacrylamide separating gel	SDS-PAGE gel buffer	33.3% (v/v)
	Bis/Acrylamide	10% (v/v)
	Glycerol	10% (v/v)
	Ammonium persulfate	0.028% (w/v)
	TEMED	0.09% (v/v)
SDS-Polyacrylamide stacking gel	SDS-PAGE gel buffer	24.8% (v/v)
	Bis/Acrylamide	3.84% (v/v)
	Ammonium persulfate	0.0672% (w/v)

	TEMED	0.224% (v/v)
TBS (10X)	Tris-HCl, pH 7.4 NaCl KCl	248 mM 1.37 M 26.8 mM
TBST (1X)	TBS (10X) Tween® 20	10% (v/v) 0.1% (v/v)
Western Blot transfer buffer	Tris-glycine buffer (10X) Methanol SDS	10% (v/v) 20% (v/v) 0.08% (v/v)

Table 19: Self-made buffers and solutions for ICC and for the work with DNA

Buffer / Solution	**Component**	**Concentration**
DAPI staining solution	DAPI	300 nM in PBS
DNA sample buffer (10X)	Tris-HCl, pH 7.6 Bromphenol blue Glycerol	50 mM 0.25% (w/v) 60%
gDNA isolation lysis buffer	Tris-HCl, pH 8.5 EDTA SDS NaCl	100 mM 5 mM 0.2% (w/v) 200 mM
Mounting solution	Tris-HCl, pH 8.5 Glycerol Mowiol DABCO®	100 mM 25% 10% 0.6%
PBS	NaCl KCl Na_2HPO_4 KH_2HPO_4	137 mM 2.7 mM 10.0 mM 1.8 mM
TAE (1X), agarose gel buffer	Tris, pH 8.0 EDTA Glacial acetic acid	200 mM 1 mM 0.114%

Table 20: Commercial buffers and solutions

Buffer / Solution	**Cat. number**	**Manufacturer**
DNA polymerase buffer (10X)	311611	Biozym (Hessisch Oldendorf, Germany)
GoTaq® DNA polymerase buffer (10X)	M780B	Promega (Madison, USA)
LongAmp® *Taq* reaction buffer (5X)	B0323S	New England Biolabs (Ipswich, USA)
Restriction buffer 2.1 (10X)	B7202S	New England Biolabs (Ipswich, USA)
RNA - Solv reagent	R6830-02	VWR (Radnor, USA)

T4 DNA ligation buffer (10X)	B0202S	New England Biolabs (Ipswich, USA)
TriFast™ peqGold	30-2010	VWR (Radnor, USA)
Tris-Tricine-SDS buffer (10X)	T1165	Sigma-Aldrich (St. Louis, USA)

4.6 Chemicals and reagents

Table 21: Molecular biology reagents and ladders

Name	Cat. number	Manufacturer
1 kb marker	N0468S	New England Biolabs (Ipswich, USA)
100 bp marker, Quick-Load®	N0467S	New England Biolabs (Ipswich, USA)
Adult brain total RNA, human	R1234035-50-BC	BioCat (Heidelberg, Germany)
dNTPs	147850010	Steinbrenner (Laborsysteme Wiesenbach, Germany)
Fetal brain total RNA, human	1F01-50	Tebu Bio (Le-Perray-en-Yvelines, France)
peqGREEN DNA/RNA binding dye	peql37-5010	VWR (Radnor, USA)
Protein marker PS 10 plus	310003	GeneOn (Ludwigshafen am Rhein, Germany)
RNase AWAY™	10666421	Thermo Fisher Scientific (Waltham, USA)
SYBR® Green nucleic acid stain	S9430	Sigma-Aldrich (St. Louis, USA)

Table 22: Chemicals

Chemical	Cat. number	Manufacturer
2-Mercaptoethanol	805740	Merck KGaA (Darmstadt, Germany)
2-Propanol	1157	Th. Geyer (Renningen, Germany)
30% Bis/acrylamide	3029.1	Carl Roth (Karlsruhe, Germany)
Acetic acid	33209	Sigma-Aldrich (St. Louis, USA)
Agar (Bacto™)	214010	BD Biosciences (Franklin Lakes, USA)
Agarose	A9539	Sigma-Aldrich (St. Louis, USA)
Ammonium persulfate	A3678	Sigma-Aldrich (St. Louis, USA)
Ampicillin	A9518	Sigma-Aldrich (St. Louis, USA)
Bacto-Tryptone	211705	BD Biosciences (Franklin Lakes, USA)
BSA	A3294	Sigma-Aldrich (St. Louis, USA)
Bromophenol blue	B8026	Sigma-Aldrich (St. Louis, USA)
Chloroform	32211	Sigma-Aldrich (St. Louis, USA)
DABCO	0718.2	Carl Roth (Karlsruhe, Germany)
DEPC	K028.1	Carl Roth (Karlsruhe, Germany)
EDTA	E3889	Across organics (Fair Lawn, USA)

Ethanol	2246.1000	Th. Geyer (Renningen, Germany)
FBS	10270-106	Thermo Fisher Scientific (Waltham, USA)
Glycerol	15523	Sigma-Aldrich (St. Louis, USA)
Glycine	10070150	Thermo Fisher Scientific (Waltham, USA)
Hydrochloric acid	836.1000	Th. Geyer (Renningen, Germany)
KH_2PO_4	1648	Th. Geyer (Renningen, Germany)
KCl	1632	Th. Geyer (Renningen, Germany)
LB medium powder	X968.4	Carl Roth (Karlsruhe, Germany)
$MgCl_2$	A351B	Promega (Madison, USA)
$MgSO_4$	105886	Merck KGaA (Darmstadt, Germany)
Methanol	0082.1	Carl Roth (Karlsruhe, Germany)
Milk powder	T145.3	Carl Roth (Karlsruhe, Germany)
Mowiol®4-88	0713.1	Carl Roth (Karlsruhe, Germany)
Na_2HPO_4	8622	Th. Geyer (Renningen, Germany)
NaCl	1367	Th. Geyer (Renningen, Germany)
PFA	16005	Sigma-Aldrich (St. Louis, USA)
Phosphatase inhibitor mini tablets	A32957	Thermo Fisher Scientific (Waltham, USA)
Protease inhibitor mini tablets	A32955	Thermo Fisher Scientific (Waltham, USA)
Puromycin dihydrochloride	540222	Merck KGaA (Darmstadt, Germany)
ROX	A351513	GENAXXON (Ulm, Germany)
SDS, pellets	CN30.1	Carl Roth (Karlsruhe, Germany)
Sodium hydroxide, pellets	6771.2	Carl Roth (Karlsruhe, Germany)
TEMED	T9281	Sigma-Aldrich (St. Louis, USA)
TRIS-HCl pH 8.5	4855.5	Carl Roth (Karlsruhe, Germany)
Triton X-100	1.08603.1000	Merck KGaA (Darmstadt, Germany)
Trypan Blue	17-942E	Lonza (Basel, Switzerland)
Tween® 20	P2287	Sigma-Aldrich(Darmstadt, Germany)
Yeast Extract	212750	BD Biosciences (Franklin Lakes, USA)

4.7 Consumables

Table 23: Consumables for cell culture, molecular biology and biochemistry

Consumable	**Format**	**Cat. number**	**Manufacturer**
TC dish	Ø 3.5 cm Ø 10 cm, Cell+	83.3900 83.3902.300	Sarstedt (Nümbrecht, Germany)
TC plates	6-well 12-well, Cell+ 24-well, Cell+	833.920.005 833.921.300 833.922.300	Sarstedt (Nümbrecht, Germany)

	48-well, Cell+ 96-well, Cell+	83.3923.300 83.3924.005	
Blotting membrane	0.2 µm PVDF Nitrocellulose	 GE10600021 GE10600001	GE Healthcare Life Science (Chicago, USA)
Bottle top filter	500 ml 1000 ml	15983307 15993307	Thermo Fisher Scientific (Waltham, USA)
Cell scraper		sc-395251	Santa Cruz Biotechnology (Dallas, USA)
Coverslips	12 mm	631-1577	VWR (Radnor, USA)
Cryotubes	1 ml	123280	Greiner (Kremsmünster, Austria)
Luna™ reusable slide			Logos Biosystems (Anyang, South Korea)
Microscopy slides		H868.1	Carl Roth (Karlsruhe, Germany)
Pasteur pipette		7691061	Th. Geyer (Renningen, Germany)
PCR strip tubes	8 x 200 µl	710971	Biozym (Hessisch Oldendorf, Germany)
Petri dish	Ø 10 cm	633180	Greiner (Kremsmünster, Austria)
Pipette tip	10 µl 200 µl 1250 µl	70.1130 70.760.002 701.186	Sarstedt (Nümbrecht, Germany)
Pipetting reservoir	25 ml	B3125-50	Parmer GmbH (Cole- Wertheim, Germany)
qPCR plate	96-well	4ti-0910/C	Steinbrenner Laborsysteme (Wiesenbach, Germany)
qPCR plate seal		4ti-0500	Steinbrenner Laborsysteme (Wiesenbach, Germany)
Reaction tubes	0.2 ml 0.5 ml 1.5 ml 2.0 ml	72.737.002 72.699 72.690.001 72.695.200	Sarstedt (Nümbrecht, Germany)
Scalpel Cutfix®		9409814	Th. Geyer (Renningen, Germany)
Screw cap tube	15 ml 50 ml	62.554.502 62.547.254	Sarstedt (Nümbrecht, Germany)
Serological pipettes	5 ml 10 ml 25 ml 50 ml	861.253.001 861.254.001 861.685.001 7695555	Sarstedt (Nümbrecht, Germany) Th. Geyer (Renningen, Germany)

Syringe	50 ml	946.077.137	Sarstedt (Nümbrecht, Germany)
Syringe filter	0.2 µm	831.826.001	Sarstedt (Nümbrecht, Germany)
Western Blot filter tissue		115-2166	VWR (Radnor, USA)

4.8 Technical Equipment

Table 24: Notable laboratory equipment

Appliance	**Name**	**Manufacturer**
Agarose gel electrophoresis chamber	EasyPhor Midi	Biozym (Hessisch Oldendorf, Germany)
Agarose gel imaging system	GeneFlash	Syngene (Bangalore, India)
Analytical balance	BP121S	Sartorius (Göttingen, Germany)
Automated cell counter	Luna™	Logos Biosystems (Anyang, South Korea)
Block heater	Thermomixer comfort	Eppendorf (Hamburg, Germany)
Camera (microscopy)	DFC9000 GT	(Wetzlar, Germany)
Centrifuge	Labofuge 400R	Thermo Fisher Scientific (Waltham, USA)
Centrifuge	5415 D	Eppendorf (Hamburg, Germany)
Centrifuge, coolable	Z216MK	Hermle (Gosheim, Germany)
Centrifuge, plates	5810	Eppendorf (Hamburg, Germany)
Electrophoresis RNA quality control	Bioanalyzer 2100	Agilent Technologies (Santa Clara, USA)
Freezer -80 °C	Hera freeze	Thermo Fisher Scientific (Waltham, USA)
Freezer -150 °C	VIP plus	Panasonic (Kadoma, Japan)
Freezing container	Mr. Frosty™	Thermo Fisher Scientific (Waltham, USA)
PCR cycler	PTC-200	Bio-Rad Laboratories (Hercules, USA)
pH meter	ProfiLab pH597	Xylem Inc. (Rye Brook, USA)
Pipetting aid	Pipet Filler S1	Thermo Fisher Scientific Scientific (Waltham, USA)
Incubator	HERAcell 150i C170 E3	Thermo Fisher Scientific (Waltham, USA) Binder (Tuttlingen, Germany)
Liquid nitrogen store	Cryotech	Thermo King (Minneapolis, USA)
Micropipettes	Research® plus	Eppendorf (Hamburg, Germany)
Microplate reader	PowerWave™ XS	BioTek (Bad Friedrichshall,

		Germany)
Microscope	Celldiscoverer 7	Carl Zeiss (Oberkochen, Germany)
Microscope	DM6B	Leica (Wetzlar, Germany)
Microscope, brightfield	DMIL LED	Leica (Wetzlar, Germany)
Microscope	DMIRB	Leica (Wetzlar, Germany)
Microscope, confocal	TCS SP5 II	Leica (Wetzlar, Germany)
Micro-Spectrophotometer	NanoDrop™ 1000	Thermo Fisher Scientific (Waltham, USA)
Nucleofector	II/2b Device	Lonza (Basel, Switzerland)
PAGE equipment	Mini-PROTEAN® Tetra	System Bio-Rad Laboratories (Hercules, USA)
qPCR cycler	QuantStudio 7 Flex	Thermo Fisher Scientific (Waltham, USA)
Qubit RNA BR Assay-Kit	Q10210	Thermo Fisher Scientific (Waltham, USA)
Sonication device	Branson Sonifier 250	Thermo Fisher Scientific (Waltham, USA)
Thermomixer	Thermomixer comfort 5355	Eppendorf (Hamburg, Germany)
Water conditioner	Milli-Q Q-POD	EMD Millipore (Burlington, USA)
Water purifier	Milli-Q® Integral 5	Merck KGaA (Darmstadt, Germany)
Western Blot imager	Odyssey IR imaging system	LI-COR Biosciences (Lincoln, USA)
Western Blot transfer system	Trans-Blot® Turbo™	Bio-Rad Laboratories (Hercules, USA)

4.9 Data processing and Software

Table 25: Software and other digital resources for data processing

Computer program	**Supplier**
ApE – A plasmid editor	M. Wayne Davis
BioRender	BioRender (Toronto, Canada)
Excel 2019	Microsoft (Redmond, USA)
ImageJ (Fiji)	National Institutes of Health (Rockville, USA)
Image Studio v 2.0	Li-Cor (Lincoln, USA)
Leica Application Suite AF	Leica (Wetzlar, Germany)
Leica Application Suite X	Leica (Wetzlar, Germany)
PowerPoint 2019	Microsoft (Redmond, USA)
Prism6	GraphPad (San Diego, USA)
QuantStudio qPCR software	Thermo Fisher Scientific (Waltham, USA)
IBM SPSS Statistics 25/26	IMB (Armonk, USA)
Word 2019	Microsoft (Redmond, USA)
ZEN	Carl Zeiss (Oberkochen, Germany)

5 Methods

5.1 Cell Culture

The cells used in this study were human-derived iPSCs from fibroblasts with no known associated disorders, which were reprogrammed in the past with the highly efficient Sendai-virus approach in the lab of Prof. Philipp Koch and were available for this thesis as stable cell lines. They were all handled under sterile conditions and regularly tested for Mycoplasma contamination by polymerase chain reaction (PCR) (124,125). All media and buffer compositions used can be found in Table 5 and Table 6.

5.1.1 Coating

For maintenance of iPSCs and neuronal progenitors, GelTrex™, a 3D physical scaffold that supported adhesion, proliferation and differentiation of the cells was used. Therefore, GelTrex™ was thawed on ice at 4 °C, diluted in cold wash medium (1:50) and then pipetted on plates (1 ml / well of a 6-well plate, 3 ml / 10 cm-dish). Plates were stored at 4 °C until further use.

To ensure the long-term cultivation of neurons a stronger coating was used. Therefore, the plates were first incubated for 10 min at room temperature (RT) with 1% polyethyleneimine (PEI), a cationic polymer that increases attachments of the cells, diluted (1:2000) in borate buffer. After that, the plates were washed three times with ddH_2O before incubating them overnight (ON) at 4 °C with Laminin diluted (1:400) in phosphate-buffered saline (PBS).

For immunocytochemistry (ICC), calcium imaging or electrophysiology, cells were plated on glass coverslips which were etched and coated as needed for the cell type of interest. Therefore, coverslips were treated with 37% hydrochloric for 1 to 2 h at RT with shaking. Then they were washed several times with ddH_2O, air-dried and autoclaved.

5.1.2 Cultivation of human iPSCs

The iPSCs were cultured as colonies on 6-well plates at a constant temperature of 37 °C and 5% CO_2. They were maintained in stem cell medium, which was changed on a daily basis. When reaching confluency of 70 to 80%, the cells were passaged in a 1:6 to 1:10 ratio. For this, the cells were washed with PBS and then incubated for 4 to 7 min with 0.5 M ethylenediamine

tetraacetic acid (EDTA) diluted 1:1000 in PBS at RT. EDTA was aspirated and the colonies were gently dissociated with stem cell medium supplemented with 5 µM Y-27632 to promote cell survival.

5.1.3 Differentiation of human iPSCs to cortical neuronal culture

To generate cortical neuronal cultures of human origin, iPSCs were first induced to cortical progenitors and subsequently differentiated into neurons.

To initiate neural cortical induction, iPSC cultures had to show confluency of about 70%. When reaching this, the stem cell medium was replaced with a neuronal progenitor induction medium (NI-I) which was changed daily. The medium composition (Table 5) is based on dual SMAD inhibition of BMP and TGF-β signaling to block mesodermal or endodermal development (121). In addition, WNT signaling was inhibited to avoid posterization to hindbrain fates. On day 4, cells were split in a 1:2 ratio and further kept in NI-I until day 8 when they were split in a 1:2 ratio into NI-II. After 8 more days cells were passaged into neural progenitor propagation medium (NP) in a 1:2 ratio and kept in this stage for up to two passages before starting terminal differentiation. All the passaging steps were done with TrypleE, a dissociation reagent, disaggregating iPSC colonies to single cells. Therefore, the cells were incubated for 7 min at 37 °C, afterward detached and collected in a Falcon™ tube containing wash medium. Cells were centrifuged at 1,200 x g at RT for 3:30 min and then resuspended in the new medium supplemented for 24 h with 5 µM Y-27632.

After the induction phase, the cortical progenitors had to differentiate into neurons and mature to form synaptic networks. The protocol used for that is based on published work (126,127) and consisted of different phases. First, progenitors are forced to exit the cell cycle by elevated Ca^{2+} levels and a synchronized neuronal differentiation is started by Notch signaling inhibition. Therefore the medium was changed to neuronal differentiation medium I (ND-I) (detailed media composition in Table 5). After one day it was renewed and on day 3 the cells were split into ND-II. For this, the cell number was counted using an automated cell counter (LUNA). For ICC, calcium imaging and patch clamp, 150,000 to 200,000 cells were plated on coverslips in a 24-well plate. For PCR or Western Blot analysis, about 3 million cells were plated on a well of a 6-well plate. The medium was half changed every two to three days. On day 10, the medium was changed to ND-III to enhance synaptogenesis and network formation by WNT signaling and again renewed every two to three days until day 17, when a

week with ND-IV started. From day 24 on ND-V was then used until the neuronal cultures were fixed or harvested for experiments.

5.1.4 Cultivation of astrocytes

Astrocytes were used for electrophysiological experiments to be co-cultivated with the neurons. They were cultured at a constant temperature of 37 °C and 5% CO_2 in astrocyte medium (Table 5) which was changed every other day. When cells grew confluent, they were split in a 1:20 ratio using TrypleE for 7 min at 37 °C. For the co-culturing 30,000 cells per well were plated on coverslips. After two to three days the medium was changed to astrocyte differentiation medium (Table 5). From this point on the medium was changed daily, until the neurons were plated on top. The co-culture was treated with neuronal media.

5.1.5 Cultivation of HEK-293 cells

Human Embryonic kidney 293 cells (HEK-293), needed for antibody and plasmid testing, were cultivated on 10 cm dishes at a constant temperature of 37 °C and 5% CO_2. They were cultured in fibroblast medium (Table 5) which was changed every other day. When cells grew confluent, they were split in a 1:12 to 1:20 ratio using TrypleE for 7 min at 37 °C.

5.1.6 Cryopreservation of cells

Since it is important to have young passages of iPSCs and not all cells or cell lines were always used for experiments, backups from all cell types and lines were done. Therefore, cells of two complete full wells of a 6-well plate were dissociated to single-cells using TrypLE™ for about 7 min at 37 °C and then diluted in wash medium. Depending on the cell type, the cells were spun down at different velocities (iPSCs at 300 x g, progenitors at 1,200 x g and day 3 neurons at 800 x g) and afterward also resuspended in different freezing media (iPSCs in stem cell freezing medium, progenitors and neurons in pause medium) all supplemented with 10 µM Y-27632. Into each cryotube 500 µl of cell suspension was transferred. The cryotubes were placed into a freezing container containing isopropanol immediately to assure gentle freezing and were stored at -80 °C. For long-term storage, the cryotubes were transferred either to liquid nitrogen or to a -150 °C freezer.

To use the backups, the cryotube were placed into a water bath at 37 ° and when the freezing medium started to melt, the cells were collected in wash medium. Afterward, the suspension was centrifuged at the correct velocity depending on the cell type (see above). The pellet was then resuspended in the corresponding medium supplemented with 10 µM Y-27632 and plated on coated plates.

5.2 Molecular biology

5.2.1 Genomic DNA isolation

For genomic desoxyribonucleic acid (gDNA) isolation, iPSCs on one well of a 6-well plate were washed with 1X PBS and subsequently harvested. The cell suspension was centrifuged for 5 min at 5,000 x g at RT and the supernatant was discarded. To the pellet 150 µl Lysis buffer solution supplemented with 1 µl Proteinase K was added and incubated at 37 °C for 1h shaking at 500 rpm. To inactivate the Proteinase K, the temperature was increased to 95 °C for 10 min. For DNA precipitation, 105 µl of 98.8% (v/v) isopropanol was added and carefully mixed for 15 s. After centrifuging at 12,000 x g for 10 min, pellets were washed twice with 70% (v/v) ethanol and centrifuged for 10 min at 12,000 x g. Then the DNA pellet was dried at RT for 20 to 30 min and resuspended depending on the size in 20 to 50 µl ddH_2O for 30 min at 37 °C. Finally, DNA concentration and purity degree were measured using the NanoDrop® ND-1000. Until further use, the samples were stored at -20 °C.

5.2.2 RNA isolation

To analyze gene expression of progenitors and neurons, RNA was isolated with an organic phenol-chloroform extraction. The procedure was performed inside a chemical hood which was sprayed with RNase AWAY™ before. Before collecting the cells, they were washed with ice-cold PBS and then centrifuged at 5,000 x g at 4 °C for 5 min. The pellet was resuspended in 1 ml TriFast™ or RNA - Solv reagent (Omega) and lysed for 5 min at RT. After adding 200 µl chloroform, the samples were vortexed for 15 s and incubated for 10 min at RT. Subsequently, they were centrifuged at 12,000 x g at RT for 5 min to allow phase separation. The upper clear phase containing the nucleic acid was transferred into a new tube, supplemented with 500 µl isopropanol and carefully inverted several times. The RNA precipitation was done ON at -20 °C. The next day, the samples were centrifuged at 12,000 x g and 4 °C for 15 min. The

supernatant was removed and pellets were washed twice with 0.5 to 1 ml 75% ethanol in diethyl pyrocarbonate (DEPC) H_2O followed by a centrifugation step of 12,000 x g for 10 min at 4 °C. After removing the ethanol, the RNA pellet was left to air-dry and then resolved in 20 to 35 µl by shaking at 400 rpm and 37 °C in the heating block for 15 min. It followed DNase treatment to remove genomic DNA contamination using the DNase I Amplification Grade Kit. For this 2.5 µl DNase I and 2.5 µl 10X reaction buffer were added per sample and incubated for 15 min at RT. The reaction was stopped by the addition of 2.5 µl stop solution followed by heat inactivation of DNase I at 70 °C for 10 min. The final RNA concentration was measured with a NanoDrop™ 1000 spectrophotometer and RNA was stored at -80 °C.

5.2.3 Complementary DNA synthesis

In order to perform PCR or quantitative PCR (qPCR) experiments, complementary DNA (cDNA) was synthesized by reverse transcription from extracted RNA. This was performed using the iScript™ cDNA Synthesis Kit. Following the manufacturer's instruction, 500 ng RNA were used for synthesis in a thermal cycler according to the protocol given in Table 26. After PCR, the product was diluted at 1:4 with ddH_2O.

Table 26: Cycling program for cDNA synthesis

Cycle Step	Temperature	Time
Priming	25 °C	5
Reverse transcription	46 °C	20
Enzyme inactivation	95 °C	1
	4 °C	∞

5.2.4 Quantitative PCR

To analyze the *BDNF* and *NTRK2* expression levels qPCR was performed. After cDNA synthesis, the qPCR reaction mix was prepared and the reaction was run as indicated in Table 27 in the QuantStudio 7 Flex cycler (Thermo Fisher Scientific). The QuantStudio software calculated threshold cycle (Ct) values as well as melting curves. Relative fold changes were determined using the ΔΔCt method with *18S* as a reference gene.

Table 27: Composition of the reaction mix for qPCR and corresponding cycling programs

GoTaq® DNA Polymerase		Temperature	Time	Cycles
200 ng	DNA/cDNA	50 °C	2 min	1
5 µl	5X *Taq* reaction buffer	95 °C	10 min	1
2.5 µl	25 mM $MgCl_2$	95 °C	20 s	|
0.25 µl	100 mM dNTPs	60 °C	20 s	40
1 µl	10 µM forward primer	72 °C	20 s	|
1 µl	10 µM reverse primer	95 °C	15 s	1
1 µl	DMSO	60 °C	1 min	1
0.02 µl	SYBR® Green	95 °C	0.05 °C/sec	1
25 nM	ROX			
0.15 µl	GoTaq® DNA polymerase			
to 25 µl	ddH_2O			

5.2.5 Polymerase Chain Reaction and DNA electrophoresis

To amplify specific regions of genes or plasmids either the *Taq* DNA Polymerase Kit (Biozym) or the LongAmp® *Taq* Polymerase Kit (NEB), which has a proofreading function and was applied during all cloning steps, were used. The reactions were done according to the instructions provided by the manufacturer (Table 28). Annealing temperature and elongation time were adjusted based on the employed primers and the expected size of the amplicon.

Table 28: Composition of the reaction mix for PCR

Taq DNA Polymerase		LongAmp® *Taq* Polymerase	
x ng	DNA/cDNA	10 ng	DNA
2.5 µl	10X *Taq* reaction buffer	5 µl	5X LongAmp® *Taq* reaction buffer
0.5 µl	40 mM dNTPs	0.75 µl	10 mM dNTPs
1 µl	10 µM forward primer	1 µl	10 µM forward primer
1 µl	10 µM reverse primer	1 µl	10 µM reverse primer
0.125 µl	*Taq* DNA polymerase	1 µl	LongAmp® *Taq* DNA polymerase
to 25 µl	ddH_2O	to 25 µl	ddH_2O

The settings selected using the MJ Research PTC-200 Thermal Cycler (Biozym Diagnostics) were as follows in Table 29.

Table 29: PCR cycling programs

	Taq DNA Polymerase			LongAmp® *Taq* Polymerase		
Cycle step	Temperature	Time	Cycles	Temperature	Time	Cycles
Initial denaturation	95 °C	1 min	1	94 °C	30 sec	1
Denaturation	95 °C	15 s	|	94 °C	30 sec	|
Annealing	60 °C	15 s	30	60 °C	60 sec	30
Extension	72 °C	15 s/kb	|	65 °C	50 s/kb	|
Final extension	72 °C		1	65 °C	5 min	1
	4 °C	∞		4 °C	∞	

To separate the fragments, each PCR sample was labeled using a 6X loading dye buffer and loaded on a 1% agarose gel (in 1X TAE-buffer, 1:15,000 PeqGREEN intercalating dye) next to a DNA ladder (100 bp or 1 kb) to determine the DNA fragment size. The gel was run inside an electrophoresis chamber with 1X TAE buffer (100 V, 400 mA, 50 min) and was developed by exposing it to UV light in a gel documentation system to visualize DNA bands. If necessary, DNA bands were cut out for further processing.

5.2.6 Gel extraction and Sanger sequencing

For sequencing analysis or cloning steps, DNA was extracted from excised gel bands using the Gel Extraction Kit (peqGOLD). The purification was performed according to the included manufacturer's instructions. After eluting the DNA in 30 µl sterile ddH_2O, the concentration was determined using the NanoDrop™ 1000 spectrophotometer.
For Sanger Sequencing, 12 µl sample and 3 µl primer were mixed and sent to an external company (Mycrosynth Seqlab Göttingen, Germany).

5.2.7 RNA quality control

For RNA bulk sequencing the RNA concentration was measured with the Qubit device according to the manufacturer's instructions.
Subsequently, to assess RNA integrity of all samples, quality control was performed with the Bioanalyzer 2100 (Agilent Technologies) using the RNA 6000 Nano Kit (Agilent Technologies) following the manufacturer's instructions. For further procedure, refer to section 5.2.8.

5.2.8 RNA bulk sequencing

For bulk sequencing, RNA of Val/Val 1 and Met/Met^{Iso} 1 neuronal cultures day 42 (n = 5) was extracted as described in 5.2.2 and quality was assessed as described in 5.2.7. For each sample having a RNA integrity number (RIN) value between 8.1 and 9.5, 40 µl of RNA solution with a concentration of 40 ng/µl was sent to the High Throughput Sequencing Unit of the Genomics & Proteomics Core Facility, German Cancer Research Center (DKFZ) to be processed. Library preparation was performed using the TruSeq Stranded protocol (Illumina) and libraries were sequenced to 50 bp on the NovaSeq 6K platform. The Omics IT and Data Management Core Facility at the DKFZ ran the Data through an RNAseq processing workflow. Analysis of total counts per feature was performed with R (128) using DESeq2 (129). All features without any counts were removed, for differential testing with DESeq2 the formula "~Batch+Condition" was used. Heatmaps for RNAseq expression data show z-scaled DESeq2 normalized counts. Gene ontology (GO) enrichment analysis was performed using enrichGO from the clusterProfiler package (130). The organism database used for this analysis is org.Hs.eg.db (131). GO circle plots were created using the GOplot package (132).
RNAseq data analysis was performed in collaboration with Dr. Anne Hoffrichter.

5.3 Generation of isogenic BDNF Val66Met lines via CRISPR/Cas9

To generate a cell line homozygous for the Val66Met polymorphism the valine residue at codon 66 of the BDNF protein had to be replaced by a methionine. This required exchange of the last nucleotide of the base triplet starting at position 196 of the open reading frame of the *BDNF* gene (196-GTG > ATG).

5.3.1 Designing and cloning of a BDNF-targeting CRISPR/Cas9 plasmid

For Cas9 gene editing the px459 V2.0 plasmid which encodes the *Streptococcus pyogenes* Cas9 enzyme fused to the puromycin N-acetyltransferase via a T2A sequence, a β-lactamase for ampicillin resistance and a restriction site for the insertion of a target-specific guide RNA (gRNA) was used (133).

Before ligation, the px459 V2.0 plasmid was digested, and the pair of oligonucleotides was phosphorylated and annealed using the following protocols.

Table 30: Composition of the reaction mix for backbone digestion and oligonucleotides phosphorylation

Backbone digestion		Oligo phosphorylation and annealing	
		1 µl	sense oligo (100 µM)
1 µg	px459 V2.0 plasmid	1 µl	anti-sense oligo (100 µM)
1 µl	BbsI	1 µl	10X T4 ligation buffer
2 µl	10X restriction buffer 2.1	0.5 µl	T4 PNK
to 20 µl	ddH_2O	to 10 µl	ddH_2O

Table 31: Thermocycler programs used for backbone digestion and oligonucleotides phosphorylation

Backbone digestion		Oligo phosphorylation and annealing		
37 °C	1 h	Phosphorylation	37 °C	30 min
		Annealing	95 °C	5 min
			Down to 25 °C	5 °C/min

Subsequently, the digested plasmid was purified after gel electrophoresis using the Extraction Kit (see chapter 5.2.6).

To ligate the backbone with the oligonucleotides for the gRNA the following reaction was prepared and incubated for 1 h at RT (Table 32).

Table 32: Composition of the reaction mix for ligation

Ligation	
50 ng	*BbsI* digested plasmid
1 µl	phosphorylated and annealed oligo duplex
1 µl	10X T4 ligation buffer
1 µl	T4 DNA Ligase
to 10 µl	ddH_2O

5.3.2 Transformation using *Escherichia coli*

To amplify plasmid DNA, *E.coli* DH5α bacteria were used. The desired DNA (5 µl) was pipetted to the thawed bacteria and incubated for 15 min on ice. Then the sample was heat shocked by placing it at the heating block at 42 °C for 40 s. Subsequently, the bacteria were again put on ice for 2 min, before 300 µl SOC medium (Table 17) was added. Then the mixture was incubated for 1 h at 37 °C while shaking at 650 rpm. Lastly, the bacteria were plated on pre-warmed 10 cm LB agar plates containing 100 µg/ml ampicillin and incubated ON at 37 °C. The next day single colonies were picked and transferred to 5 ml LB medium (Table 17) supplemented with 100 µg/ml ampicillin. Tubes were again incubated ON at 37 °C and 400 rpm for bacteria growth to be able to isolate the plasmid DNA.

5.3.3 Plasmid DNA Isolation

For plasmid isolation from small-scale, bacterial cultures the peqGOLD Plasmid miniprep Kit (VWR) was used. All steps of the Kit were performed according to the instructions of the Kit. The plasmid DNA was eluted in 30 µl ddH_2O. DNA concentration was measured using the spectrophotometer NanoDrop™ 1000.

High plasmid DNA concentrations were gained using the PureLink HiPure Plasmid Maxiprep Kit (Thermo Fisher Scientific). For this purpose, bacteria were grown in 200 ml LB ON at 37 °C and 400 rpm and centrifuged at 4,600 x g for 10 min. The DNA isolation was performed as described in the manufacturer's instructions. Only the centrifugation steps for precipitation

and washing were performed at a lower velocity (4,600 x g) but therefore for a longer time (2 h and 1 h). DNA concentration was determined again using a NanoDrop™ spectrophotometer. To validate the correct insertion of the BDNF gRNA, the plasmid DNA isolated was analyzed by Sanger sequencing using the hU6-forward primer (Table 10).

5.3.4 Nucleofection of human iPSCs and clone selection

The CRISPR/Cas9-mediated generation of a BDNF Val66Met cell line was performed on iPSCs of a healthy control subject homozygous for the G allele (Val/Val 1) using the Lonza Cell Line Nucleofector Kit V. For electroporation, $1x10^6$ cells pre-incubated with 5 µM Y-27632 for 1 h were mixed with 82 µl Nucleofector™ Solution V, 18 µl Supplement 1 and total of 6 µg of DNA (2 µg BDNF gRNA targeting CRISPR/Cas9 px459, 4 µg single-stranded oligonucleotide repair template harboring the G196A mutation) and transferred to the provided cuvette avoiding any air bubbles. The program used for nucleofection was B-023 of the Lonza Cell Line Nucleofector. Afterwards, iPSCs were plated on four wells of a 6-well plate at different densities (400,000; 300,000; 200,000 and 100,000 cells). As a control, non-nucleofected cells were seeded on another well. The cells were kept for one day in Pen/Strep-free stem cell medium with 5 µM RI, before starting the selection with 0.33 µg/ml puromycin for three days. After two days Pen/Strep was reintroduced to the medium. The surviving colonies were picked, as soon as, they reached an appropriate size and expanded for further testing and genotyping (sections 5.3.5 and 5.3.6).

5.3.5 Validation of potential $BDNF^{Met/Met}$ clones

To verify the insertion of the point mutation, pellets of each clone were harvested and gDNA was isolated (chapter 5.2.1). Afterward, the region around codon 66 was amplified by PCR using specific BDNF primers. The resulting amplicon was extracted from the gel and sent to Microsynth-Seqlab to be sequenced (see chapter 5.2.6). Clones harboring the desired GTG > ATG nucleotide exchange but no further alterations in the sequenced DNA stretch were further propagated. The remaining clones were disposed.

5.3.6 Whole genome SNP genotyping

For SNP analysis, genomic DNA was isolated from cells, using the EXTRACTME® GENOMIC DNA Kit according to the manufacturer's instructions. For elution, 30 µl sterile ddH_2O was used and the concentration of nucleic acids was determined with the NanoDrop™ 1000 spectrophotometer. For high-resolution SNP array karyotyping 900 ng of the purified DNA (50 ng/µl) were sent to the Institute of Human Genetics at the University (Life&Brain, Bonn, Germany) where the whole genome genotyping was performed using an Illumina Infinium® Global Screening Array – 24v1.0 BeadChip. Data were processed and analyzed by Josef Frank (Genetic Epidemiology Department, Zi Mannheim, Germany) using Genome Studio software v2.0.4, module Genotyping v2.0.4/Illumina BeadStudio.

5.4 Biochemistry

5.4.1 Cell lysis and protein quantification

Cells were washed with ice-cold PBS and scraped off from the plate with a cell 49 scraper. After centrifugation at 5,000 x g for 5 min at 4 °C, the pellets were resuspended in 100 to 150 µl of lysis buffer (Table 18). The suspension was incubated for 10 min at RT and 50 min on ice. Lysates were sonicated to shear genomic DNA and reduce sample viscosity with 5 pulses (duty cycle 20%, output control 5.5) from a Branson Ultrasonics™ sonifier 250 (Thermo Fisher Scientific). Subsequently, cell debris was removed by centrifugation for 15 min at 16,000 x g and 4 °C. To determine protein concentration the PierceTM BCA protein assay Kit was used according to the manufacturer's protocol. Samples were diluted at 1:5 in ddH2O and mixed with assay reagent in a 96-well plate. After incubation at 37 °C for 30 min, the absorption at 562 nm was measured in a PowerWave™ XS (BioTek) microplate reader. The protein concentration of samples was calculated based on the included bovine serum albumin (BSA) standard dilution series. Protein samples were stored at -20 °C until being analyzed by SDS-PAGE and Western Blot (section 5.4.2).

5.4.2 SDS-PAGE and Western Blot

For protein analysis, protein extracts were separated by sodium dodecyl sulfate-polyacrylamide gel electrophoresis (SDS-PAGE). Therefore, 15 to 25 µg of total protein were

diluted in protein sample buffer (final 1X), incubated at 95 °C for 5 min and loaded on SDS-polyacrylamide gels. Electrophoresis was started at 30 V for 20 to 30 min until the samples were concentrated at the stacking gel border, and then voltage was increased to 120 V for 1.5 to 2 h to separate proteins according to molecular weight.

Proteins were transferred from the gel onto nitrocellulose membrane by semi-dry blotting with transfer buffer in a Trans-Blot® Turbo™ transfer system (Bio-Rad Laboratories) for 30 to 45 min at 20 V and 1 A. Afterwards, membranes were blocked for 1 h at RT either in 5% (w/v) milk powder or 5% BSA in tris-buffered saline with Tween®20 (TBS-T). Proteins of interest were stained with primary antibodies diluted in blocking buffer ON at 4 °C. The next day, membranes were washed three times with TBS-T for 10 min at RT before being incubated for 1 h at RT with secondary antibodies diluted in TBS-T. Afterwards, the membranes were washed again 3 times and then imaged with the Odyssey imaging system (Li-Cor).

5.4.3 Immunocytochemistry

To visualize specific proteins and analyze their localization and expression, ICC was performed. After one washing step with 1X PBS, cells on coverslips were fixed either with 4% paraformaldehyde (PFA) for 10 min at RT or Methanol for 5 min at -20 °C to reserve cell structures and crosslinking proteins. The coverslips were washed three times with 1X PBS, before blocking the cells for at least 1 h at RT with blocking solution (PBS containing 10% FBS) supplemented with 0.1% Triton-X. To stain proteins localized in the nucleus, the Triton-X concentration was increased to 0.3% for better permeabilization. Primary antibodies were diluted according to the location of their targets in the blocking solution and incubated ON at 4 °C in a humid chamber. The next day the coverslips were washed 3 times with 1X PBS. Subsequently, the secondary antibodies were diluted in the blocking solution and incubated for 1 h at RT. Then the cells were washed twice with 1X PBS before incubating them with 4,6-diamidino-2-phenylindole (DAPI) for 5 to 10 min at RT. Before mounting the coverslips with Mowiol on slides, they were washed twice with 1X PBS and once with ddH_2O. Samples were airdried ON at RT before imaging them. An overview of the primary and secondary antibodies used for the experiments and their dilution factor can be found in Table 12 and Table 14.

5.5 Calcium imaging

Neuronal cultures on day 42 of three independent batches were incubated for 30 min at 37 °C with 1.1 µg/ml Fluo-4 AM (1:1000) and 20% Pluronic (1:1000). Before starting the recording, cells were washed twice with warmed imaging buffer. Calcium imaging was performed at 37 °C in the Celldiscoverer 7 automated microscope (Zeiss) with the 20X objective (0.5 zoom). Fluo-4 fluorescence was recorded with the 488 nm filter for 3 min per position at a frame interval of 170 ms and an exposure time of 150 ms. Approximately 800 to 900 time-lapse images depending on the frame rate were acquired. Per coverslip 3 visual fields with evenly distributed cells were imaged and analyzed offline for single neuron dynamics and network activity with a R script (by Dr. Anne Hoffrichter) based on scripts published earlier (Sun & Südhof, 2021). From the 20 to 30 analyzed cells per visual field the script determined one mean value per parameter which is depicted as single dot in the respective figure. Raster plots and synchronization index were created and calculated using the PaekCaller script for MATLAB (Artimovich et al., 2017). Afterwards, recordings were repeated with stimulation buffer.

5.6 Electrophysiological characterization

Whole-cell patch-clamp recordings were performed by Dr. Mahnaz Davoudi in the group of PD Dr. Georg Köhr at the Central Institute of Mental Health on neuronal cultures day 55 to 60 co-cultured with and without astrocytes using an EPC9 amplifier and PatchMaster (HEKA Elektronik GmbH). Neuronal cultures on coverslips were perfused at 2 ml/min (peristaltic pump; Ismatec GmbH) with carbogen (95% O_2 / 5% CO_2)-saturated artificial cerebrospinal fluid (ACSF) in a recording chamber at RT. To identify the single neurons, a Zeiss Axioskop with infrared differential interference contrast video microscopy was used. Before, pipettes were pulled from borosilicate glass capillaries with a P-97 micropipette puller (Sutter Instrument) and afterwards filled with intracellular solution having resistances between 4 to 6 MΩ. In voltage-clamp, input resistance was determined at -70 mV based on currents evoked by small voltage steps (-3 mV; 300 ms), whereas with increasing depolarizing steps (10 mV; 300 ms) inward and outward currents were evoked. In current-clamp, the resting membrane potential (RMP) was defined and action potentials (APs) were evoked with increasing current injections (10 pA; 300 ms) in ten depolarizing steps. Further, the total number of all evoked APs was summed up and the amplitude of the first AP was determined. In addition, spontaneous

excitatory postsynaptic currents (sEPSCs) as well as miniature EPSCs (mEPSCs) in the presence of 1 µM TTX were recorded at -70 mV. Analysis of the recordings was performed with FitMaster (HEKA Elektronik GmbH) and MiniAnalysis (Synaptosoft).

5.7 Microscopy and quantitative image analysis

5.7.1 Image acquisition

Images of immunofluorescence stainings were taken using either the fluorescence microscope DM6B (Leica) with the corresponding Leica imaging software Las X or the confocal microscope TCS SP5II (Leica). With the Leica DM6B images were taken with the 20X or 40X objective. To better, visualize synapses and small proteins, the confocal was used with a 60X objective.
The Celldiscoverer 7 automated microscope (Zeiss) with the corresponding software was used for live cell experiments like calcium imaging or to take images of living cells using the 20X objective (0.5 zoom).
Brightfield images of fixated cells were done with the DMIRB (Leica) using the 10X and 20X objective.
All images acquired were processed with ImageJ. For the analysis part, different plugins and macros were used (see 5.7.2, 5.7.3 and 5.7.4).

5.7.2 Early outgrowth assay

To identify morphological changes in neuronal cultures different approaches were used.
At an early stage of differentiation, the neurite length and the number of branch points can change rapidly, since the neurons are in the growing phase. To identify differences between the $BDNF^{Val/Val}$ and the $BDNF^{Met/Met}$ lines in this phase an early outgrowth assay was performed. Therefore, cells were plated at a low density at 6-well plates coated with PEI/Laminin. After one, three and five days the neurons were fixed and brightfield images were taken for analysis. To measure the length and the number of branchpoints, the plugin NeuronJ (ImageJ) was used. Furthermore, the effects of extracellular BDNF on different cell lines were analyzed.

5.7.3 Sholl analysis

In a second experiment, a Sholl analysis was performed to analyze the effects of the Val66Met polymorphism at a later stage of differentiation. Therefore, neurons of both variants were grown in high density (200,000/well of a 24-well plate) and after 28 days transduction with an adeno-associated vector (AAV_CamKIIa p-hCHR2(134a)-mcherry provided by Grinevich Lab, ZI) was performed. Two to three weeks after transduction the neurons were fixed and stained for mcherry. The images were analyzed using the Sholl macro of ImageJ. Here, the number of intersections was measured in 25 µm steps until reaching a distance of 200 to 300 µm from the soma. Furthermore, the total length, the primary neurites and sum of intersections were calculated.

5.7.4 Protein density

To identify the density of different proteins such as BDNF, SYN or PSD95, the number of puncta was analyzed with the ComDet v.0.4.1 plugin (ImageJ). Therefore, per image ten ROIs were set around neurites based on the structural proteins (MAP2 or TAU). Afterwards, the number of puncta in these ROIs as well as the length of the ROIs was measured. Finally, the number per 100 µm length was calculated.

5.8 Statistical analysis

Unless indicated otherwise, at least three independent biological replicates were analyzed for quantitative statistical analysis. Results are displayed as means with standard error of the mean (SEM) which were calculated using GraphPad Prism 8 statistical analysis software. In case multiple groups influenced by a single variable were compared, a Kruskal-Wallis test (with Dunn's post hoc test) was performed. If only two groups were compared, a Mann-Whitney-U test was performed. Significance levels against the respective controls are *$p < 0.05$, **$p < 0.01$, ***$p < 0.001$ and ****$p < 0.0001$.

6 Results

So far, the BDNF Val66Met polymorphism was mainly studied in non-human model systems, such as mice. Human iPSC technology can be used either to verify existing molecular mechanisms or to identify human-specific ones. With the generation of human iPSC-derived neuronal cultures, it is possible to decipher the consequences of the human-specific BDNF Val66Met polymorphism in a human context. The focus of this study was the analysis of the BDNF localization as well as to identify if morphological and functional changes caused by this polymorphism can be detected in an iPSC-derived model system.

6.1 Generation of a cell culture cohort carrying Val66Met BDNF variants

A common SNP (rs6265) in the *BDNF* gene causes a substitution of Val to Met at codon 66 in the pro-domain of the protein (Val66Met) (67). This is due to a substitution from G to A at position 196 of the coding sequence (Figure 6 A).

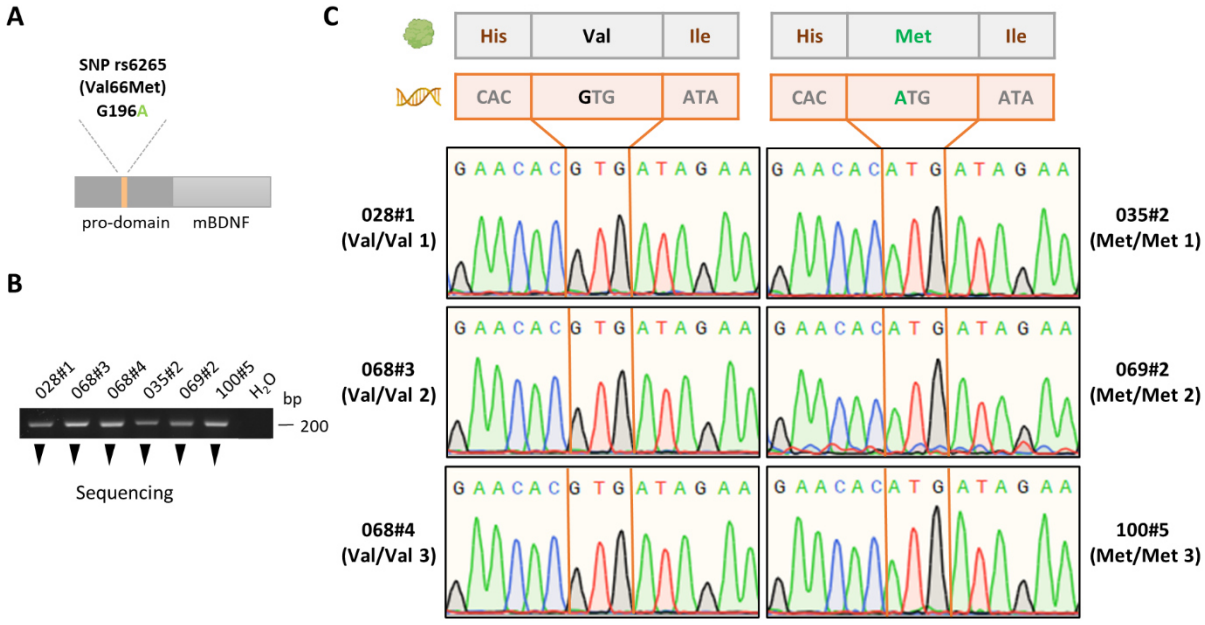

Figure 6: Identification of human iPSCs carrying Val66Met BDNF variants

(A) Schematic illustration of the BDNF protein with the SNP (rs6265; Val66Met; G196A) located in the pro-domain. **(B)** PCR to identify the *BDNF* SNP rs6265 genotype of the different lines. A 199 bp region surrounding the SNP was amplified and sent to sequencing. **(C)** Sanger sequencing results confirming homozygous G196 or A196 genotype for each three human iPSC lines.

From a repository of > 30 iPSC lines generated from dermal fibroblast of healthy donors by Sendai virus-based reprogramming available in the lab, three lines homozygous for *BDNF*$^{Val/Val}$ allele and three lines homozygous for *BDNF*$^{Met/Met}$ allele were selected to analyze the effects of Val66Met polymorphism on cortical neurons. Therefore, the BDNF locus was amplified by PCR and sequenced to identify homozygous carriers of both variants (Figure 6 B, C). The cohort comprised healthy female and male donors between the age of 23 and 44 (Table 1).

Additionally, cell lines were generated via CRISPR/Cas9-based genome editing to directly compare the two *BDNF* genotypes in a highly controlled and isogenic genetic background eliminating the impact of secondary genetic variation which is given in the before selected lines from different individuals. For this purpose, one of the iPSC lines (Val/Val 1) homozygous for the G196 allele was transfected with a guide RNA (gRNA) designed to target the rs6265 SNP located in the pro-domain of the *BDNF* gene and a 141 bp single-stranded oligodeoxynucleotide (ssODN) carrying A196 for homology-directed repair (Figure 7 A, B). The transfected clones were selected for only 48 h with 0.33 µg/ml puromycin since there was no stable integration of a resistance gene, but only a transient one. The clones that survived the selection were analyzed by Sanger sequencing as previously described (5.2.6). Two of the clones (Met/Met^{Iso} 1, Met/Met^{Iso} 2) were carrying the desired A196 mutation homozygous with no detectable other mutations in this region (Figure 7 C). The other clones were either missing the A196 mutation or showed more mutations or deletions in the sequence. Alignment of the BDNF protein sequence of isogenic Val/Val 1 line (G196) and A196 mutants showed the desired Val > Met substitution but no additional amino acid exchanges (data not shown). On the two clones, genomic and karyotypic integrity by SNP analysis were performed to exclude off-target effects (Figure 7 D). For the two clones, the B allele frequencies (BAF) and the Log R ratio (LRT) graph for every chromosome are depicted. None of the clones showed marked genomic aberrations. By ICC for the markers OCT3/4, SOX2 and stage-specific embryonic antigen 4 (SSEA4) the pluripotency capacity of all lines was confirmed (Figure 7 E). SOX2 and OCT3/4 are important transcription factors for the promotion of self-renewal of undifferentiated stem cells and SSEA4 is a cell surface glycosphingolipid which is important for cell signaling and specific for mammalian pluripotent stem cells (134–136).

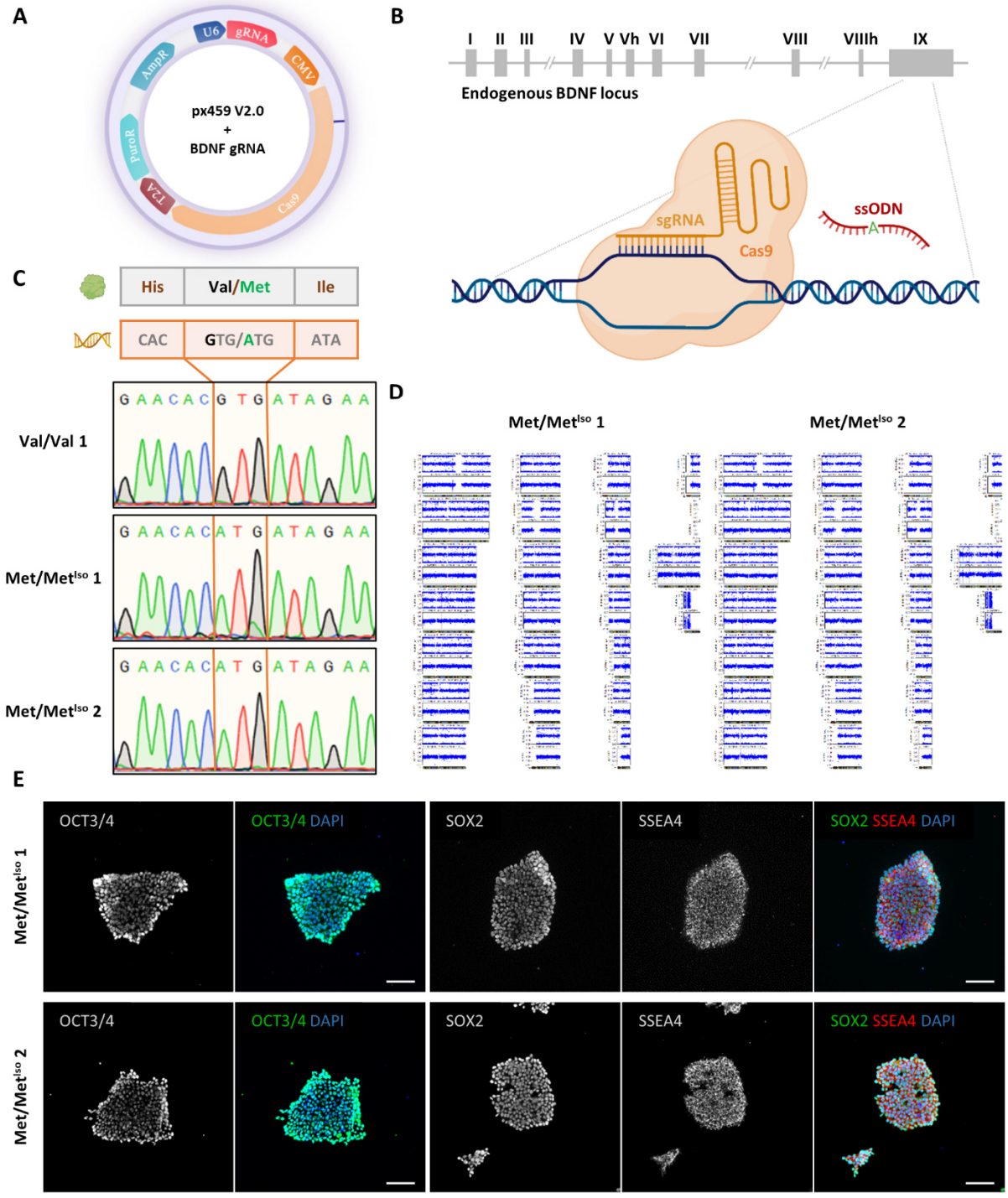

Figure 7: Generation of an isogenic line carrying Met66 BDNF variant

(A) Plasmid (px459 V2.0) cloned for CRISPR/Cas9-mediated genome editing harboring guide RNA designed to target the rs6265 SNP. **(B)** Illustration of the targeting strategy for CRISPR/Cas9-based generation of isogenic iPSC lines carrying endogenous *BDNF* A196. **(C)** Sequencing of Val/Val 1 cell line carrying homozygous *BDNF* G196 alleles used for gene editing and isolated clones (Met/Met^{Iso} 1 and Met/Met^{Iso} 2) carrying homozygous *BDNF* A196 alleles after nucleofection. **(D)** Full genome SNP analysis of Met/Met^{Iso} 1 and Met/Met^{Iso} 2. The two validated iPSC clones did not display genomic alterations. **(E)** ICC of CRISPR/Cas9-based generated iPSC lines for pluripotency markers OCT3/4, SOX2 and SSEA4. Scale bars: 100 µm

6.2 Generation and characterization of human cortical neuronal cultures from iPSCs

To investigate the effects of the BDNF Val66Met polymorphism on human cortical neurons, iPSC lines carrying Val66Met BDNF variants were used to generate human neuronal cultures of cortical identity. In the first step, dual SMAD inhibition (121) in combination with inhibitors for ventralization and caudalization was used to differentiate stem cells into an ectodermal lineage by preventing mesodermal and endodermal specification. In the second step, the progenitors were differentiated into mature neurons by small molecules-driven cell cycle arrest and inhibition of Notch signaling (126,127). Further, they were temporarily exposed to GABA and cultured with an increased concentration of $CaCl_2$ to mimic the milieu during embryonic development (Figure 8).

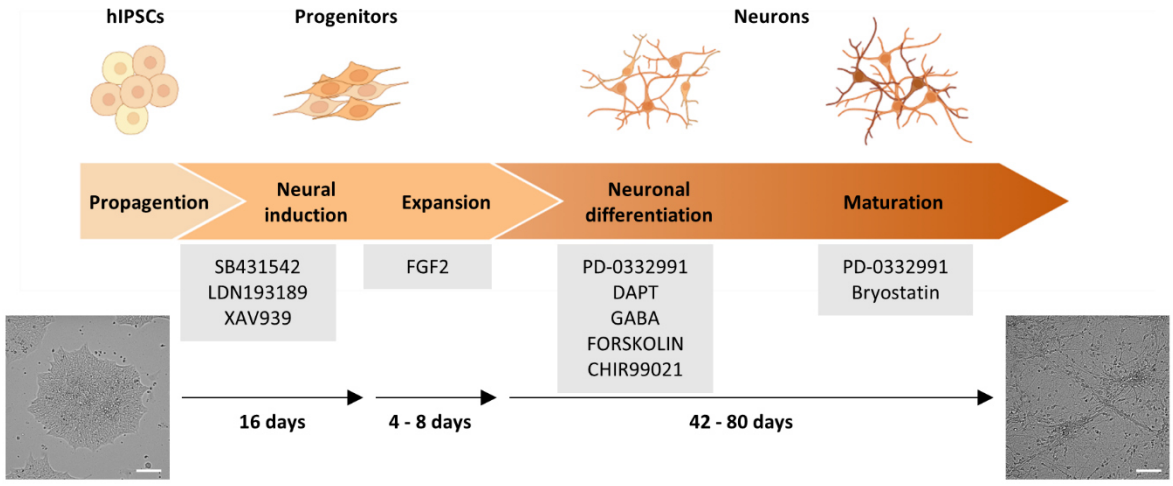

Figure 8: Differentiation from human iPSCs into cortical neurons

Illustrative scheme of the protocol used for the generation of iPSC-derived cortical neurons via dual SMAD inhibition with representative brightfield pictures from iPSCs and neurons day 42. Scale bars: 100 µm

In the first weeks the cells were expressing markers for progenitor cells like *NES* (Nestin) or *PAX6* shown by PCR and ICC (Figure 9 A, B). Furthermore, forebrain genes like *OTX2* and *FOXG1*, proneuronal marker (*ASCL1*) but not ventral forebrain (*DLX2*) and hindbrain (*HOXB2*) genes were detectable in the cultures (Figure 9 A). The majority of cells were expressing a signal for the transcription factor FOXG1 also on a protein level, while only a few cells were positive for the neuronal marker TUBB3 (Figure 9 B), as expected at this stage. Many cells showed a Ki-67 signal, marking proliferating cells (data not shown).

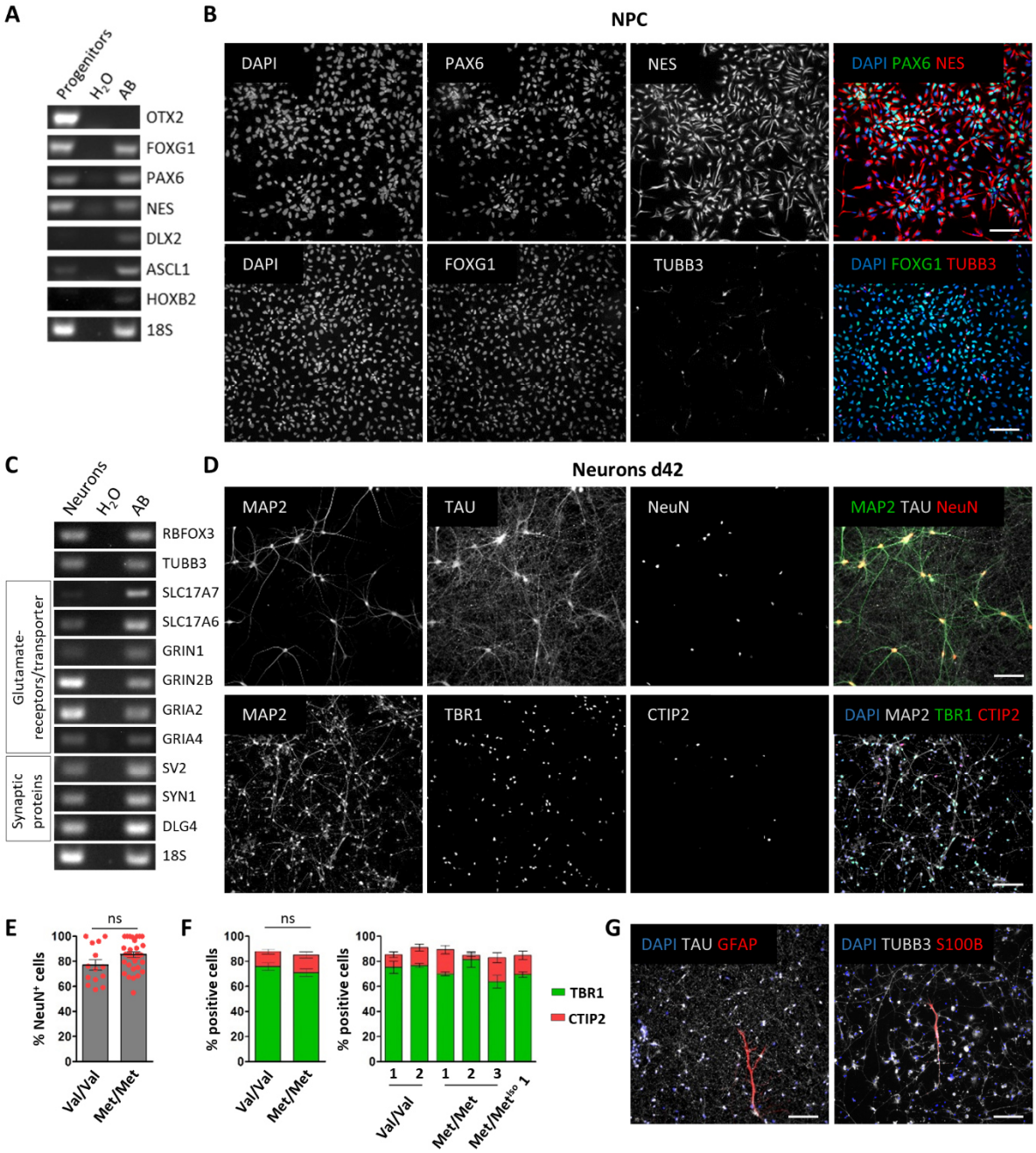

Figure 9: Characterisation of progenitors and neurons

(A) RT-PCR analysis of canonical marker genes in progenitors. AB: adult brain. **(B)** ICC of neuronal progenitors expressing DAPI, PAX6, NES, FOXG1 and TUBB3. Scale bars: 50 µm. **(C)** RT-PCR analysis of canonical marker genes in neuronal cultures day 42. AB: adult brain. **(D)** ICC of mature neurons day 42 expressing dendritic marker MAP2, axonal marker TAU, NeuN and cortical layer V/VI markers TBR1 and CTIP2. Scale bars: 100 µm. **(E)** Quantification of the percentage of NeuN$^+$ nuclei in neuronal cultures (n ≥ 14 ROIs per BDNF variant, Mann Whitney-U test; means ± SEM). **(F)** Quantification of the percentage of TBR1$^+$ and CTIP2$^+$ nuclei in neuronal cultures (n ≥ 7 per BDNF variant, Mann Whitney-U test; means ± SEM). **(G)** ICC of neuronal cultures day 42 expressing TAU, TUBB3 and the astrocyte markers S100B and GFAP. Scale bar: 100 µm. ns: not significant

For a broader transcriptional characterization of the generated neuronal cultures, PCR was performed on neuronal cultures on day 42 of differentiation (Figure 9 C). The cultures expressed mRNA levels for *RBFOX3* (NeuN) and *TUBB*. Furthermore, synaptic markers important for functional mature neurons like *SV2*, *SYN1* (Synapsin) and *DLG4* (PSD95) were present at this stage of differentiation. The neuronal cultures consisted in part of glutamatergic neurons as illustrated by the expression of genes for vesicular glutamate transporters like *SLC17A6* (vGlut2) and *SLC17A7* (vGlut1). Furthermore, also ionotropic glutamate receptors, like the NMDA receptor subunit *GRIN1* and *GRIN2B* and AMPA receptor subunits *GRIA2* and *GRIN4,* were detectable. The differentiated and maturated human neuronal cultures on day 42 showed advanced separation of pan-neuronal markers MAP2 (dendritic) and TAU (axonal) by ICC (Figure 9 D). About 77.08 ± 15.42% of the $BDNF^{Val/Val}$ and 85.36 ± 12.36% of the $BDNF^{Met/Met}$ cells were expressing a nuclear signal for the mature neuron marker NeuN (Figure 9 E). Further, neuronal cultures were expressing the cortical layer V/VI markers TBR1 and CTIP2 (Figure 9 D) in similar percentages. In fact, $BDNF^{Val/Val}$ cultures had 75.88 ± 7.52% $TBR1^+$ and 11.87 ± 5.09% $CTIP2^+$ cells and $BDNF^{Met/Met}$ cultures 70.88 ± 11.48% $TBR1^+$ and 14.24 ± 9.49% $CTIP2^+$ (Figure 9 F). However, only a few S100B and GFAP positive cells thus astrocytes were present in the cultures (Figure 9 G).

6.3 Localization of BDNF expression in cortical neurons

There have been various studies examining the localization of BDNF Val66Met in overexpression models (67,84), but no localization studies on an endogenous level on cultured neurons have been conducted, specifically not in a human neuronal context. When GFP-tagged and overexpressed in murine neurons, the $BDNF^{Met/Met}$ variant showed reduced distribution to dendrites and an accumulation in the soma compared to $BDNF^{Val/Val}$. I thus became interested in the distribution of BDNF in our human neuronal cultures.

6.3.1 Human iPSC-derived cortical neurons express BDNF

First, to identify if the neuronal cultures were expressing *BDNF*, quantitative RT-PCR was performed. The mRNA expression levels of *BDNF* increased from the progenitor state to neurons (Figure 10 A). Neuronal cultures around day 42 from all lines used in this study

showed similar *BDNF* expression levels (Figure 10 B). Taking together the expression levels for all BDNF$^{Val/Val}$ neuronal cultures versus the expression level of all BDNF$^{Met/Met}$ neuronal cultures, BDNF$^{Met/Met}$ neurons showed an approximately 0.5-fold increase (Figure 10 C).

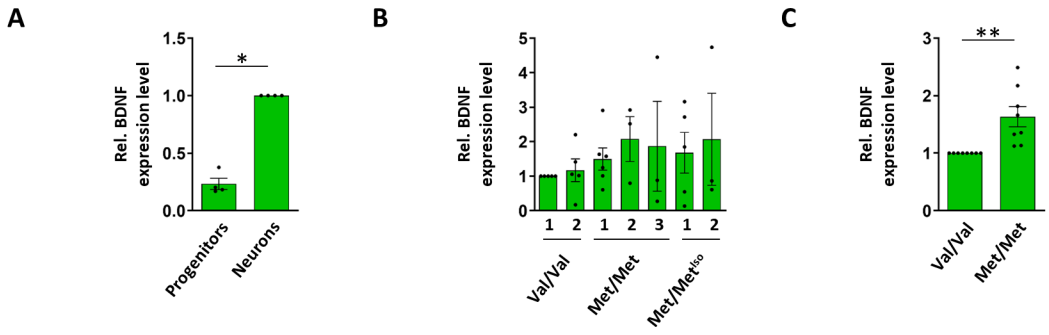

Figure 10: Human iPSC-derived neurons express the BDNF gene

(A - C) Expression levels of *BDNF* measured by quantitative RT-PCR and normalized to *18S* expression levels (A) in progenitors and neuronal cultures day 42, (B) in all lines used in this study on day 42 and (C) in BDNF$^{Val/Val}$ vs BDNF$^{Met/Met}$ neurons day 42 ($n \geq 3$ from three independent experiments, Mann Whitney-U test or Kruskal-Wallis test with Dunn's multiple comparison test; means ± SEM). *$p < 0.05$, **$p < 0.01$

Before looking for protein expression and localization in our neuronal cultures, I validated the BDNF antibody in HEK cells overexpressing HA-tagged BDNF (Figure 11 A). In this model BDNF and HA signals were colocalizing. Furthermore, Western Blot analysis showed a band at 14 kDa for recombinant BDNF as well as a higher band for proBDNF in the neuronal cultures (Figure 11 B).

To analyze the intracellular distribution of BDNF, I performed ICC on BDNF, the dendritic marker MAP2 and the axonal marker TAU on neuronal cultures on day 42. Both BDNF variants showed a punctate signal which was localized in all three compartments, axons, dendrites and soma (Figure 11 C). To look more closely into the BDNF density, I measured the amount of BDNF^{+} puncta per 100 µm in the neurites of BDNF$^{Val/Val}$ and BDNF$^{Met/Met}$ neurons. Quantification showed that the BDNF density was higher on dendrites than on axons in BDNF$^{Val/Val}$ as well as BDNF$^{Met/Met}$ neurons (Figure 11 D). To analyze if the distribution between axons and dendrites was varying depending on the BDNF variant, the number of puncta was calculated in percentages. This distribution of BDNF^{+} puncta didn't differ between BDNF$^{Val/Val}$ (MAP2: 76.21 ± 6.76%, TAU: 23.79 ± 4.10%) and BDNF$^{Met/Met}$ neurites (MAP2: 67.49 ± 4.26%, TAU: 32.5 ± 6.7%) (Figure 11 E).

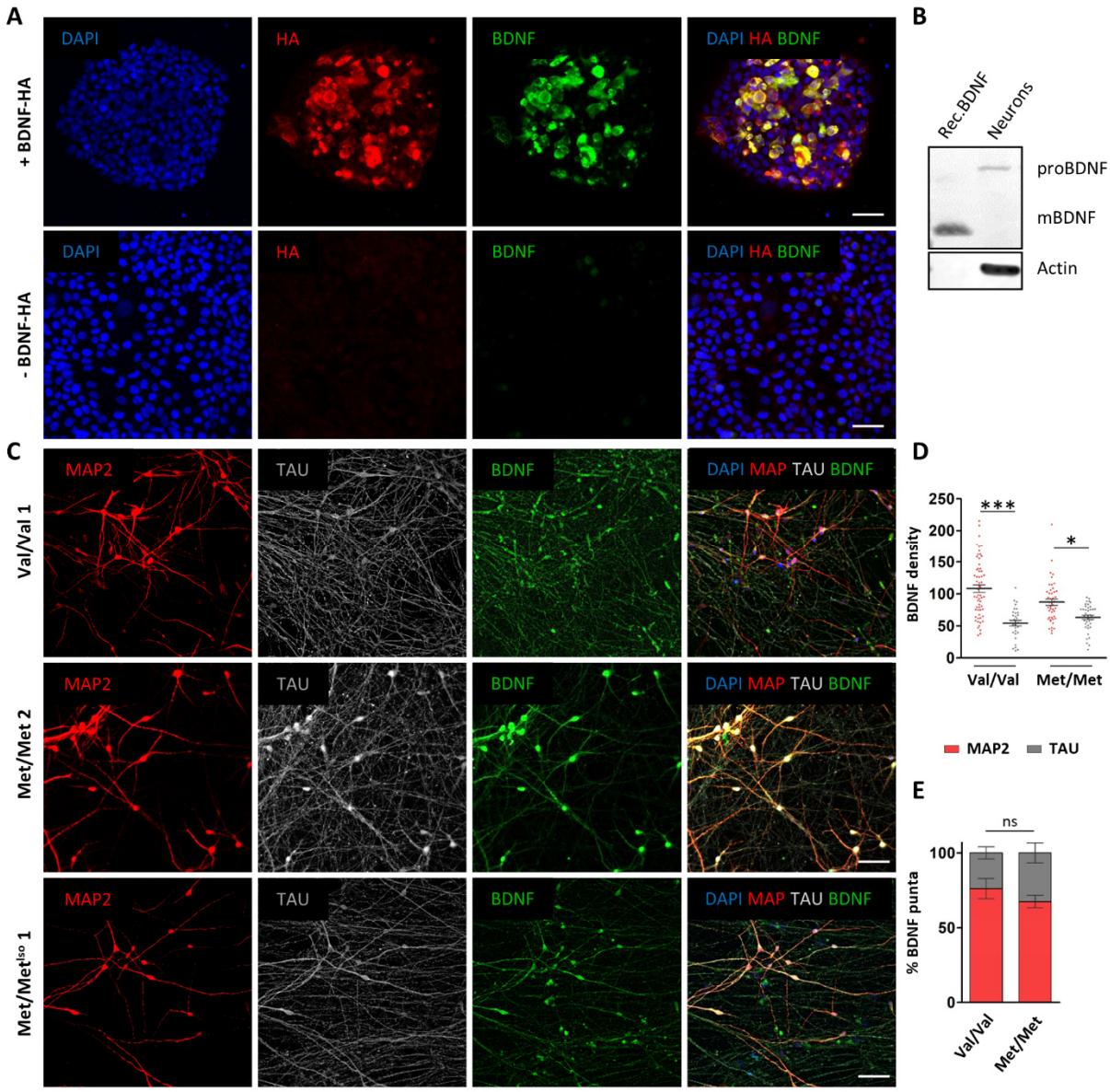

Figure 11: Human iPSC-derived neurons express BDNF on axonal and dendritic structures

(A) ICC of HEK cells overexpressing BDNF-HA for DAPI, HA and BDNF. Scale bars: 50 µm. **(B)** Western Blot of BDNF for recombinant BDNF and in neurons. **(C)** ICC of neuronal cultures for MAP2, TAU and BDNF. Scale bars: 50 µm. **(D)** Quantification of axonal vs dendritic BDNF density ($BDNF^{+}$ puncta per 100 µm length). Summary graphs are shown as merged data of two $BDNF^{Val/Val}$ and two $BDNF^{Met/Met}$ lines (n ≥ 30 per BDNF variant, Mann Whitney-U test; means ± SEM). **(E)** Quantification of the percentage of $BDNF^{+}$ puncta on axonal (TAU) and dendritic (MAP2) structures. Summary graphs are shown as merged data of two $BDNF^{Val/Val}$ and two $BDNF^{Met/Met}$ lines (n ≥ 30 per BDNF variant, Mann Whitney-U test; means ± SEM). *p < 0.05, ***p < 0.001, ns: not significant

Further, I analyzed the localization of the uncleaved proBDNF (Figure 12). The signal was punctuated, but not as extended into the neurites as the mature BDNF signal (Figure 12 A). It was mainly localized at the soma around the nucleus speaking for an ER or Golgi localization. A closer look showed a difference between $BDNF^{Val/Val}$ neurons and $BDNF^{Met/Met}$ neurons. The

proBDNF^{Val} signal was more extended into the neurites compared to proBDNF^{Met} (Figure 12 A').

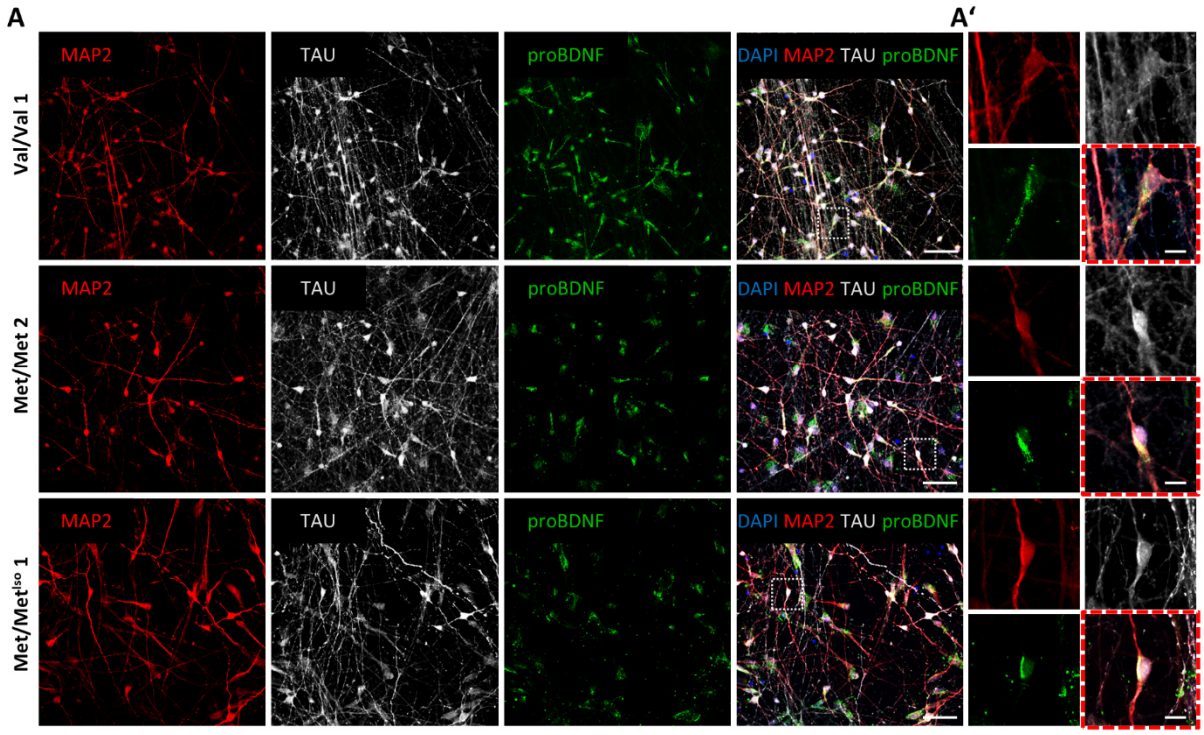

Figure 12: Localization of proBDNF in human iPSC-derived neurons

(A) ICC of neuronal cultures day 42 for dendritic marker MAP2, axonal marker TAU and proBDNF. Scale bars: 50 µm. **(A')** Representative high-magnification images of a soma for MAP, TAU and proBDNF. Scale bars: 10 µm

6.3.2 Reduced BDNF abundance in neurites of BDNF$^{Met/Met}$ neurons

To look more closely into the BDNF density in the neurites, I measured the amount of BDNF^{+} puncta in neurites of BDNF$^{Val/Val}$ and BDNF$^{Met/Met}$ neurons (Figure 13 A). Quantification showed that neuronal cultures exhibit on average between 91.89 ± 13.63 and 130.6 ± 29.71 BDNF^{+} puncta per 100 µm length. Looking at the BDNF density from all individual lines, a trend was visible: BDNF$^{Met/Met}$ neurites showed a decrease in BDNF density in comparison to BDNF$^{Val/Val}$ neurites. This decrease in BDNF was significantly in two BDNF$^{Met/Met}$ lines (Met/Met 1: 100.1 ± 24.40, $p < 0.01$ and Met/Met 3: 91.89 ± 13.63, $p < 0.001$) in comparison to Val/Val 2 (130.6 ± 29.71) (Figure 13 B) and in Met/Met ($p < 0.05$) 3 in comparison to Val/Val 1 (123.1 ± 51.92). Taken together all data of each three lines for a BDNF variant, neurons derived from BDNF$^{Val/Val}$ carriers (122.3 ± 49.85) showed a significant ($p = 0.0009$) higher amount of BDNF^{+} puncta in the neurites in comparison to BDNF$^{Met/Met}$ neurons (100.6 ± 28,68) (Figure 13 C).

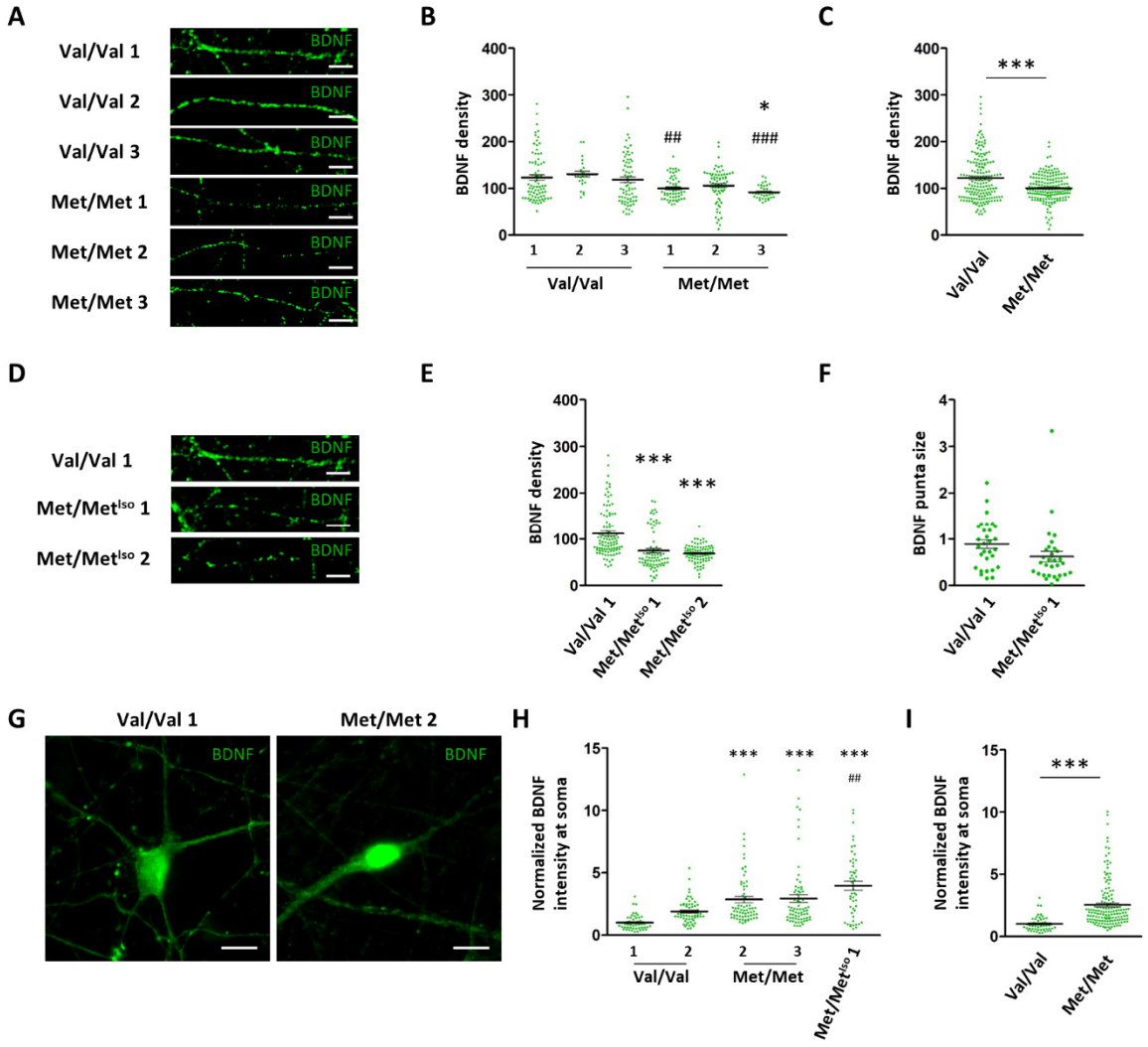

Figure 13: BDNF$^{Met/Met}$ neurons have a decreased amount of BDNF^{+} puncta on neurites

(A, D) Representative high-magnification images of ICC for BDNF in neurites of (A) each three BDNF$^{Val/Val}$ and BDNF$^{Met/Met}$ lines and (D) isogenic lines. Scale bars: 5 µm. **(B)** BDNF density (BDNF^{+} puncta per 100 µm length) in different BDNF$^{Val/Val}$ and BDNF$^{Met/Met}$ lines (n ≥ 25 per cell line, Kruskal-Wallis test with Dunn's multiple comparison test, means ± SEM). **(C)** Summary graph of BDNF density showing merged data of two BDNF$^{Val/Val}$ and two BDNF$^{Met/Met}$ lines (n ≥ 172 per BDNF variant, Mann Whitney-U test, means ± SEM). **(E)** BDNF density of isogenic lines (n ≥ 78 per cell line, Kruskal-Wallis test with Dunn's multiple comparison test, means ± SEM). **(F)** Comparison of BDNF^{+} puncta size between Val/Val 1 and Met/Met^{Iso} 1 (n ≥ 30 per BDNF variant, Mann Whitney-U test, means ± SEM). **(G)** Representative ICC images for BDNF from the soma. Scale bars: 10 µm. **(H)** Normalized BDNF intensity at soma for each line (n ≥ 50 somata per line, Mann Whitney-U test, means ± SEM). **(I)** Summary graph of normalized BDNF intensity at the soma showing merged data of two BDNF$^{Val/Val}$ and three BDNF$^{Met/Met}$ lines (n ≥ 111 somata per BDNF variant, Mann Whitney-U test, means ± SEM). *p < 0.05, **p < 0.01, ***p < 0.001. (B, H) * marks statistical significance in relation to Val/Val 1, # in relation to Val/Val 2

To exclude the impact of the genetic heterogeneity of the different cell lines, the density of BDNF^{+} puncta was additionally analyzed in the isogenic lines (Figure 13 D). Both isogenic

BDNF$^{Met/Met}$ (Met/Met^{Iso} 1: 74.69 ± 43.22, Met/Met^{Iso} 2: 68.79 ± 18.64) lines showed a reduced BDNF density in comparison to Val/Val 1 (123.1 ± 51.92) (Figure 13 E).

The plugin used to analyze the number of puncta takes into account the size of the puncta analyzed, nevertheless to ensure the visible effect was not due to unevenly sized puncta, the puncta size was also measured (Figure 13 F). Surprisingly, BDNF^{Val} puncta had a bigger size in comparison to BDNF^{Met} ones, suggesting that the difference in BDNF density between BDNF$^{Val/Val}$ and BDNF$^{Met/Met}$ neurons could be even higher.

On the one hand, *BDNF* expression was increased in BDNF$^{Met/Met}$ neurons in comparison to BDNF$^{Val/Val}$ (Figure 11), but on the other hand, the BDNF density in the neurites was decreased. So, the question arose if BDNF$^{Met/Met}$ was accumulating in the soma or was being degraded. Therefore, BDNF intensity at the soma was analyzed and normalized to the soma size. The intensity was significantly higher at the soma of BDNF$^{Met/Met}$ neurons (1.00 ± 0.60) in comparison to BDNF$^{Val/Val}$ (2.53 ± 1.88) (Figure 13 G - I).

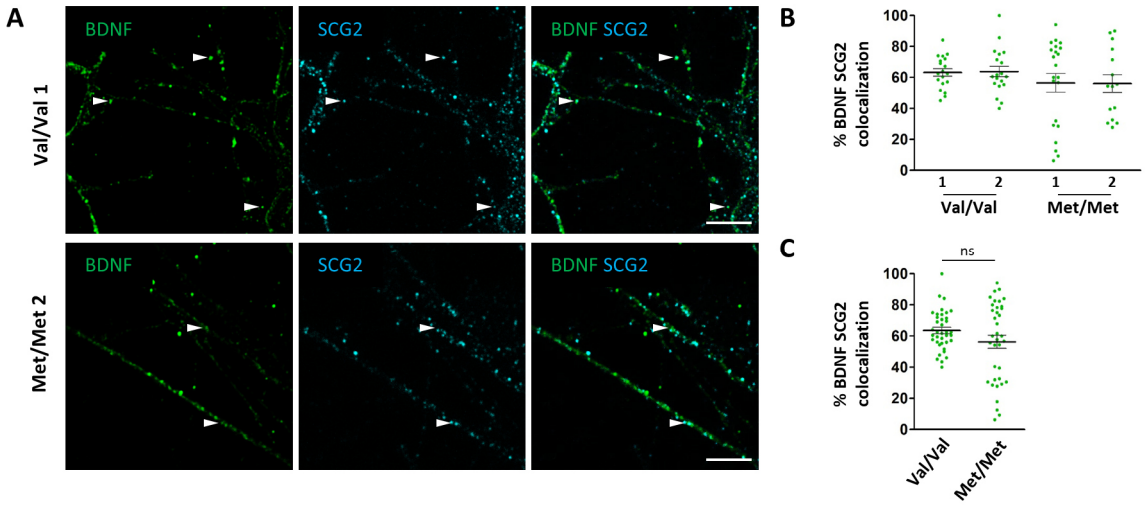

Figure 14: Subcellular localization of BDNF^{Val} and BDNF^{Met}

(A) ICC of neuronal cultures for BDNF and SCG2. Arrows depicting colocalizing signals. Scale bars: 5 µm **(B)** Quantification of the percentage of BDNF/SCG2^{+} puncta in two BDNF$^{Val/Val}$ and two BDNF$^{Met/Met}$ lines (n ≥ 15 per cell line, Kruskal-Wallis test with Dunn's multiple comparison test, means ± SEM). **(C)** Quantification of the percentage of BDNF/SCG2^{+} puncta. Summary graph showing merged data of two BDNF$^{Val/Val}$ and two BDNF$^{Met/Met}$ lines (n ≥ 37 per BDNF variant, Mann Whitney-U test, means ± SEM). ns: not significant

To further look at the subcellular localization of BDNF, I performed ICC for BDNF and the secretory vesicle marker SCG2. Both BDNF variants colocalized partially with SCG2 (Figure 14

A, B). Specifically, BDNF$^{Val/Val}$ neurons had a 63.54 ± 12.65% and BDNF$^{Met/Met}$ neurons 56.31 ± 25.56% of colocalization between both signals (Figure 14 C).

6.3.3 Human iPSC-derived cortical neurons express TrkB receptor

Secreted mature BDNF binds extracellularly with high affinity to the TrkB receptor (33). Therefore, it is important that human iPSC-derived neurons also express this receptor to be sure that BDNF can affect the cells.

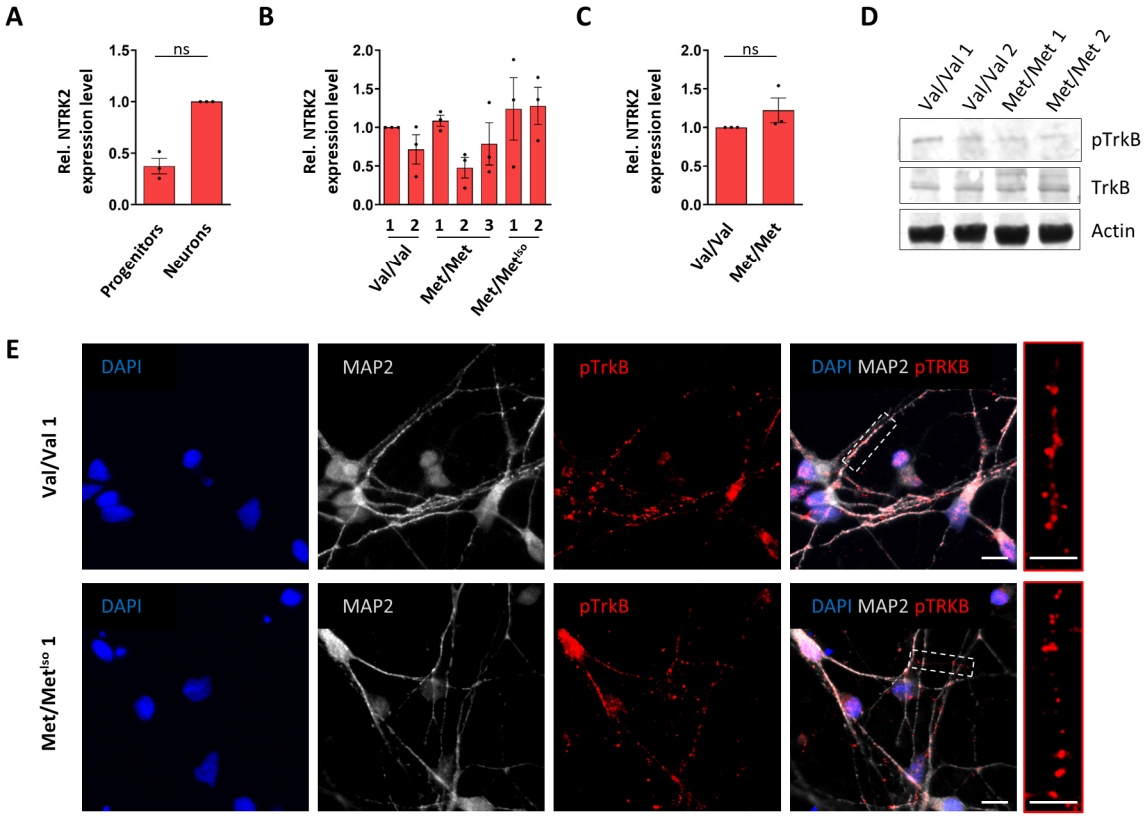

Figure 15: Human iPSC-derived neurons express TrkB receptor

(A - C) Expression levels of *NTRK2* measured by quantitative RT-PCR and normalized to *18S* expression levels (A) in progenitors and neuronal cultures on day 42, (B) in all lines used in this study on day 42 and (C) in BDNF$^{Val/Val}$ vs BDNF$^{Met/Met}$ neurons day 42 (n ≥ 3 from three independent experiments, Mann Whitney-U test or Kruskal-Wallis test with Dunn's multiple comparison test, means ± SEM). **(D)** Western Blots of TrkB, pTrkB and Actin in each of two different BDNF$^{Val/Val}$ and BDNF$^{Met/Met}$ neuronal cultures day 42. **(E)** ICC for phosphorylated TrkB (pTrkB) and MAP2 on neuronal cultures day 42. Scale bars: 10 µm, zoom 5 µm. ns: not significant

Quantitative RT-PCR on progenitors and neuronal cultures on day 42 revealed that the mRNA expression level of *NTRK2* had a trend to increase from progenitor state to more mature

neurons, but it was not significant (Figure 15 A). Comparing $BDNF^{Val/Val}$ to $BDNF^{Met/Met}$ neuronal cultures on day 42, no differences in the mRNA expression level of *NTRK2* were detected (Figure 15 B, C). Next, Western Blot analysis showed that $BDNF^{Val/Val}$ as well as $BDNF^{Met/Met}$ neurons express TrkB receptor and his phosphorylated (thus activated) variant (pTrkB) (Figure 15 D). In parallel, ICC was performed on day 42 old neuronal cultures (Figure 15 E). Val/Val 1 neurons as well as Met/Met^{Iso} 1 neurons showed a punctuated signal for pTrkB which was mainly localized in the neurites.

6.4 Val66Met affects neuronal morphology

To identify cellular processes and pathways affected by the BDNF Val66Met polymorphism, whole transcriptome RNA bulk sequencing of neuronal cultures at 42 was performed. Analysis revealed a total of 814 significantly changed DE transcripts. Of these transcripts, 280 were significantly downregulated and 534 upregulated. GO analysis revealed an enrichment of transcripts whose functions are related to signaling pathways associated with BDNF for example ERK1 and ERK2 cascade, activation of MAPK activity and the regulation of NF-kappaB signaling (Figure 16A). For instance, the ERK pathway is known to influence neurite outgrowth (137), speaking for the enrichment of GO terms like regulation of axon guidance, neuron projection guidance and actin cytoskeleton reorganization (Figure 16 B). Relative expression levels of molecules involved in axon guidance like semaphorins (*SEMA3C*, *SEMA3A*, *SEMA5B*) and ephrins (*EPHA2*, *EPHB4*, *EPHB3*) showed significantly different expression levels between the two neuronal cultures (Figure 16 C).

In the next part, I examined the consequences of the BDNF Val66Met SNP on morphology and neurite complexity on neurons at early (day 1 to 5) and later stages (day 50 to 55) of differentiation.

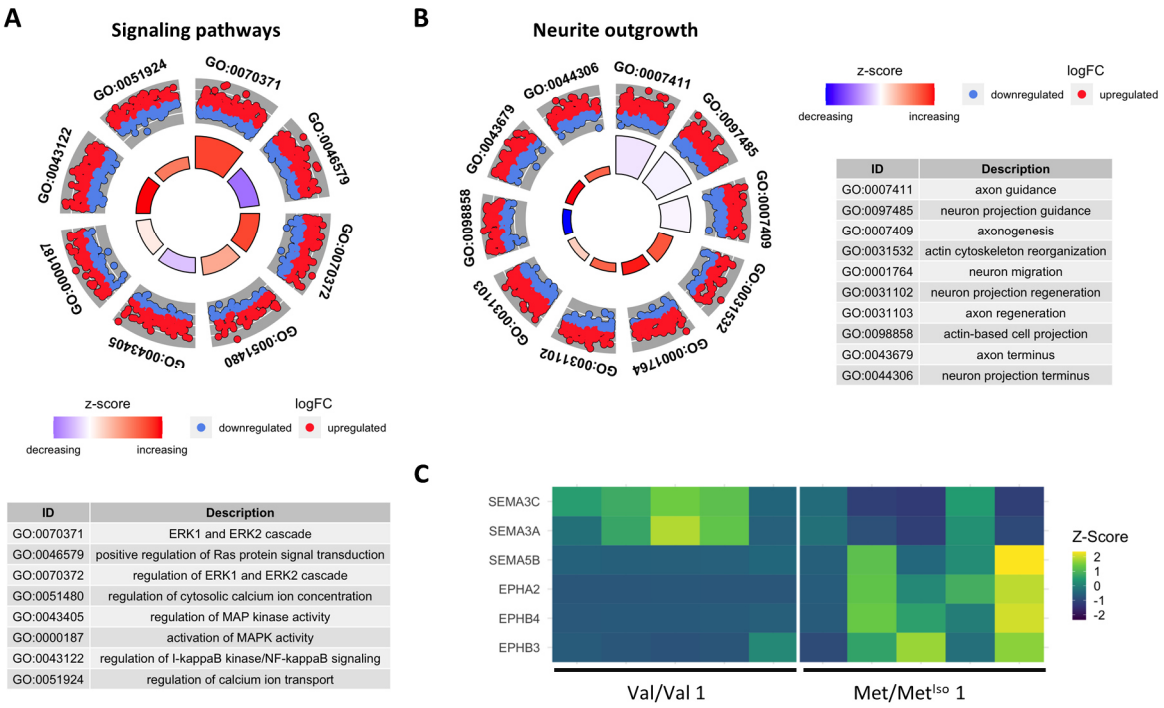

ID	Description
GO:0070371	ERK1 and ERK2 cascade
GO:0046579	positive regulation of Ras protein signal transduction
GO:0070372	regulation of ERK1 and ERK2 cascade
GO:0051480	regulation of cytosolic calcium ion concentration
GO:0043405	regulation of MAP kinase activity
GO:0000187	activation of MAPK activity
GO:0043122	regulation of I-kappaB kinase/NF-kappaB signaling
GO:0051924	regulation of calcium ion transport

ID	Description
GO:0007411	axon guidance
GO:0097485	neuron projection guidance
GO:0007409	axonogenesis
GO:0031532	actin cytoskeleton reorganization
GO:0001764	neuron migration
GO:0031102	neuron projection regeneration
GO:0031103	axon regeneration
GO:0098858	actin-based cell projection
GO:0043679	axon terminus
GO:0044306	neuron projection terminus

Figure 16: Enrichment of GO terms related to neurite outgrowth

(A, B) Circle plot depicting enriched GO terms between Val/Val 1 and Met/Met^{Iso} 1 neuronal cultures related to (A) signaling pathways associated to BDNF and (B) neurite outgrowth. **(C)** Heat map (z-scaled) showing expression of semaphorin and ephrin genes for Val/Val 1 and Met/Met ^{Iso} 1 neuronal cultures.

6.4.1 Reduced neurite outgrowth in neurons expressing BDNF$^{Met/Met}$

To directly compare both Val66Met BDNF variants on human cortical neurite outgrowths, early (day 4) neurons of both variants were trypsinized, seeded in low density and neurite length and branching were quantified at day 1, 3 and 5 (representative reconstructions in Figure 17 A). The analysis showed that all six cell lines grew over time from about 69.7 ± 32.9 to 108.4 ± 44.8 µm on day 1 to 161.0 ± 80.2 to 344.6 ± 127.9 µm on day 5 (Figure 17 B). Already at day 1, some lines showed a reduced length in comparison to others, but no clear differences between BDNF$^{Val/Val}$ and BDNF$^{Met/Met}$ neurons were depicted. On day 5 the changes increased. All three BDNF$^{Val/Val}$ neurons had significantly longer neurites in comparison to each BDNF$^{Met/Met}$ line (Figure 17 C). The number of primary neurons also increased slightly over time, but only in the BDNF$^{Val/Val}$ neurons from 2.2 ± 0.9 to 2.6 ± 1.2 on day 1 to 2.9 ± 0.9 to 3.8 ± 1.2 neurites on day 5. In BDNF$^{Met/Met}$ neurons, the number of primary neurites remained stable (day 1: 2.1 ± 1.0 to 2.4 ± 1, day 5: 2.1 ± 0.7 to 2.5 ± 1.1) (Figure 17 D). Regarding the number of branch points, all cell lines showed almost no branch points (0.3 ± 0.5 to 0.6± 0.9) on day 1. On day 3, the number of branch points had increased in all BDNF$^{Val/Val}$ neurons to

around 1.0 ± 1.0 to 2.0 ± 1.6 branch points and was significantly higher for each line compared to each $BDNF^{Met/Met}$ line (0.5 ± 0.8 to 0.7 ± 1.2). This difference was also visible on day 5. Here, $BDNF^{Val/Val}$ neurons had about 1.4 ± 1.2 to 2.2 ± 1.9 branch points and $BDNF^{Met/Met}$ 0.6 ± 1.1 to 0.8 ± 1.1 (Figure 17 E). Taken together all $BDNF^{Val/Val}$ neurons in comparison to all $BDNF^{Met/Met}$ neurons, the total neurite length was significantly increased at all three quantified timepoints (day 1: $p < 0.001$, day 3: $p < 0.001$, day 5: $p < 0.001$) (Figure 17 F). Specifically, neurite length from $BDNF^{Val/Val}$ neurons increased from 102.3 ± 50.27 µm (day 1) to 288.0 ± 115.3 µm (day 5) compared to the neurite length from $BDNF^{Met/Met}$ neurons which only increased from 91.76 ± 51.15 µm (day 1) to 207.5 ± 107.0 µm (day 5). Primary neurites were significantly decreased (day 1: $p = 0.0034$, day 3: $p < 0.001$, day 5: $p < 0.001$) over all timepoints in $BDNF^{Met/Met}$ neurons in comparison to $BDNF^{Val/Val}$ neurons. Furthermore, while only a few branch points were visible in both genotypes by day 1, neuronal complexity was significantly more elaborated from day 3 (Val/Val: 1.4 ± 1.3, Met/Met: 0.6 ± 1.0). Direct comparison of all neurons derived from $BDNF^{Val/Val}$ lines to all $BDNF^{Met/Met}$ neurons showed a significantly increased number of branch points from day 3 (day 1: ns, day 3: $p < 0.001$, day 5: $p < 0.001$) (Figure 17 F).

The same outgrowth assay was performed on the isogenic lines to directly compare the two *BDNF* genotypes in genetically identical backgrounds (representative reconstructions Figure 18 A). Both isogenic Met/Met^{Iso} lines grew like all other lines over time from 93.3 ± 65.0 µm to 222.2 ± 104.2 µm (Met/Met^{Iso} 1) and from 91.1 ± 49.6 µm to 248.7 ± 110.4 µm (Met/Met^{Iso} 2). Neurons from Met/Met^{Iso} 1 and Met/Met^{Iso} 2 showed significantly reduced total neurite length in comparison to Val/Val 1 from day 1 (day 1: $p < 0.001$, day 3: $p < 0.001$, day 5: $p < 0.001$). The number of primary neurites and branch points was not significant between the lines on day 1. The primary neurites from day 3 Met/Met^{Iso} 1 (0.7 ± 1.0) and Met/Met^{Iso} 2 (0.6 ± 0.9) neurons showed a reduced number of branch points compared to Val/Val 1 (1.2 ± 1.2) reaching half of the branch points at day 5 (Figure 18 B).

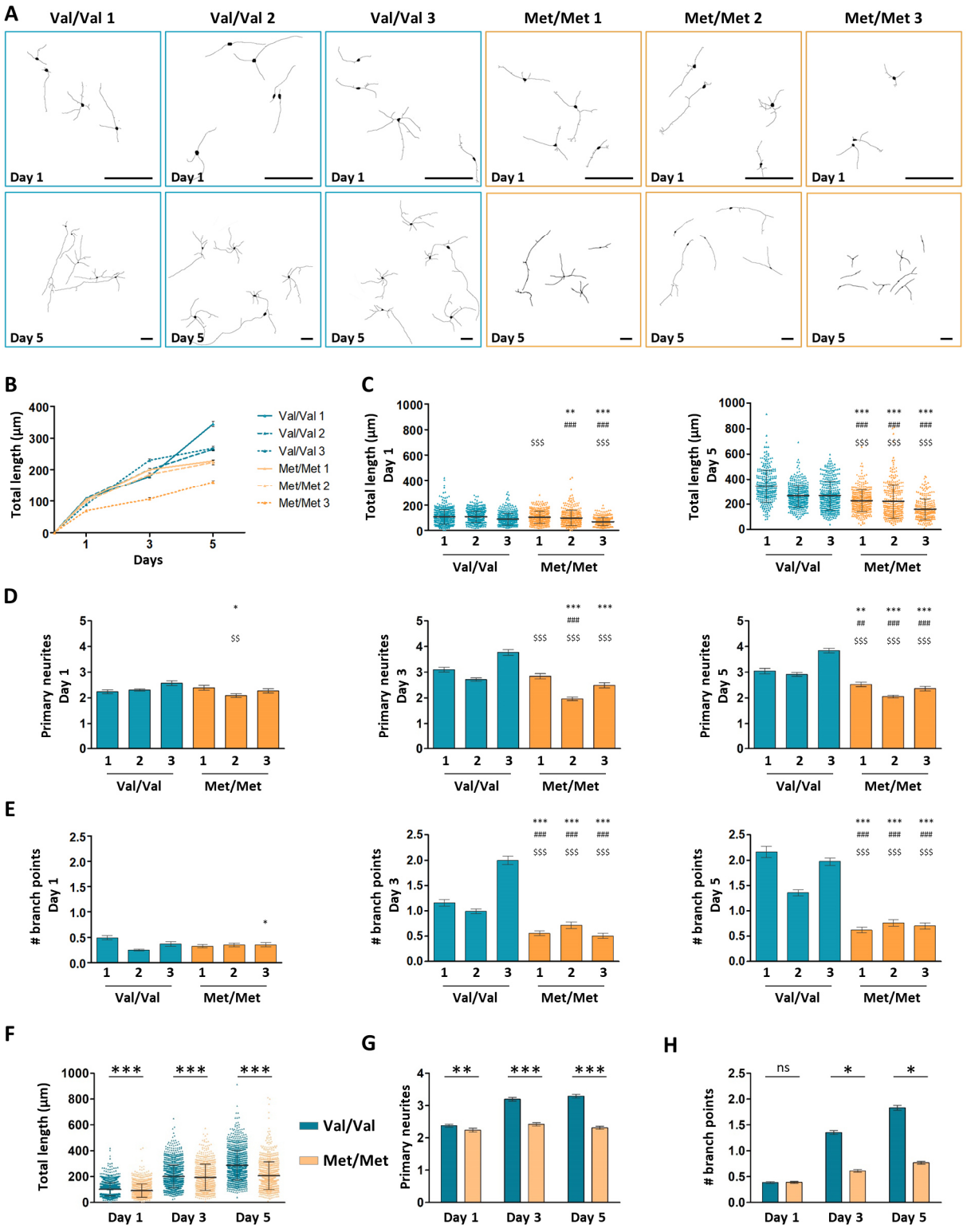

Figure 17: BDNF$^{Met/Met}$ neurons have an altered outgrowth

(A) Representative reconstructions of neuronal cultures used for early outgrowth assay on days 1 and 5 after seeding. Scale bars: 100 µm. **(B)** Total neurite length between day 1 and day 5 after seeding from each three BDNF$^{Val/Val}$ and BDNF$^{Met/Met}$ lines. **(C)** Quantitative analysis of total length from BDNF$^{Val/Val}$ and BDNF$^{Met/Met}$ neurons on days 1 and 5 (n ≥ 263 neurons per cell line from three independent experiments, Mann Whitney-U test; means ± SEM, dot blots: means ± SD). **(D, E)** Quantitative analysis of the number of (D) primary neurites and (E) branch

points from BDNF$^{Val/Val}$ and BDNF$^{Met/Met}$ neurons on days 1, 3 and 5 (n ≥ 126, n ≥ 259 neurons per cell line from three independent experiments, Mann Whitney-U test; means ± SEM). **(F - H)** Quantitative analysis of (F) total neurite length, (G) primary neurites and (H) the number of branch points. Summary graphs are shown as merged data of each three BDNF$^{Val/Val}$ and BDNF$^{Met/Met}$ lines (n ≥ 706, n ≥ 349, n ≥ 1002 neurons per BDNF variant from three independent experiments, Mann Whitney-U test; means ± SEM, dot blots: means ± SD). *p < 0.05, **p < 0.01, ***p < 0.001, ns: not significant. (C -E) * marks statistical significance in relation to Val/Val 1, # marks statistical significance in relation to Val/Val 2 and9 $ marks statistical significance in relation to Val/Val 3

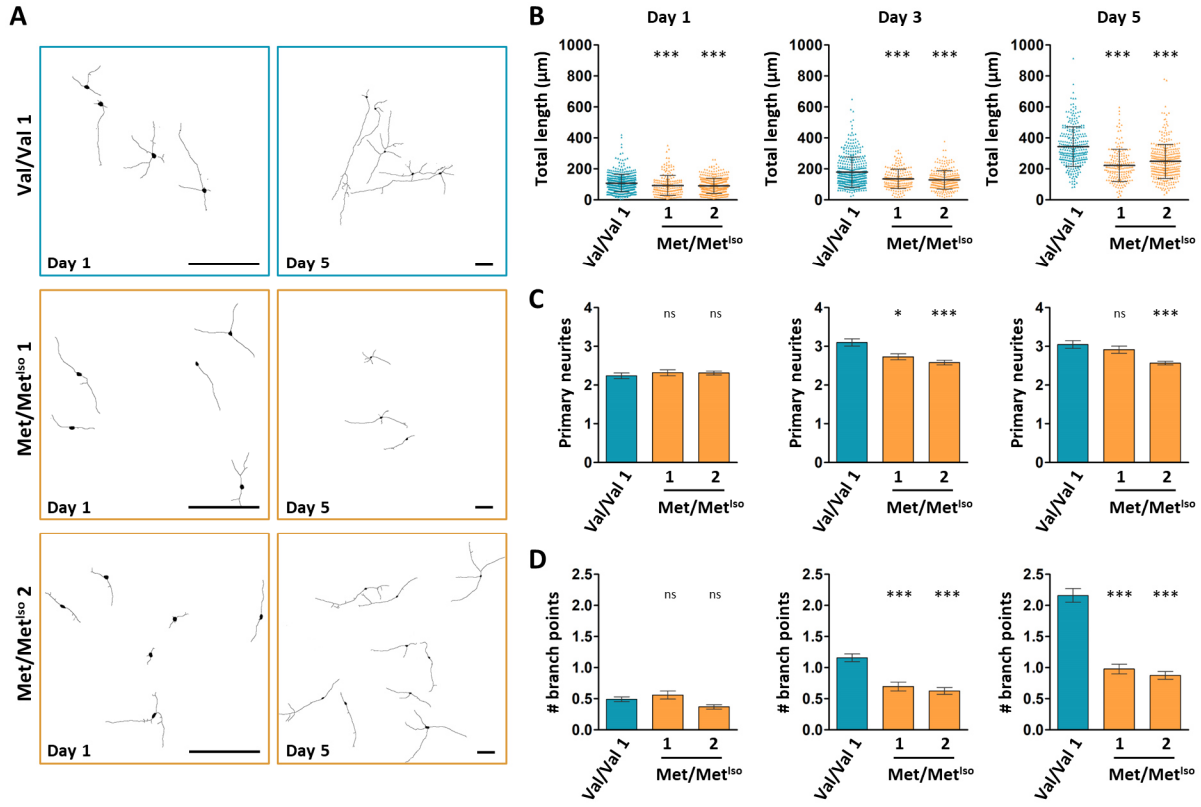

Figure 18: Isogenic BDNF$^{Met/Met}$ neurons have a reduced length and complexity

(A) Representative reconstructions of neuronal cultures used for outgrowth assay from Val/Val 1, Met/Met^{Iso} 1 and Met/Met^{Iso} 2 neurons on days 1 and 5. **(B - D)** Quantitative analysis of (B) total length, (C) primary neurites and (D) the number of branch points in Val/Val 1, Met/Met^{Iso} 1 and Met/Met^{Iso} 2 neurons at day 1, 3 and 5. (n ≥ 186 neurons per cell line from three independent experiments, Mann Whitney-U test; dot blots: means ± SD). *p < 0.05, ***p < 0.001, ns: not significant

To evaluate, whether these differences could be rescued by external application of mature BDNF, the isogenic lines were treated with 10 ng/ml and 20 ng/ml recombinant BDNF (representative reconstructions Figure 19 A). The addition of recombinant BDNF increased neurite outgrowth of BDNF$^{Met/Met}$ neurons in a dose-dependent matter while BDNF$^{Val/Val}$ neurons showed no further enhancement by external BDNF addition. Specifically, total neurite

length of Met/Met^{Iso} 1 neurons increased from 238.6 ± 201.6 µm to 334.5 ± 258.0 µm (10 ng/ml) and to 353.5 ± 353.5 µm (20 ng/ml), reaching the length of untreated Val/Val 1 neurons (354.3 ± 164.1 µm) (Figure 19 B, C). On primary neurites, BDNF didn't have an effect (Figure 19 D). Besides, the number of branch points could be increased in Met/Met^{Iso} 1 neurons with both BDNF concentrations, but not in Val/Val 1 neurons. Specifically, the number of branch points increased from 0.4 ± 0.7 to 0.7 ± 1.2 with 10 ng/ml BDNF and was even duplicated to 1.95 ± 1.45 branch points per neuron with 20 ng/ml BDNF treatment (Figure 19 E).

Taken together, this data suggests that the BDNF Val66Met polymorphism has an effect on early neurite outgrowth in human iPSC-derived cortical neurons leading to reduced neurite outgrowth and branching in BDNF$^{Met/Met}$ neurons. This impairment can be rescued by the external addition of recombinant BDNF in a dose-dependent manner.

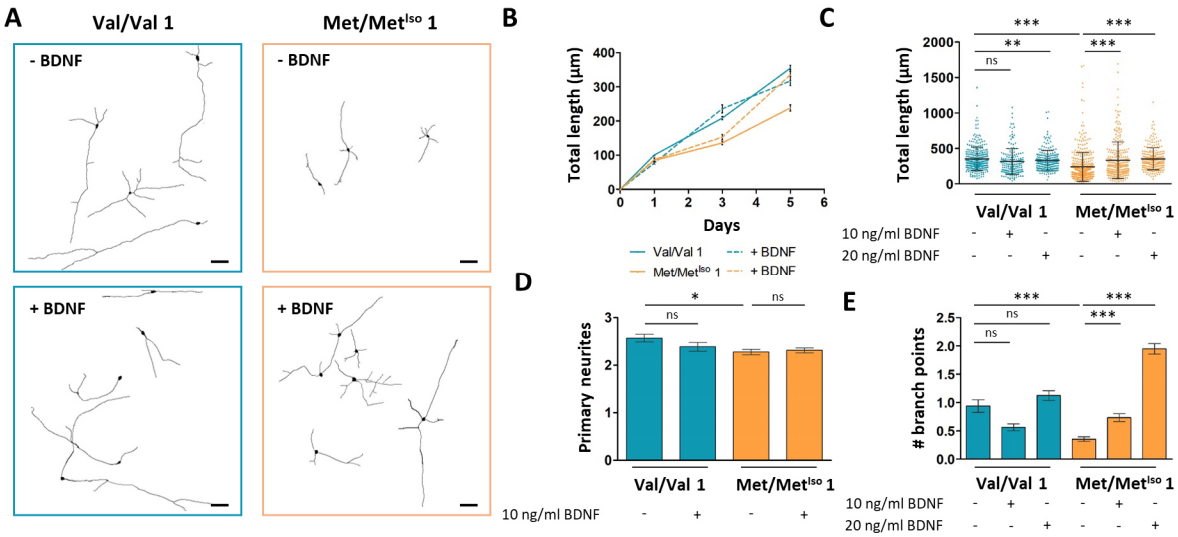

Figure 19: BDNF treatment rescued impaired outgrowth of Met/Met^{Iso} 1 neurons

(A) Representative reconstructions of neuronal cultures used for outgrowth assay from Val/Val 1 and Met/Met^{Iso} 1 at day 5 treated with and without 20 ng/ml BDNF for five days. Scale bars: 100 µm. **(B)** Total neurite length between day 1 and day 5 after seeding from isogenic lines with and without 10 ng/ml BDNF. **(C -E)** Quantitative analysis of (C) total neurite length, (D) primary neurites and (E) the number of branch points with and without BDNF treatment for the isogenic cell lines at day 5 (n ≥ 185 neurons per cell line from three independent experiments, Mann Whitney-U test; means ± SEM; dot blots: means ± SD). *p < 0.05, **p < 0.01, ***p < 0.001, ns: not significant

6.4.2 Reduced neuronal complexity in neurons expressing BDNF$^{Met/Met}$

To further explore, if the effect of Val66Met polymorphism detectable on neurite outgrowth was still present in more mature neurons and to provide additional details of the effects of Val66Met on neurite complexity, neuronal cultures around day 36 were transduced with AAVs coding for mCherry driven by the CamKIIa promotor. Two to three weeks (neurons day 50 to 55) after virus transduction, dense neuronal cultures were fixed and stained to increase the mCherry^{+} signal. Single mCherry^{+} neurons were quantified by Sholl analysis to investigate the neural complexity (representative reconstructions Figure 20 A). Shortly, this analysis quantifies how many neurites intersected a circumference that originated from the soma and increased his radius in steps of 25 µm until a maximal distance of 200 µm.

The course of the Sholl traces was similar between all the lines. At 25 µm all lines showed the highest number of intersections (3.76 ± 2.00 to 6.58 ± 2.80) which decreased with distance (Figure 20 C). Neurons from all three BDNF$^{Met/Met}$ lines showed a decreased number of processes from the soma compared to each BDNF$^{Val/Val}$ line (Val/Val: 6.06 ± 2.56 to 6.58 ± 2.80, Met: 3.76 ± 2.00 to 4.77 ± 2.36). Not only the primary neurites but also the total number of intersections were reduced in all neurons of BDNF$^{Met/Met}$ lines (16.11 ± 6.37 to 18.07 ± 7.25) compared to neurons of BDNF$^{Val/Val}$ lines (29.05 ± 13.30 to 35.27 ± 17.62). This reduction in complexity was also reflected in the total length, where neurons of BDNF$^{Met/Met}$ carriers showed a decreased total length in comparison to BDNF$^{Val/Val}$ neurons (Figure 20 B). Taken all neurons from BDNF$^{Val/Val}$ carriers together versus all neurons from BDNF$^{Met/Met}$ carriers showed the same results (Figure 20 D). Specifically, BDNF$^{Val/Val}$ neurons had on average two more primary neurites than BDNF$^{Met/Met}$ neurons (Val/Val: 6.32 ± 2.69, Met: 4.33 ± 2.22). The increase was even higher looking at the number of total intersections. Here, BDNF$^{Val/Val}$ neurons had even the double amount compared to BDNF$^{Met/Met}$ neurons (Val/Val: 32.16 ± 15.90, Met/Met: 16.84 ± 6.94). This reduction was also present in the total length. BDNF$^{Val/Val}$ neurons were on average twice as long as BDNF$^{Met/Met}$ neurons (Val/Val: 804.0 ± 397.6 µm, Met/Met: 421.0 ± 173.5 µm).

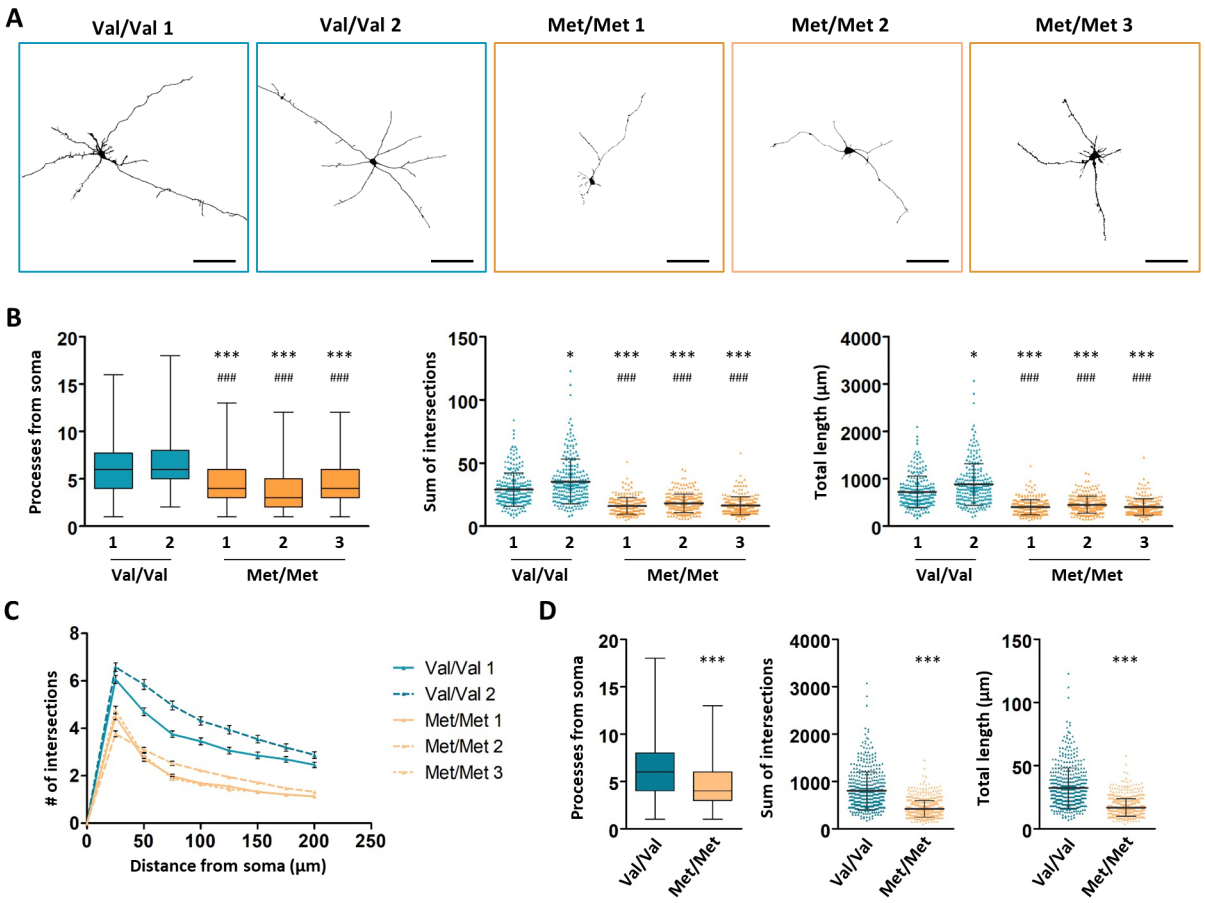

Figure 20: BDNF$^{Met/Met}$ neurons have altered neuronal morphology

(A) Representative reconstructions of CamKIIa-mcherry-transduced neurons with their dendritic arbors around day 55 from BDNF$^{Val/Val}$ and BDNF$^{Met/Met}$ neurons. Scale bars: 100 µm. **(B)** Processes from the soma, sum of intersections and the total length of CamKIIa-mcherry^{+} BDNF$^{Val/Val}$ and BDNF$^{Met/Met}$ neurons. (n ≥ 220 neurons per cell line from three independent experiments, Kruskal-Wallis test with Dunn's multiple comparison test; means ± SD; * marks statistical significance in relation to Val/Val 1, $^{\#}$ marks statistical significance in relation to Val/Val 2). **(C)** Sholl analysis measuring the number of dendritic intersections in 25 µm increments from the soma of two BDNF$^{Val/Val}$ and three BDNF$^{Met/Met}$ lines (means ± SEM). **(D)** Summary graphs of processes from the soma, sum of intersections and total length are shown as merged data of two BDNF$^{Val/Val}$ and three BDNF$^{Met/Met}$ lines (n ≥ 480 neurons per BDNF variant from three independent experiments, Mann Whitney-U test; means ± SD). *p < 0.05, ***p < 0.001

Next, to exclude any effects originating from the heterogenous genomic background of the other lines, Sholl analysis was performed on the isogenic pair. The morphological changes observed before could be recapitulated here (representative reconstructions Figure 21 A). Both lines displayed a similar graph course, having their maximum amount of intersections at a 25 µm distance from the soma (Val/Val 1: 6.06 ± 2.55, Met/Met^{Iso} 1: 5.44 ± 3.12) and then with increasing distance from the soma reducing the number of intersections to 0.96 ± 0.93

for Met/Met^{Iso} 1 and 2.46 ± 1.80 intersections for Val/Val 1 (Figure 21 B). Furthermore, neurons from Met/Met^{Iso} 1 displayed a significantly less sum of total intersections. While Val/Val 1 neurons had on average 29.05 ± 13.30 intersections, Met/Met^{Iso} 1 neurons had only 18.73 ± 10.00. This reduced complexity was also reflected by the total length. Specifically, the neurite length of Met/Met^{Iso} 1 neurons was on average 468.3 ± 250.0 µm in comparison to 726.3 ± 332.5 µm neurite length of the isogenic Val/Val 1 (Figure 21 B).

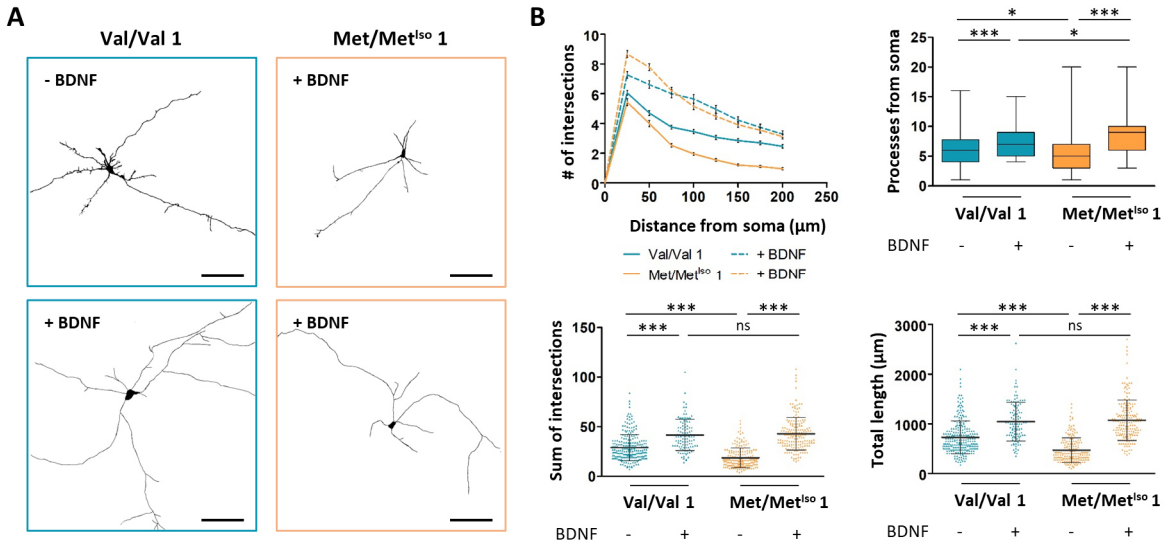

Figure 21: BDNF treatment increases reduced neuronal complexity and length in Met/Met^{Iso} 1 neurons

(A) Representative reconstructions of CamKIIa-mCherry-transduced neurons with their dendritic arbors around day 55 from Val/Val 1 and Met/Met^{Iso} 1 lines with and without 10 ng/ml BDNF treatment. Scale bars: 100 µm. **(B)** Sholl analysis, sum of intersections, processes from the soma and total length of CamKIIa-mCherry^{+} Val/Val 1 and Met/Met^{Iso} 1 neurons with and without 10 ng/ml BDNF treatment (n ≥ 100 neurons per cell line from three independent experiments, Kruskal-Wallis test with Dunn's multiple comparison test; means ± SEM, dot blots: means ± SD). *p < 0.05, ***p < 0.001, ns: not significant

To detect if this phenotype could be rescued, neuronal cultures of both Val66Met BDNF variants were treated with 10 ng/µl endogenous BDNF during the complete differentiation (representative reconstructions Figure 21 B). After treatment, both lines showed an increase in processes from the soma, sum of intersections and total length (Figure 21 B). Specifically, neurons from Met/Met^{Iso} 1 (8.68 ± 3.07) showed even more processes from the soma with BDNF treatment than neurons from Val/Val 1 (7.28 ± 2.31). The number of total intersections in both lines increased from 29.05 ± 13.30 (Val/Val 1) and 18.73 ± 10.00 (Met/Met^{Iso} 1) to about 41.73 ± 15.68 and 42.88 ± 16.37 respectively. The same effect was reflected in the total

length. It was increased from 468.3 ± 250.0 µm (Met/Met^{Iso} 1) and 726.3 ± 332.5 µm (Val/Val 1) to around 1072 ± 409.3 and 1043 ± 392.1 µm correspondingly.

Summing up, the Val66Met polymorphism reduced the complexity and length of neurons carrying BDNF$^{Met/Met}$. The addition of the endogenous BDNF had beneficial effects on neurons of both Val66Met BDNF variants, increasing length and complexity. However, the impact was higher on the Met/Met^{Iso} 1 neurons than on the Val/Val 1 neurons.

6.5 Val66Met affects synaptic transmission

BDNF is crucial for the development, maturation and control of synapses in the adult brain and leads to structural and functional effects (39,40). Here, the activity-dependent neurotrophin is critical for synaptic plasticity (41,42) and is particularly involved in the activity-dependent regulation of the structure and function of glutamatergic synapses (138). Previous studies suggest that the BDNF Val66Met polymorphism affects the abundance of excitatory synapses and neuron function (84). Analysis of the bulk sequencing data revealed enriched GO terms related to neuronal function, including synapse organization, modulation of chemical synaptic transmission, and regulation of trans-synaptic signaling (Figure 22 A). Furthermore, relative expression levels of individual genes associated to pre- and postsynapses as *GRIN2B, SV2B*, *SYN3*, *PCLO*, *DLG2* or *HOMER1* were reduced in Met/Met^{Iso} 1 lines in comparison to Val/Val 1 (Figure 22 B).

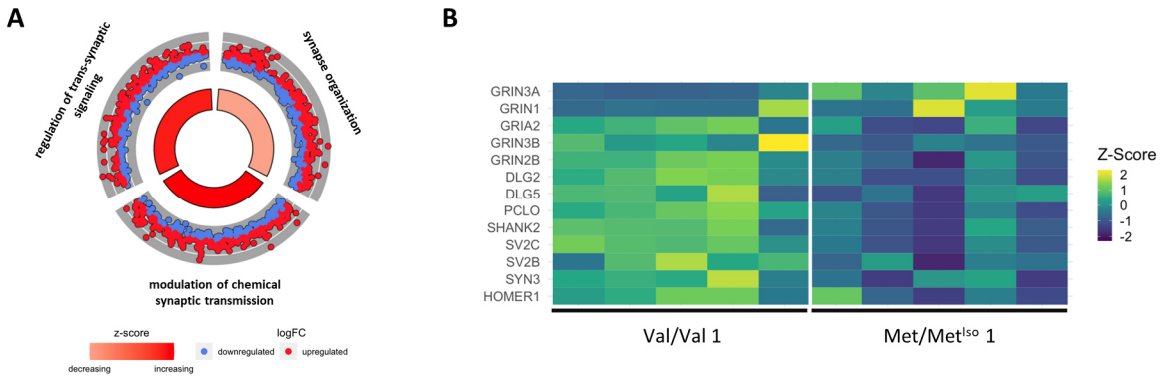

Figure 22: Enrichment of GO terms related to neuronal function

(A) Circle plot depicting enriched GO terms between Val/Val 1 and Met/Met^{Iso} 1 neuronal cultures associated to neuronal function. **(B)** Heat map (z-scaled) showing expression of pre- and postsynaptic genes for Val/Val 1 and Met/Met^{Iso} 1 neuronal cultures.

6.5.1 Reduced synaptic density in BDNF$^{Met/Met}$ neurons

To assess whether synapse development is also affected in human-derived neurons, the expression of the presynaptic protein synapsin (SYN) and postsynaptic density protein 95 (PSD95) were analyzed by ICC in each two lines carrying one Val66Met BDNF variant (Figure 23 A, B). The quantification was done around day 70 of culture to make sure that both signals were detectable, since before that timepoint SYN but not PSD95 signal was present (data not shown). Both signals show a punctuated structure. In general, PSD95^{+} puncta had in comparison to SYN^{+} puncta a smaller size and the density (number of puncta per 100 µm neurite length) was lower. Neurites from Val/Val 2 (91.35 ± 34.11) neurons showed higher SYN density in comparison to each BDNF$^{Met/Met}$ line (Met/Met 2: 61.56 ± 30.37, Met/Met 3: 48.01 ± 24.11). Besides, neurites of Val/Val 1 (65.72 ± 29.46) neurons had only a higher density than neurites of Met/Met 3 (48.01 ± 24.11) neurons. Quantification revealed that neurons of both BDNF$^{Val/Val}$ lines (Val/Val 1: 52.79 ± 38.73, Val/Val 2: 82.00 ± 38.15) had a higher density of PSD95^{+} puncta in comparison to each BDNF$^{Met/Met}$ line (Met/Met 2: 25.96 ± 20.16, Met/Met 3: 28.30 ± 20.55). Furthermore, the density of colocalizing (SYN/PSD95) puncta, representing active synapses, was quantified. In general, this density was much lower than the density of the single proteins. Here, neurons of both BDNF$^{Val/Val}$ (Val/Val 1: 23.33 ± 28.32, Val/Val 2: 13.15 ± 8.56) lines showed an increased density of SYN/PSD95 in comparison to Met/Met 3 (3.62 ± 4.53). The number of colocalizing puncta was not significantly changed between both BDNF$^{Val/Val}$ lines and Met/Met 2 (Figure 23 C).

Next, data of both BDNF$^{Val/Val}$ and both BDNF$^{Met/Met}$ lines were taken together to analyze if there was an even more clear difference between both Val66Met BDNF variants (Figure 23 D). BDNF$^{Val/Val}$ neurons had a significantly higher density of SYN, PSD95 and SYN/PSD95 compared to BDNF$^{Met/Met}$. Neurites of BDNF$^{Val/Val}$ neurons were expressing on average 78.54 ± 34.31 SYN^{+} puncta and neurites of BDNF$^{Met/Met}$ neurons 54.51 ± 28.08 SYN^{+} puncta. Regarding PSD95 density, BDNF$^{Val/Val}$ neurons (67.4 ± 41.07) had over the doble amount than BDNF$^{Met/Met}$ neurons (27.18 ± 20.36). The colocalizing puncta showed a similar distribution as the density of PSD95 (Val/Val: 18.24 ± 21.50, Met/Met: 8.192 ± 10.64).

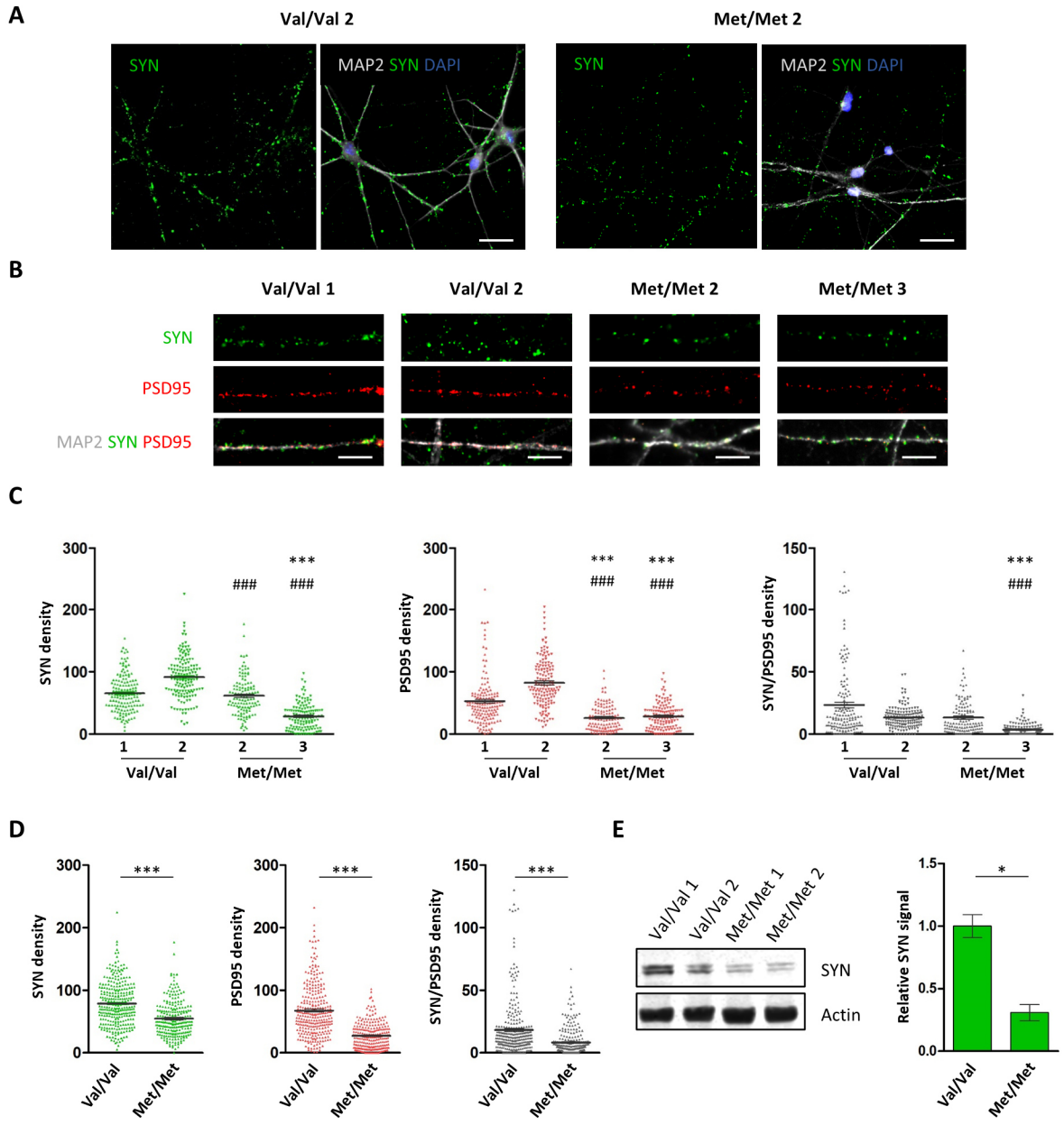

Figure 23: BDNF$^{Met/Met}$ neurons display a reduction in synaptic density

(A) ICC for MAP2, SYN and DAPI of BDNF$^{Val/Val}$ and BDNF$^{Met/Met}$ neuronal cultures day 70. Scale bars: 25 µm. **(B)** High-magnification images of dendrites stained for dendritic marker MAP2, presynaptic marker SYN and postsynaptic marker PSD95 of BDNF$^{Val/Val}$ and BDNF$^{Met/Met}$ lines. Scale bars: 10 µm. **(C)** SYN, PSD95 and SYN/PSD95 density (SYN^{+}, PSD95^{+} and colocalizing (SYN/PSD95^{+}) puncta per 100 µm dendritic length) (n ≥ 120 per cell line from three independent experiments, Kruskal-Wallis test with Dunn's multiple comparison test; means ± SEM; * marks statistical significance in relation to Val/Val 1, $^{\#}$ marks statistical significance in relation to Val/Val 2). **(D)** SYN, PSD95 and SYN/PSD95 density. Summary graphs are shown as merged data of two BDNF$^{Val/Val}$ and two BDNF$^{Met/Met}$ lines (n ≥ 250 per BDNF variant from three independent experiments, Kruskal-Wallis test with Dunn's multiple comparison test; means ± SEM). **(E)** Western Blot against SYN and Actin of BDNF$^{Val/Val}$ and BDNF$^{Met/Met}$ neurons day 42 and respective quantifications (n = 7, Mann Whitney-U test; means ± SEM). *p < 0.05, ***p < 0.001

In parallel, Western Blot analyses were performed to quantify the protein expression levels of different synaptic proteins like SYN, SNAP25 or SV2 (data not shown). According to the ICC quantification, the amount of SYN was also decreased in total protein level in BDNF$^{Met/Met}$ neurons compared to BDNF$^{Val/Val}$ neurons by about 50% (Figure 23 E). The quantification of the other synaptic proteins didn't show a difference between the Val66Met BDNF variants.

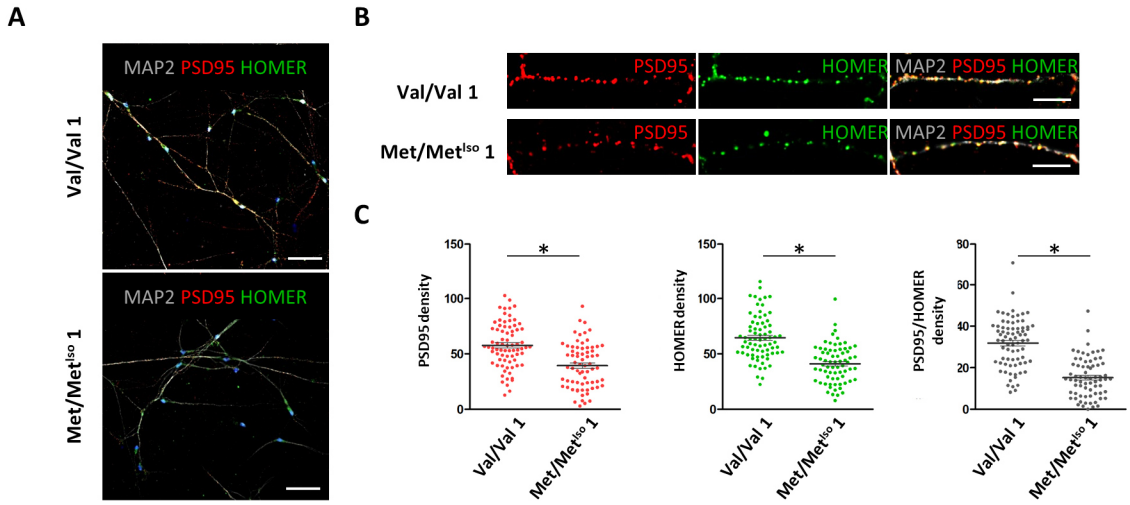

Figure 24: BDNF$^{Met/Met}$ neurons display a reduction in postsynaptic proteins

(A) ICC for MAP2, PSD95, HOMER and DAPI of Val/Val 1 and Met/Met^{Iso} 1 neuronal cultures. Scale bars: 50 µm. **(B)** High-magnification images of dendrites stained for dendritic marker MAP2, postsynaptic markers PSD95 and HOMER. Scale bars: 10 µm. **(C)** PSD95, HOMER and PSD95/HOMER density (PSD95$^+$, HOMER$^+$ and colocalizing (PSD95/HOMER$^+$) puncta per 100 µm dendritic length) (n ≥ 70 per cell line from three independent experiments, Kruskal-Wallis test with Dunn's multiple comparison test; means ± SEM). *p < 0.05

Next, to identify if the reduction in synaptic proteins was also present in an isogenic manner and not due to other genetic players, ICC for PSD95 and HOMER (Figure 24 A, B) as well as for SYN and PSD95 (Figure 25 A, B) was performed at around day 70 neuronal cultures from Val/Val 1 and Met/Met^{Iso} 1. Like the other synaptic markers, the postsynaptic marker HOMER was showing a punctate signal in the neurites. The density of HOMER was comparable to the one of PSD95 in both lines. However, the PSD95 and HOMER density were lower in the Met/Met^{Iso} 1 (PSD95: 39.41 ± 20.33, HOMER: 41.07 ± 17.10) neurons in comparison to the Val/Val 1 (PSD95: 57.74 ± 20.15, HOMER: 64.52 ± 20.12). A reduction was also detectable in the number of colocalizing PSD95/HOMER$^+$ puncta (Figure 24 C). As seen before, PSD95$^+$ puncta appear smaller than SYN$^+$ puncta (Figure 25 B). Quantification of the density showed that Met/Met^{Iso} 1 (42.59 ± 17.36) had on average less SYN$^+$ puncta per 100 µm neurite length

in comparison to Val/Val 1 (65.72 ± 29.46). The density of PSD95 was also reduced in Met/Met^{Iso} 1 neurites compared to Val/Val 1 by about 21.71 ± 30.26 puncta. The density of SYN/PSD95 colocalizing puncta reflected these results, also showing a lower density in Met/Met^{Iso} 1 neurons (12.66 ± 14.35) compared to Val/Val 1 (23.33 ± 28.32) (Figure 25 C).

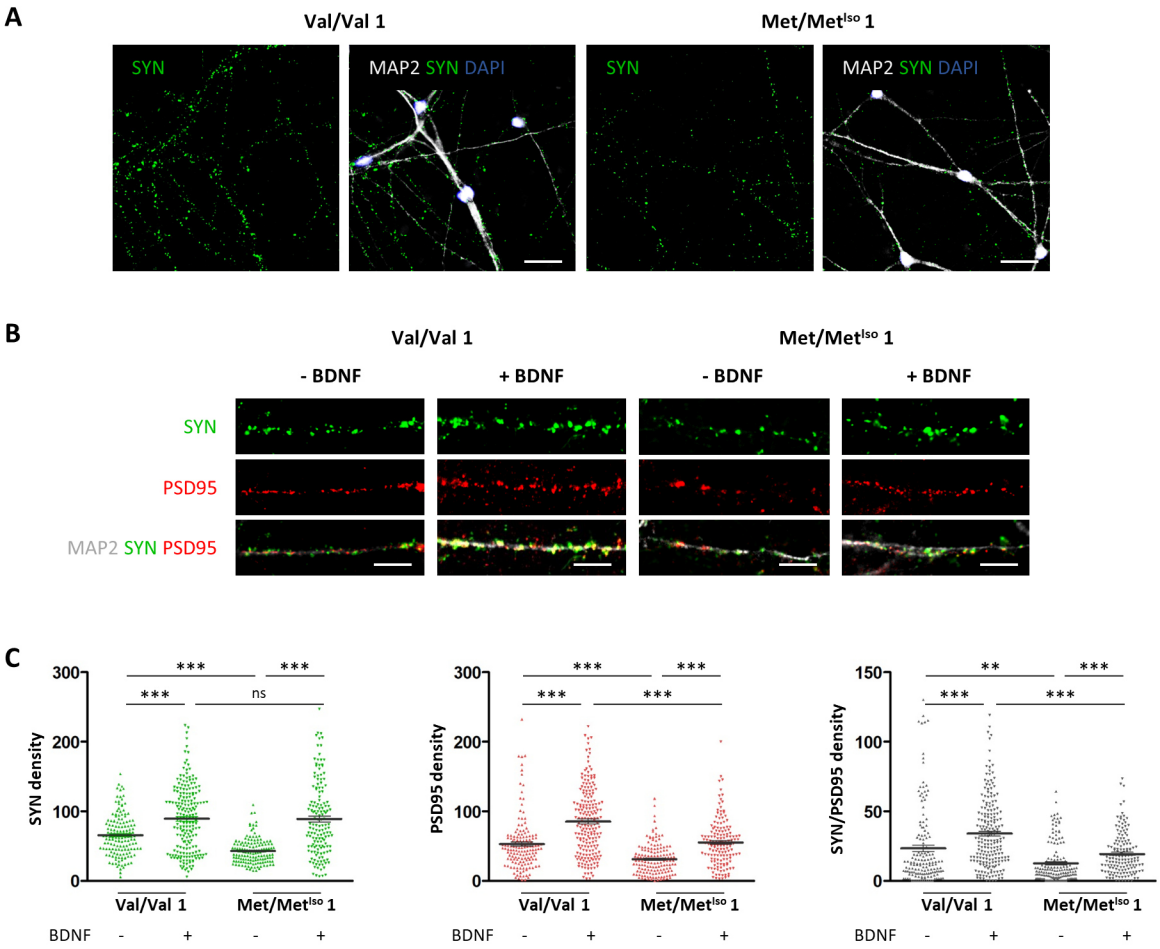

Figure 25: BDNF treatment rescued reduction in synaptic density in Met/Met^{Iso} 1 neurons

(A) ICC for MAP2, SYN and DAPI of Val/Val 1 and Met/Met^{Iso} 1 neuronal cultures. Scale bars: 25 µm. **(B)** High-magnification images of dendrites stained for dendritic marker MAP2, presynaptic marker SYN and postsynaptic marker PSD95 of isogenic lines with and without 20 ng/ml BDNF treatment. Scale bars: 10 µm. **(C)** SYN, PSD95 and SYN/PSD95 density (SYN$^+$, PSD95$^+$ and colocalizing (SYN/PSD95$^+$) puncta per 100 µm dendritic length) (n ≥ 150 per cell line from three independent experiments, Kruskal-Wallis test with Dunn's multiple comparison test; means ± SEM). **p < 0.01, ***p < 0.001, ns: not significant

Further, to detect if exogenous BDNF could rescue this effect, the neuronal cultures were treated for three days with 20 ng/ml BDNF. This led to an increase in the density of SYN, PSD95 and SYN/PSD95 in both lines (Figure 25 C). SYN density increased significantly for the Val/Val

1 and Met/Met^{Iso} 1 neurons to a comparable level of 89.06 ± 46.94 and 88.87 ± 52.96 respectively. The PSD95 density showed an increase of about 32.58 ± 43.52 for Val/Val 1 neurites and from about 23.96 ± 27.58 for Met/Met^{Iso} 1 neurites. However, Met/Met^{Iso} 1 neurons only reached a similar PSD95 density as the untreated Val/Val 1 neurons. This was also the case for the SYN/PSD95 density. Specifically, Val/Val 1 increased it to 33.94 ± 24.98 and Met/Met^{Iso} 1 by 19.37. Thus, the Met/Met^{Iso} 1 neurons had a similar number of colocalizing puncta as the untreated Val/Val 1 neurons.

6.5.2 Excitatory synaptic transmission is impaired in Met/Met^{Iso} 1 neurons

Calcium imaging was performed, since it allows monitoring of large populations of neurons and can visualize the activity modes of individual neurons as well as the synchronous firing of multiple neurons in networks which increases with the synapse density. Therefore, neuronal cultures of Val/Val 1 and Met/Met^{Iso} 1 neurons on day 48 were incubated with Fluro4 dye in 1.8 mM Ca^{2+}, 2.5 mM K^{+} imaging buffer to evaluate the neuronal performance and the neuronal network. Neuronal cultures of both BDNF variants showed random spontaneous Ca^{2+} transients (Figure 26 A). Quantification of Ca^{2+} transients was performed with two different scripts. Scatter plots depicting the amount of Ca^{2+} transients peaks demonstrate the reduced frequency in Met/Met^{Iso} 1 (Figure 26 B). On single-neuron dynamics Val/Val 1 neurons exhibit a increased amplitude of Ca^{2+} transients (Val/Val 1: 0.34 ± 0.10, Met/Met^{Iso} 1: 0.23 ± 0.06) as well as a significantly increased frequency compared to Met/Met^{Iso} 1 neurons (Val/Val 1: 1.02 ± 0.18, Met/Met^{Iso} 1: 0.79 ± 0.21) (Figure 26 C). Regarding the network activity, no differences could be detected in Ca^{2+} transient frequency and synchronization index, only a decreased amplitude in Met/Met^{Iso} 1 neurons (Figure 26 D, E, G). The cross-correlation matrix showed in both lines a low correlation between most of the neurons measured (Figure 26 F).

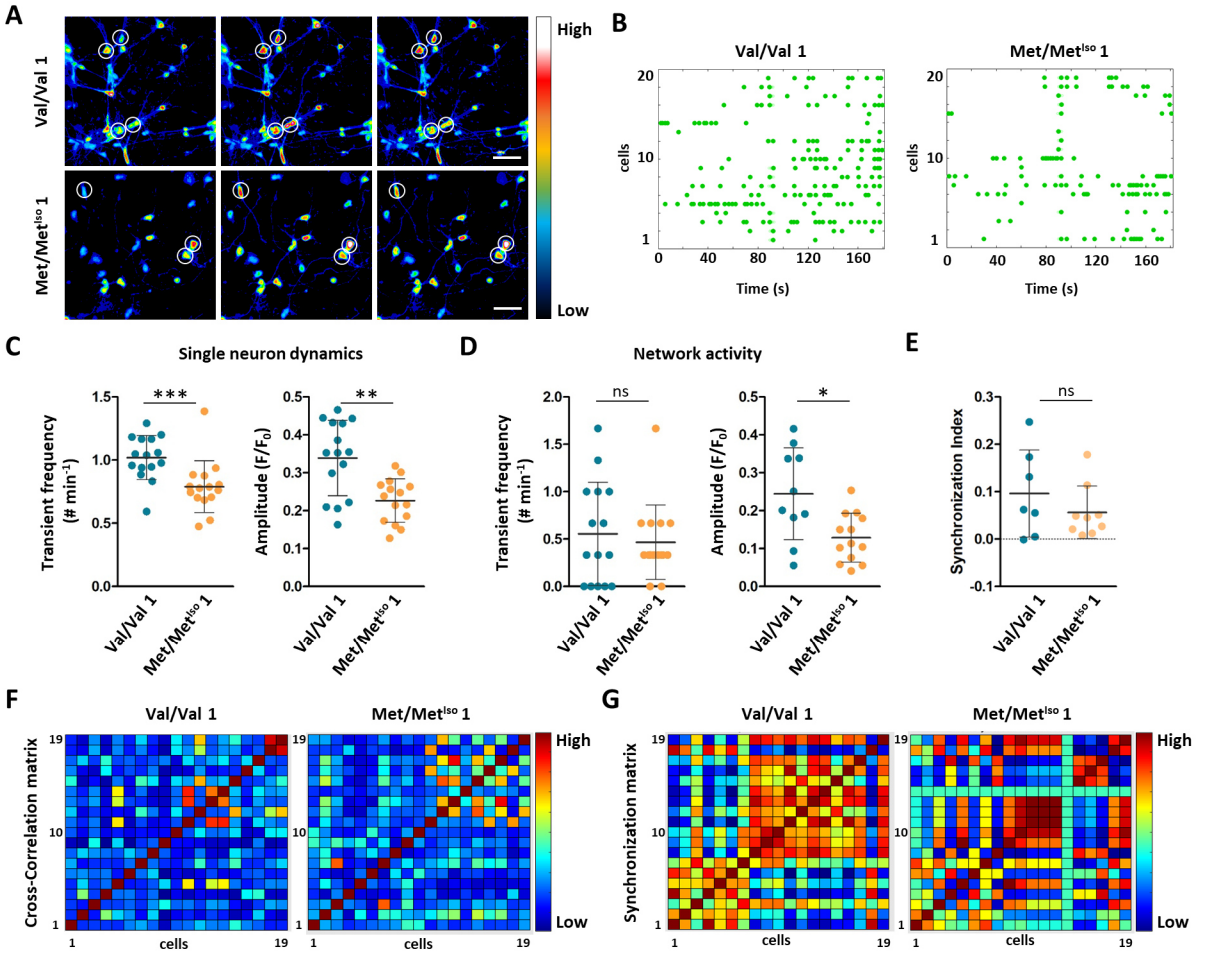

Figure 26: BDNF$^{Met/Met}$ neurons display a reduction in Ca^{2+} transient frequency and amplitude

(A) Fluo-4 depicting Ca^{2+} transients in Val/Val 1 and Met/Met^{Iso} 1 neuronal cultures in 1.8 mM Ca^{2+}, 2.5 mM K^{+} imaging buffer. **(B)** Representative raster plots depicting Ca^{2+} transients. **(C)** Quantification of single-neuron dynamics (transient frequency and amplitude) of Val/Val 1 and Met/Met^{Iso} 1 neuronal cultures around day 48 (n = 15, Mann Whitney-U test; means ± SEM). **(D)** Quantification of network activity (frequency = synchronous firing rate and amplitude) of Val/Val 1 and Met/Met^{Iso} 1 neuronal cultures around day 48 (n ≥ 10, Mann Whitney-U test; means ± SEM). **(E)** Synchronization index of Val/Val 1 and Met/Met^{Iso} 1 neuronal cultures around day 48 (n ≥ 7, Mann Whitney-U test; means ± SEM). **(F)** Representative Cross-Correlation matrix from 20 cells. **(G)** Representative Synchronization matrix from 20 cells. *p < 0.05, **p < 0.01, ***p < 0.001, ns: not significant

Since the neuronal cultures didn't show high network activity, a stimulation buffer (4 mM Ca^{2+}, 8 mM K^{+}) was applied trying to increase the activity and thereby induce synchronicity (Figure 27 A). Indeed, the stimulation buffer tended to increase the synchronous firing rate, which was not significant (Figure 27 D). On a single neuron, dynamic Ca^{2+} transient frequency was not changed (Figure 27 C). Furthermore, the amplitude for single neuron dynamics and network activity had a tendency to decrease. This was only significant in the network activity of Val/Val 1 neurons. In neither single neuron dynamics nor network activity, significant

differences could be detected with stimulation buffer (Figure 27 C, D). The cross-correlation and synchronization matrixes showed a slightly higher amount of neurons with a higher correlation and synchronization compared to the condition in 1.8 mM Ca^{2+}, 2.5 mM K^{+} imaging buffer but not between the lines (Figure 27 E, F).

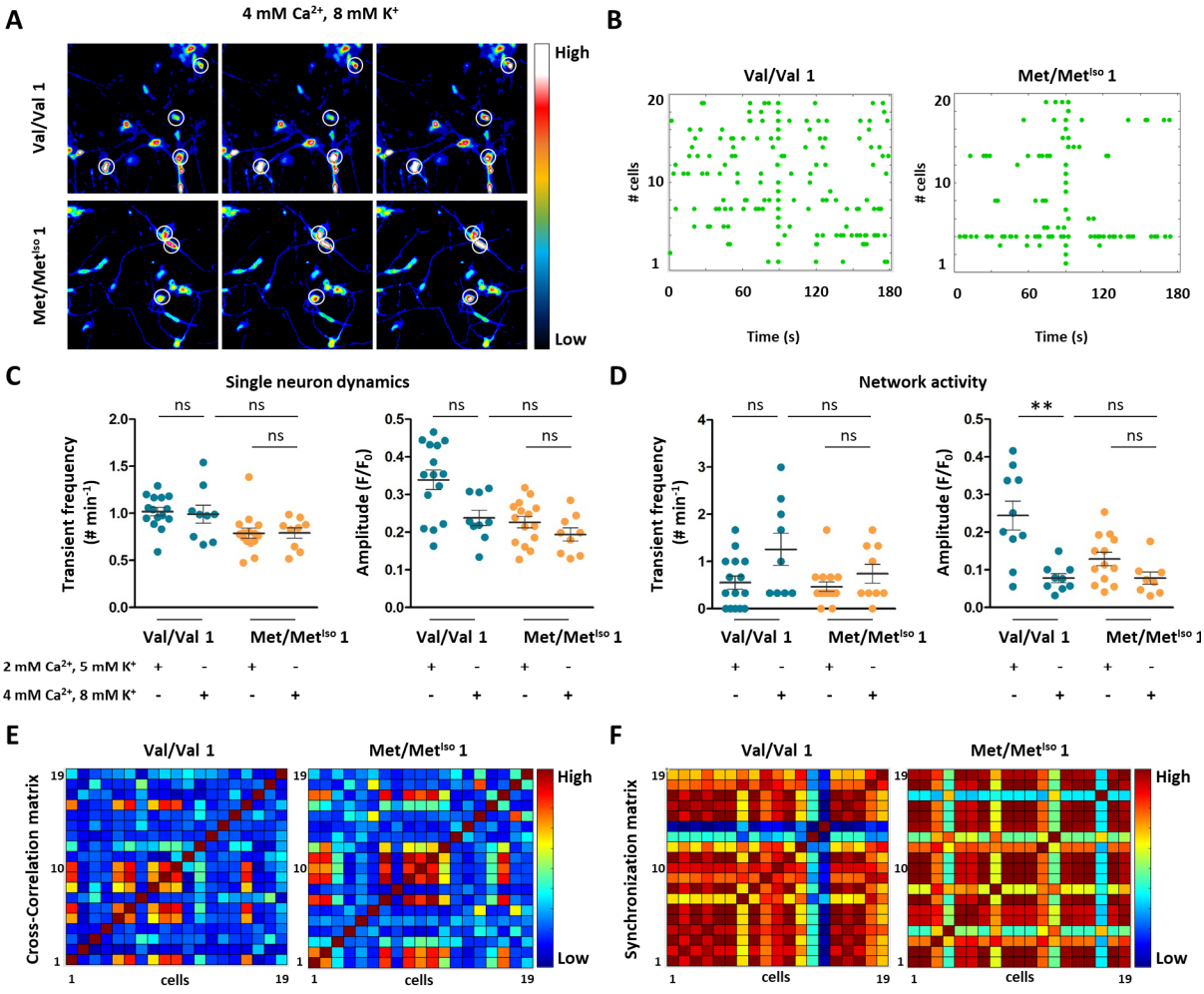

Figure 27: High calcium and potassium tend to increase network activity

(A) Fluo-4 depicting Ca^{2+} transients in Val/Val 1 and Met/Met^{Iso} 1 neuronal cultures in stimulation buffer. **(B)** Scatter plots depicting Ca^{2+} transients in stimulation buffer. **(C)** Quantification of single-neuron dynamics (Ca^{2+} transient frequency and amplitude) of Val/Val 1 and Met/Met^{Iso} 1 neuronal cultures around day 48 in stimulation buffer (n ≥ 9, Kruskal-Wallis test with Dunn's multiple comparison test; means ± SEM). **(D)** Quantification of network activity (synchronous firing rate and amplitude) of Val/Val 1 and Met/Met^{Iso} 1 neuronal cultures around day 48 in stimulation buffer (n ≥ 8, Kruskal-Wallis test with Dunn's multiple comparison test; means ± SEM). ns: not significant

In parallel, the electrophysiological properties were characterized by patch-clamp recordings on single neurons of 50 to 60 days neuronal cultures to test whether the reduced synaptic

density was accompanied by a decreased synaptic function. First, the intrinsic properties of neurons were measured. Neurons did not show a difference in most of the intrinsic properties. They had a similar peak sodium current (Val/Val 1: -2078 ± 306.3 pA, Met/Met^{lso} 1: -1641 ± 214.5 pA) and peak potassium current (Val/Val 1: 1894 ± 242.5 pA, Met/Met^{lso} 1: 1914 ± 242.2 pA) (Figure 28 A). The total number of evoked APs (Val/Val 1: 33.8 ± 3.86, Met/Met^{lso} 1: 36.25 ± 5.64) as well as the amplitude (Val/Val 1: 94.64 ± 4.95 mV, Met/Met^{lso} 1: 91.99 ± 7.34 mV) also didn't differ between the neuronal cultures (Figure 28 B). Only the input resistance was decreased in Met/Met^{lso} 1 (-2.46 ± 0.16 GΩ) neurons compared to Val/Val 1 (-1.89 ± 0.16 GΩ) neurons (Figure 28 C).

Furthermore, sEPSCs were recorded on 50 to 60 days old Val/Val 1 and Met/Met^{lso} 1 neuronal cultures cultivated on astrocytes to asses synaptic activity (Figure 28 D). Consistent with the reduced number of synapses detected by ICC, the frequency of the sEPSCs in Met/Met^{lso} 1 neurons compared to Val/Val 1 neurons was significantly decreased from 1.08 ± 0.30 Hz to 0.37 ± 0.10 Hz (Figure 28 E). The amplitude of sEPSCs didn't show a significant difference (Figure 28 E). Since astrocytes also produce BDNF, the sEPSCs were also measured in neuronal cultures without astrocytes to exclude possible side effects. Met/Met^{lso} 1 neurons (0.92 ± 1.35) tended to have a decreased sEPSCs frequency in comparison to Val/Val 1 (1.71 ± 2.37). In the amplitude, again no differences between the variants could be detected (Figure 28 F).

Next, the cultures were treated with TTX to measure the action potential independent mEPSCs. The mEPSCs frequency had the same trend, namely to be decreased in Met/Met^{lso} 1 neurons (0.68 ± 0.14 Hz) compared to Val/Val 1 neurons (1.12 ± 0.17 Hz) and was even significant decreased compared to Met/Met^{lso} 2 (0.25 ± 0.21 Hz) (Figure 28 G, H). The amplitude was similar between Val/Val 1 and Met/Met^{lso} 1 neurons, but reduced compared to Met/Met^{lso} 2 (Figure 28 G, H).

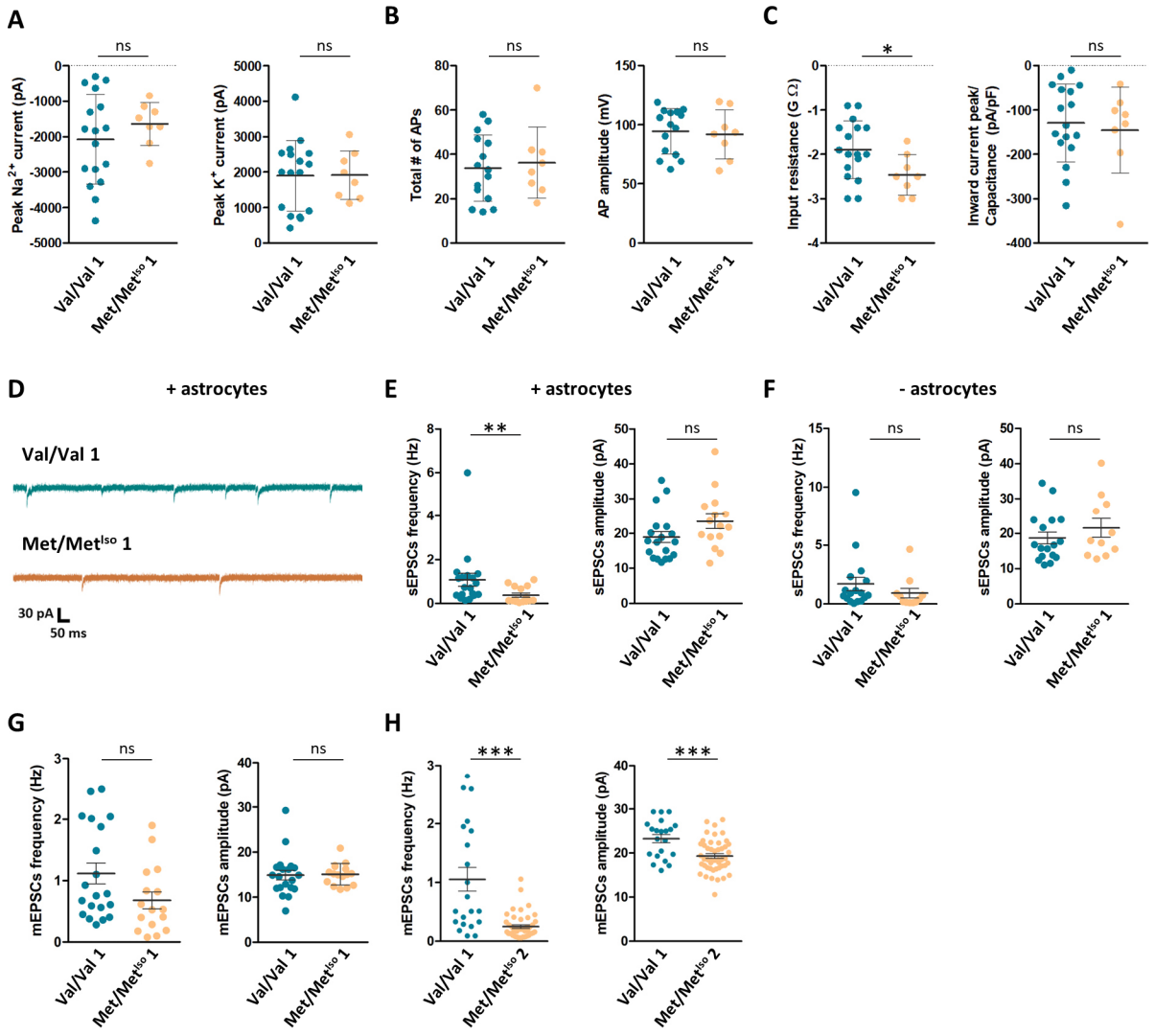

Figure 28: BDNF$^{Met/Met}$ neurons display a reduction in sEPSCs frequency

(A) Peak Na^{2+} and K^{+} currents from Val/Val 1 and Met/Met^{Iso} 1 neurons (n ≥ 8, Mann Whitney-U test; means ± SEM). **(B)** The number of evoked AP and their amplitude (n ≥ 8 neurons, Mann Whitney-U test; means ± SEM). **(C)** Input resistance and inward current peak/ Capacitance (n ≥ 8, Mann Whitney-U test; means ± SEM). **(D)** Representative traces of sEPSCs from Val/Val 1 and Met/Met^{Iso} 1 neurons. **(E, F)** Quantification of the total amount of sEPSC frequency (Hz) and amplitude (pA) from Val/Val 1 and Met/Met^{Iso} 1 neurons cultured (E) with and (F) without astrocytes (n ≥ 11 neurons, Mann Whitney-U test; means ± SEM). **(G, H)** Quantification of mEPSC frequency (Hz) and amplitude (pA) from Val/Val 1 and (G) Met/Met^{Iso} 1 or (H) Met/Met^{Iso} 2 neurons cultured on astrocytes (n ≥ 16 neurons, Mann Whitney-U test; means ± SEM). **p < 0.01, ***p < 0.001, ns: not significant

Since BDNF is particularly involved in the induction and maintenance of LTP (43,44), I also became interested in analyzing the effects on LTP formation and maintenance in the iPSC-derived neuronal cultures. For chemically LTP induction, neuronal cultures were treated for 10 min with 50 µM Forskolin and 0.1 µM Rolipram (Figure 29 A), leading to an increase in

mEPSC frequency in both cell lines, which decreased during the recovery phase again (Figure 29 B). The amplitude was constant over time in both cell lines (Figure 29 C).

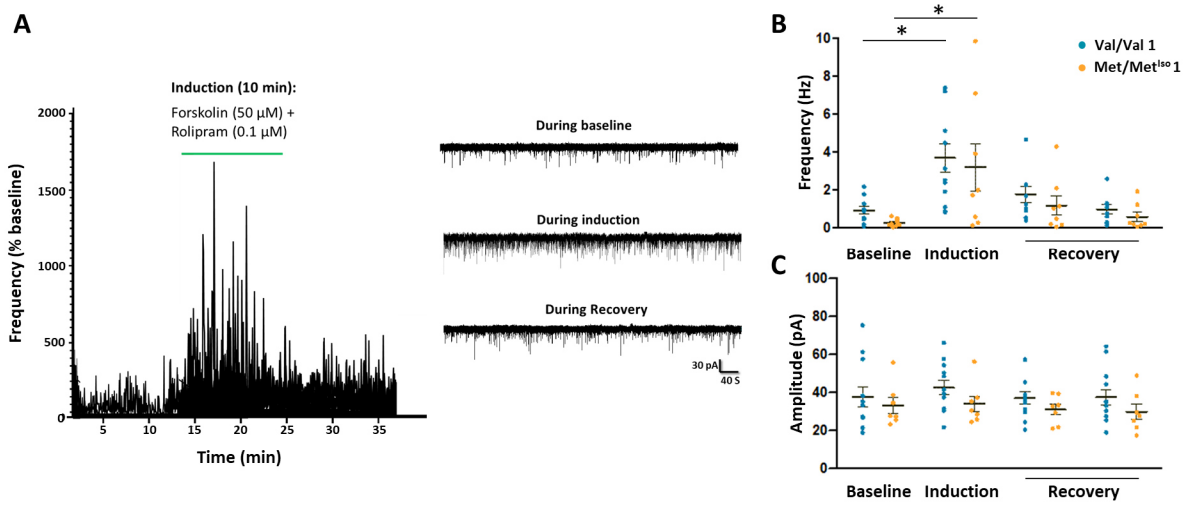

Figure 29: Chemical LTP induction

(A) Induction protocol and representative traces during baseline, induction and recovery from Val/Val 1 and Met/Met^{Iso} 1 neurons. **(B)** Frequency (n ≥ 8 neurons, Kruskal-Wallis test with Dunn's multiple comparison test; means ± SEM) **(C)** Amplitude (n ≥ 8 neurons, Kruskal-Wallis test with Dunn's multiple comparison test; means ± SEM). *p < 0.05

Together, these data show the advanced electrophysiological functionality of the generated iPSC-derived neurons after 50 to 60 days of cultivation with and without astrocytes. Further, the reduction in synaptic density in Met/Met^{Iso} 1 neurons detected by ICC could be recapitulated by electrophysiological experiments.

6.5.3 Reduced density of NDMAR2B in BDNF$^{Met/Met}$ neurons

BDNF regulates the expression and traffic of NMDA receptors, which play an important role in controlling synaptic plasticity (49,139). That is why I became interested if the Val66Met polymorphism also affected NMDA receptors expression and localization.

First, to identify if neuronal cultures were expressing NMDA receptors, quantitative RT-PCR for *GRIN1* and *GRIN2B* on neuronal cultures on day 42 was performed. All cell lines showed expression for *GRIN1* and *GRIN2B*. Interestingly, the mRNA expression levels of *GRIN1* and *GRIN2B* were approximate 2-fold increased in BDNF$^{Val/Val}$ neurons in comparison to BDNF$^{Met/Met}$ neurons (Figure 30 A, B).

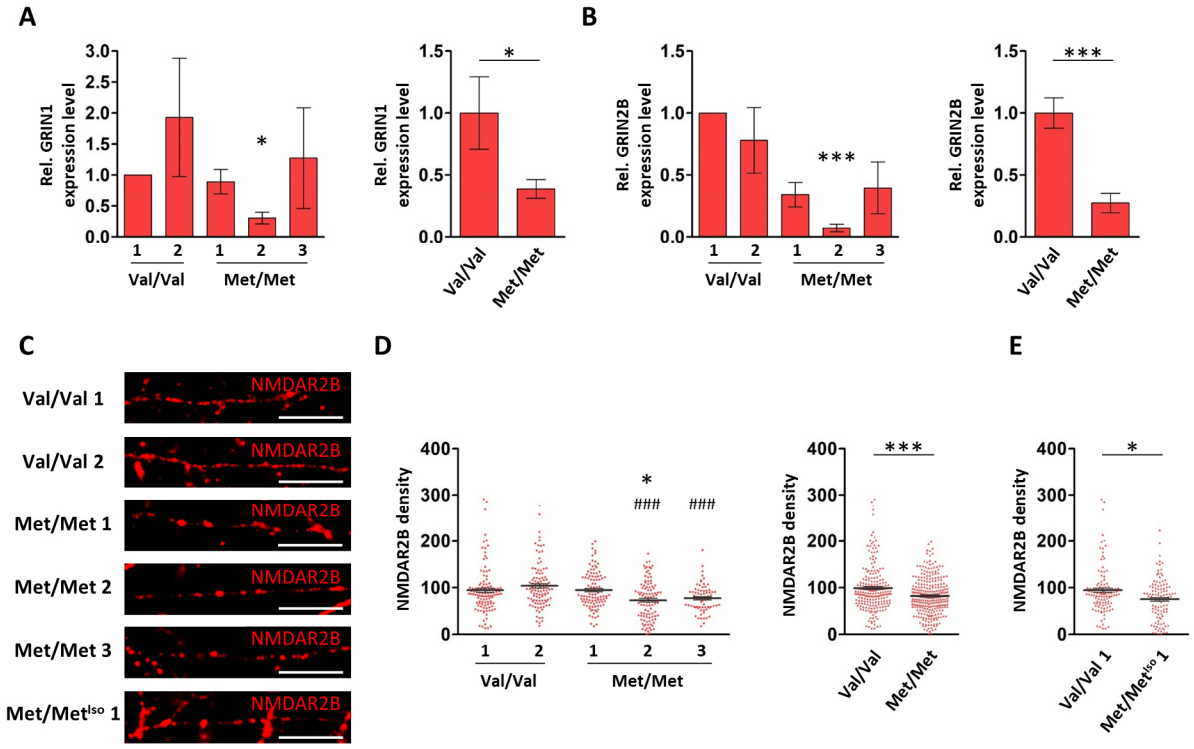

Figure 30: BDNF$^{Met/Met}$ neurons display a reduction in NMDAR2B density

(A) Expression levels of GRIN1 measured by quantitative RT-PCR and normalized to *18S* expression levels in two BDNF$^{Val/Val}$ and three BDNF$^{Met/Met}$ lines on day 42 (n ≥ 4, Kruskal-Wallis test with Dunn's multiple comparison test; means ± SEM) and the corresponding summary graph with merged data (n ≥ 14, Mann Whitney-U test; means ± SEM). **(B)** Expression levels of GRIN2B measured by quantitative RT-PCR and normalized to *18S* expression levels in two BDNF$^{Val/Val}$ and three BDNF$^{Met/Met}$ lines on day 42 (n ≥ 4, Kruskal-Wallis test with Dunn's multiple comparison test; means ± SEM) and the corresponding summary graph with merged data (n ≥ 14, Mann Whitney-U test). **(C)** High-magnification images of dendrites stained for NMDAR2B. Scale bars: 10 µm. **(D)** NMDAR2B density (NMDAR2B$^+$ puncta per 100 µm dendritic length) in different BDNF$^{Val/Val}$ and BDNF$^{Met/Met}$ lines (n ≥ 72 per cell line from three independent experiments, Kruskal-Wallis test with Dunn's multiple comparison test; means ± SEM) and a summary graph of NMDAR2B density showing merged data of two BDNF$^{Val/Val}$ and three BDNF$^{Met/Met}$ lines (n ≥ 218 per cell line from three independent experiments, Mann Whitney-U test; means ± SEM; * marks statistical significance in relation to Val/Val 1, # marks statistical significance in relation to Val/Val 2). **(E)** NMDAR2B density in the isogenic pair (n ≥ 110 per cell line from three independent experiments, Mann Whitney-U test; means ± SEM). *p < 0.05, ***p < 0.001

To detect, if this effect was also visible on protein level, day 42 neurons were stained without permeabilization for membrane-bound NMDAR2B (Figure 30 C), since here the difference in mRNA level was higher. ICC for NMDAR2B showed a punctuate signal in the neurites of the neuronal cultures of all cell lines. For quantification NMDAR2B density (number of $NMDAR2B^{+}$ punta per 100 µm length) was analyzed (Figure 30 D, E). NMDAR2B density from $BDNF^{Val/Val}$ neurons averaged 99.29 ± 49.42 and was significantly increased in comparison to the density in $BDNF^{Met/Met}$ neurons which constituted 82.35 ± 38.59 $NMDAR2B^{+}$ puncta per 100 µm neurite length. This analysis was also performed in the isogenic pair. Here, the result was the same, Val/Val 1 neurons had a density of 94.78 ± 50.79 that was significantly higher than the density of 75.41 ± 44.30 in Met/Met^{Iso} 1 neurons (Figure 30 E).

7 Discussion

7.1 Human iPSC-derived neuronal cultures – a model system to analyze the human-specific BDNF Val66Met polymorphism

A common (30 to 60 % of the population is homozygous or heterozygous) SNP (rs6265, Val66Met) in the *BDNF* gene has been associated since its discovery in 2003 with different psychiatric disorders including bipolar disorder or schizophrenia (91,140). So far, most of the research regarding BDNF and the Val66Met polymorphism has been done in murine models. Thanks to the ability to genetically manipulate mice, they are a powerful tool for examining genetic mechanisms. Consequently, knock-in mice carrying the human *BDNF* gene have been generated leading to the identification of several morphological and functional effects caused by the Val666met polymorphism (83,141). However, animal models have been valuable in elucidating molecular mechanisms and in providing insights into the function of specific genes, but when it comes to translating findings into human therapeutics, they have a poor track record (142,143). Furthermore, a lot of studies regarding the localization, trafficking and sorting of BDNF are based on the over-expression of BDNF in neurons (67,84). Although these studies have their advantages, it is a highly artificial model with an unphysiologically high expression level of BDNF. This can lead to incorrect protein folding or mislocalization of the protein by overwhelming the trafficking machinery. One can also speculate that this could also lead to increased BDNF-dependent cellular mechanism and therefore, misrepresent the physiological activity of the protein of interest in his signaling pathways.

The discovery of iPSCs in 2006 (108) and the resulting opportunities that have been continuously developed since then, have provided an enormous potential to generate and study any type of human tissue like human neurons *in vitro* without using an ethical-controversial embryonic origin (104). Over recent years, many differentiation protocols to generate neuronal cultures of different regionalities have been established and improved. Thus in this thesis, human iPSC-derived neurons were assessed as a potential model system to investigate the human-specific BDNF Val66Met polymorphism, more specifically to study the effects of the polymorphism on BDNF trafficking, morphological alterations, neuronal network formation and function on an endogenous expression level in a human system.

For this purpose, the rs6265 locus in a cohort of iPS cells generated from healthy voluntaries was sequenced and iPSCs from individuals carrying homozygous alleles for either *BDNF*$^{Val/Val}$ or *BDNF*$^{Met/Met}$ were identified. To further directly compare the two *BDNF* genotypes in identical genetic backgrounds, thereby eliminating the impact of secondary genetic variations, isogenic iPSC lines were additionally generated. Here, the coding sequence of *BDNF* Val66 was exchanged to *BDNF* Met66 by CRISPR/Cas9-mediated gene editing. This approach allowed a controlled modification of endogenously expressed BDNF without the need of using large viral expression constructs which can have the disadvantages of random genomic integration and silencing expression by chromatin remodeling during prolonged differentiation processes (144). Furthermore, the risk of analyzing biological artifacts resulting from unphysiological overexpression is eliminated.

BDNF is predominantly expressed by glutamatergic neurons (12) nearly in all brain regions, but especially in the hippocampus and cerebral cortex (6). Besides, it can also be expressed by other cells like astrocytes that are also involved in synapse formation and maintenance which was one of the aspects I was interested in (145). Therefore, for analysis of the effects caused by the Val66Met polymorphism in the previously mentioned iPSC lines, highly pure neuronal cultures of cortical glutamatergic identity are required, to avoid potential side effects caused by other cells. For this purpose, different small molecules like the GSK-3α/β inhibitor CHIR-99021, the CDK4/6 inhibitor PD-0332991 and the γ-secretase inhibitor DAPT were combined to force the progenitors to exit cell cycle and promote the neuronal differentiation (126,127). Independent from the iPSC line used, the generated neuronal cultures of cortical identity, marked by the expression of the cortical layer V/VI transcription factors TBR1 and CTIP2, showed only a few astrocytes, marked by GFAP and S100B, and had a high percentage of neurons expressing NeuN (Figure 9). This indicates that the composition of the human iPSC-derived neuronal cultures used, was comparable independent of the genetic background and therefore further analysis should be practicable.

A milestone to determine if iPSC-derived neuronal cultures could be used as a model system to decipher the effects of the Val66Met polymorphism was to secure that the cultures were expressing BDNF. Indeed this neurotrophin is broadly expressed in the brain but only in very small amounts (1). Furthermore, BDNF is a very small and sticky protein which makes it difficult to detect by Western Blot. The generated neuronal cultures were expressing *BDNF* mRNA showed by PCR and qPCR (Figure 10). Interestingly, BDNF$^{Met/Met}$ neurons showed an

increased *BDNF* expression compared to $BDNF^{Val/Val}$ neurons. The cultures were also expressing proBDNF (Figure 12), as well as mature BDNF on protein level, showed by ICC (Figure 11).

The effect of secreted mature BDNF is first exhibited in presynaptic or postsynaptic neurons by extracellular binding of the protein with a high affinity to TrkB (33). Therefore, I looked for the expression of the receptor in the neuronal cultures. In fact, not only the TrkB receptor but also his phosphorylated and thereby activated form (pTrkB) could be detected, indicating that the neuronal cultures indeed were expressing and secreting BDNF (Figure 15).

All in all, these results showed that it is possible to use an *in vitro* human iPSC-derived model system to study the influence of the BDNF Val66Met polymorphism on human cortical neurons.

7.2 BDNF trafficking – impairments in the sorting of $BDNF^{Met}$

After establishing defined cortical neuronal cultures of different BDNF variants, the next step was to investigate the localization and trafficking of BDNF dependent on the genotype.

Regarding the distribution and secretion sites of BDNF in neurons, there are contradictory findings in the literature. On one hand, it is claimed that BDNF is only present in somatodendritic compartments (146), but on the other hand, publications are indicating that BDNF is found exclusively in nerve endings (10,147,148). However, there are studies asserting that BDNF is transported both anterogradely and retrogradely along axons and dendrites (24,26,27).

Our neuronal cultures reflect the latter. Both BDNF variants showed somatodendritic ($MAP2^+$ structures) as well as an axonal (TAU^+ structures) localization of the mature protein, indicating anterogradely and retrogradely transport of BDNF in the neurons in both BDNF variants (Figure 11). The signal was punctuated for both variants. This is the case since proBDNF/BDNF is sorted into granular vesicles at the trans-Golgi (149). Further, looking in more detail at the distribution of BDNF particles in the axons and dendrites, I started to quantify the BDNF density (number of $BDNF^+$ particles per neurite length) which turned out to be significantly higher in dendrites than in axons in both genetic backgrounds. Thereby the subcellular distribution didn't differ between $BDNF^{Val}$ and $BDNF^{Met}$. These first results were partially contradictory to previous findings, where was claimed that in primary hippocampal neurons

overexpressing one of both variants there is evidence of differences in the subcellular BDNF localization. Precisely, $BDNF^{Met}$ seemed to appear diffused and restricted to the soma whereby $BDNF^{Val}$ was punctuated and extended into dendrites (67,84). However, comparing the total BDNF density in neurites showed a significant decrease of the BDNF density in $BDNF^{Met/Met}$ neurons (100.6 ± 28.68) in comparison to $BDNF^{Val/Val}$ neurons (122.3 ± 49.85) which was also detectable in the isogenic lines (Figure 13). This finding speaks for the restricted intracellular transport caused by the amino acid substitution located in the pro-domain (67,76). Proteins involved in sorting into the secretion vesicles such as sortilin are normally binding to this important region. Due to the mutation, this interaction is impaired and leads to the reduced trafficking of BDNF into the neurites (23,24).

A difference between the so far published studies and the model system I used is that I am looking at endogenous *BDNF* expression and not at an overexpressed construct. That means I have to take into account that the *BDNF* gene has a very complex regulation with alternative promoters, splicing and polyadenylation sites which results in a higher amount of transcripts that can lead to more human BDNF pre-pro-proteins isoforms. One of these regulation steps, the different alternative polyadenylation sites, leads to mRNAs with either a short 3'UTR or long 3'UTR (18). Depending on the UTR type *BDNF* mRNA distribution differs in the neurons. Short 3'UTR *BDNF* mRNA is restricted to the soma while long 3'UTR *BDNF* mRNA is enriched in dendrites of cortical neurons (19). All this complex information for regulation steps gets lost, overexpressing only the CDS of the *BDNF* gene. This may explain the fact that $BDNF^{Met}$ is localized in the neurites of human iPSC-derived cultures and is not limited to the soma. In addition, the trafficking of some and not all *BDNF* transcripts or isoforms may be affected by the Val66Met polymorphism. Future studies need to be performed to elucidate if this is the case.

Further, I addressed the BDNF abundance in the soma. First of all, at the perinuclear localization, the BDNF signal is more concentrated and has a flatter shape that in the neurites. Probably, the structure could be the ER, the site of synthesis of the proBDNF and the Golgi apparatus. Colocalizations of BDNF with markers of the ER and the Golgi apparatus have already been reported (67,150). As single particles couldn't be detected, the overall intensity of the BDNF signal was measured. Indeed, the signal intensity was significantly higher in the somata of $BDNF^{Met/Met}$ neurons, which was also the case in the isogenic $BDNF^{Met/Met}$ line (Figure

13), indicating an accumulation of BDNF in the perinuclear region and thereby impaired trafficking of $BDNF^{Met}$ as already described in other studies.

Dense-core vesicles are involved in neuropeptide storage and secretion at nerve terminals (151). It is assumed that BDNF is transported in this kind of vesicle to the secretion sides (148,152). To analyze that, co-stainings with BDNF and SCG2, a protein involved in sorting into secretory vesicles, were performed. Contradictory to previous studies that couldn't find any colocalization between $BDNF^{Met}$ and SCG2 in primary hippocampal neurons (67), both BDNF variants showed a co-localization with SCG2 which was not significantly different (Figure 14). Interestingly, neurons carrying $BDNF^{Met/Met}$ showed a higher variation in the percentage of colocalizing particles. In detail two clusters, one with a similar percentage of colocalizing particles compared to $BDNF^{Val}$ and one with a decreased percentage could be identified. These two clusters could either be due to axonal versus dendritic differences in BDNF trafficking, or different sorting depending on the different *BDNF* transcripts. It is important to mention, that the investigation of the activity dependent release of BDNF was not possible in the neuronal cultures as the extracellular BDNF concentrations were below the detection level of ELISA sensitivities (data not shown).

Together these data indicate that the BDNF Val66Met polymorphism influences the distribution of $BDNF^{Met}$. Specifically, decreasing the BDNF density in the neurites and accumulating it in the soma. The previously mentioned increased *BDNF* expression in $BDNF^{Met/Met}$ neurons could be a mechanism of the neurons trying to compensate for the impairment in $BDNF^{Met}$ trafficking and therefore maybe also in secretion.

7.3 Neuronal morphology – effects of $BDNF^{Met}$ on neurite complexity and growth

As previously mentioned, secreted BDNF activates the TrkB receptor and is involved in nerve growth through the activation of the MAPK/ERK pathway (137). The effect of BDNF on neurite morphology has already been analyzed in different neuron populations. Particularly, neurite outgrowth and the branching pattern have been often examined. BDNF has been shown to locally regulate dendritic growth in pyramidal cells in the cortex and hippocampus and lead to an increase in dendritic length (153–156). Furthermore, the autocrine BDNF effect is claimed to have an impact on axon development, whereby BDNF promotes axonal outgrowth in cultured rat hippocampal neurons (157). Inhibition of the receptor leads to reduced dendritic

complexity in neurons of the visual cortex (156) and reduced axonal length in hippocampal neurons (157). The Val66Met polymorphism leads to an impaired regulated secretion of $BDNF^{Met}$ (67,76) which makes it interesting to evaluate the morphological alterations caused by the Val66Met polymorphism. Two sets of measurements were performed to analyze the effect on early outgrowth as well as on a later time point of differentiation. Generally, the neurons of both BDNF variants were able to grow and get more complex over time. $BDNF^{Met/Met}$ neurons showed a reduced neurite length as well as a reduced number of primary neurites and branch points in comparison to $BDNF^{Val/Val}$ neurons in the initial phases of development (Figure 17). In addition to BDNF, other factors are involved in nerve growth. For instance, the other members of the neurotrophins such as NGF and NT-3 also have an influence on neurite outgrowth (158–160). Furthermore, other growth factors such as GDNF or IGF (insulin-like growth factors) are associated with axonal growth (161,162). The detected morphological changes could be due to the genotypic-specific characteristics of the lines. Therefore, I validated the influence of the Val66Met polymorphism on the neurite morphology in isogenic lines. Actually, the isogenic pair revealed the same results (Figure 18), indicating that the defects in neurite outgrowth are due to the endogenous BDNF and thereby attributed to the Val66Met polymorphism.

This reduced neuronal complexity was persistent up to later stages of development where neuronal cultures around day 50 to 60 carrying $BDNF^{Met/Met}$ displayed fewer intersections, primary neurites and a reduced total length measured by Sholl analysis (Figure 20). These results confirmed previous studies analyzing primary cultures of hippocampal neurons that showed that transfected $BDNF^{Met}$ leads to reduced growth, as well as less branching of dendrites in comparison to $BDNF^{Val}$ (84). The reduced complexity can be correlated with previous findings showing reduced hippocampal volumes in humans and rodents of $BDNF^{Met/Met}$ carrier (67,82,86,163). Reduced volume of various brain regions has also been observed in patients suffering from neuropsychiatric disorders like major depression, schizophrenia or bipolar disorder (58,59). In particular, lower hippocampal volume in patients with bipolar disorder has been correlated to Val66Met polymorphism (93,94).

The deficit in early neurite outgrowth in $BDNF^{Met/Met}$ neurons could be rescued and even increased in comparison to $BDNF^{Val/Val}$ neurons by external addition of recombinant BDNF in a dose-dependent manner (Figure 19). Surprisingly, $BDNF^{Val/Val}$ neurons were not affected by the addition of recombinant BDNF neither in length nor in branching. One potential

explanation may be that the TrkB receptors are saturated by the autocrine-secreted BDNF and an increased amount of available BDNF isn't able to activate more TrkB receptors. Second, BDNF can also lead to dendritic instability and branching limitation (164) and thereby leading to a stable state regarding length and branching. Interestingly, long-term BDNF treatment (during complete differentiation) leads to an increase in complexity in neurons of both BDNF variants (Figure 21). This suggests that at later stages of differentiation eventually less BDNF is secreted by the neurons and thereby the addition of external BDNF still can bind and activate TrkB receptors in $BDNF^{Val/Val}$ neurons or a higher amount of TrkB receptor is expressed leading to an increase in length and branching. Furthermore, neurons of both BDNF variants reached a similar length and total amount of intersection speaking for a saturation of the TrkB receptor.

To conclude, the human iPSC-derived neurons from $BDNF^{Met/Met}$ carrier displayed an impaired early outgrowth. The reduced dendritic complexity endures until later development stages with more mature neurons and can be rescued by exogenous BDNF treatment. Gene expression studies support this observation as many axonal outgrowth and guidance genes show differential expression in the neuronal cultures.

7.4 Synaptic transmission – functional consequences of $BDNF^{Met}$

Altered neuron morphology is likely to affect neuron function. Furthermore, BDNF is crucial in the development, maturation and control of synapses in the adult brain and leads to structural and functional effects (39,40). Especially, in the activity-dependent regulation of the structure and function of glutamatergic synapses, neurotrophin signaling plays a role (45). Therefore, I was interested, in whether functional effects caused by the polymorphism also could be detected in human iPSC-derived neuronal cultures. For that, the neuronal cultures were differentiated for 60 to 80 days to ensure mature neurons with robust synaptogenesis even in the absence of astrocytes. $BDNF^{Met/Met}$ neurons showed a reduced synapse density (identified by the co-localization of presynaptic SYN and postsynaptic PSD95), indicating a reduced total number of synapses (Figure 23). In line with the identified differences, comparative gene expression shows several synaptic proteins associated to vesicle release and postsynaptic density proteins to be differentially expressed in both genotypes. Consistently, previous studies have shown that overexpressed $BDNF^{Met}$-GFP in contrast to $BDNF^{Val}$-GFP reduces the

abundance of excitatory synapses (84). Exposure to exogenous BDNF was able to increase synaptic density in both genotypes (Figure 25), underlying once again the ability of the neuronal cultures to respond to external BDNF treatment.

To further analyze the connectivity of the cultures, calcium imaging with Fluro4 dye at day 48 neuronal cultures of $BDNF^{Val/Val}$ and $BDNF^{Met/Met}$ was performed. Even if this approach does not have the resolution and depth of more refined methods, such as patch-clamp electrophysiology, it allows the monitoring of large populations of neurons and can visualize the activity modes of individual neurons without the need for advanced instrumentation that may not be available. Furthermore, the synchronous firing of multiple neurons in networks can be detected and analyzed. Calcium imaging allows statements about a variety of neuronal properties in cultured neurons like developmental maturity or synaptic connectivity based on the firing pattern (165,166). The quantification was performed based on two only recent published methods that enables scalable analyses of single-neuron dynamics and network activity (167,168).

Under standard conditions (1.8 mM Ca^{2+}, 2.5 mM K^{+}) cortical neurons showed random calcium transients in cultures of both BDNF variants, indicating that the cultures were active. The reduced synapse density measured by ICC could be correlated to calcium imaging results. Specifically, $BDNF^{Val/Val}$ neurons exhibit an increased calcium transients frequency, but no differences in amplitude in comparison to $BDNF^{Met/Met}$ neurons (Figure 26), indicating a reduced synaptic transmission in $BDNF^{Met/Met}$ neurons. Previous studies have shown that BDNF rises Ca^{2+} concentration in the cell by releasing it from IP_3-gated stores (169). Regarding network activity, no differences could be detected between the lines. Therefore, calcium imaging was also performed with a stimulation buffer (4 mM Ca^{2+}, 8 mM K^{+}) trying to stimulate the cultures and thereby increase network events (Figure 27). Indeed, calcium transient frequency was increased under this condition and the amplitude decreased, displaying a trend towards functional differences of BDNF variants. The reason that the neuronal cultures didn't show a high amount of burst and synchronous firing can be due to several facts. Actually, not only synaptic density influences network connectivity but also dendritic and axonal development as well as the overall cellular state of the single neurons (165,166).

To further analyze if the synaptic transmission and neuronal excitability of the cultures were affected by the Val66Met polymorphism, patch-clamp recordings were performed (Figure 28). Intrinsic properties, like peak Na^{+} current and peak K^{+} current, didn't show any differences

between $BDNF^{Val/Val}$ and $BDNF^{Met/Met}$ neurons. Furthermore, the neuronal cultures showed a similar amount of evoked action potentials (APs). Overall, these results indicate comparable neuronal excitability of the neurons. However, the Val66Met polymorphism affects the baseline synaptic function, which can be seen based on the decreased frequency of baseline sEPSCs and mEPSCs in $BDNF^{Met/Met}$ neurons underlying the impaired synaptic density shown by ICC. In line with that, the addition of BDNF increases rapidly spontaneous firing rate as well as the frequency and amplitude of EPSC (170). Furthermore, previous studies have shown an impaired synaptic transmission and plasticity in the prefrontal cortex of $BDNF^{Met/Met}$ mice as well as in other brain regions like the hippocampus which strongly indicates that the polymorphism should have detectable effects in iPSC-derived cultures (171–173). Moreover, the activity-dependent neurotrophin is critical for synaptic plasticity, especially in the hippocampus which is important for cognitive functions such as learning and memory (41,42). It is particularly involved in the induction and maintenance of LTP (43,44). Thus, I became interested in analyzing the effects on LTP formation and maintenance in the iPSC-derived neuronal cultures. Chemically LTP induction leaded to an increase in mEPSC frequency in both cell lines. During the recovery phase, $BDNF^{Val/Val}$ and $BDNF^{Met/Met}$ neurons reduced their frequency again (Figure 29). Technical difficulties resulted in to short recordings. To improve the culturing conditions and thereby the overall state of the cells, co-cultures with astrocytes were generated. However, the improvement of the recording was unsuccessful. Nevertheless, in the future different and better cell culture conditions should be tested to boost neuronal maturity and thereby allow longer more reliable recordings of the cells.

The reduced synaptic connectivity may be related, at least partially, to the decreased surface levels of NMDAR2B detected in $BDNF^{Met/Met}$ neurons (Figure 30), indicating a decline in glutamatergic synaptic transmission. NMDAR are known to play an important role in controlling synaptic plasticity (139). Furthermore, previous studies in different rodent brain regions have consistently shown an impaired NMDA receptor-dependent synaptic plasticity caused by the Val66Met polymorphism (171–174). A reason could be that postsynaptically BDNF affects the activity of the glutamate receptors by inducing phosphorylation of the receptor subunits or by increasing the amount of membrane-bound NMDA receptor subunits (48–50).

Summing up, my experimental model was capable of recapitulating results already gained with animal studies for a human disease model and verified that the BDNF Val66Met

polymorphism has an effect on neuronal functionality in human neurons. Specifically, $BDNF^{Met/Met}$ neuronal populations display a reduced pre- and postsynaptic density and reduced amount of ionotropic glutamate receptors on the surface which is reflected in a decreased sEPSC frequency. Overall, this suggests a reduced glutamatergic transmission in $BDNF^{Met/Met}$ neurons which partially can be reversed by external BDNF addition. In a large part of the positive association studies, the $BDNF^{Met}$ allele is seen as the risk allele for psychiatric disease. The fact that external BDNF addition increases the synaptic density and the neuronal complexity, concludes that future studies will be required to elucidate in more detail the mechanisms behind the impairment in BDNF trafficking as well as to unravel the impact of the polymorphism in patient-derived neurons in order to investigate the potential of BDNF-based therapies for clinical use in neuropsychiatric disorders associated to the Val66Met polymorphism.

8 Conclusion and Outlook

In the here present work, a human iPSC-based model to quantitative analyze the BDNF Val66Met polymorphism on an endogenous expression level in a highly controlled cell population *in vitro* was established and characterized. My data demonstrate that the use of human iPSCs advances our understanding of the fundamental cellular and synaptic alterations associated with the Val66Met polymorphism in a human neuronal context and give first experimental evidence that the exchange of the amino acid Val to Met in the human *BDNF* gene has measurable implications in human neuronal development. In conclusion, the main findings presented in this thesis were the following:

1.) An accumulation of $BDNF^{Met}$ at the soma accompanied by a reduction of BDNF density in the neurites indicating impaired trafficking of $BDNF^{Met}$

2.) A reduction in neurite length and complexity in the initial phases of development indicating defects in neurite outgrowth which is persistent up to later stages of development caused by $BDNF^{Met}$

3.) An impaired synaptic transmission in neuronal cultures carrying $BDNF^{Met}$

4.) An external application of recombinant BDNF declined morphological and functional alterations caused by Val66Met

This model is not only capable of recapitulate results already gained with animal studies such as reduced complexity (84), but rather helps to understand human-specific aspects which can now be unraveled with a starting point set by this thesis. Furthermore, it helps to clarify mechanistic discrepancies previously observed in the literature like the secretion sites of BDNF. Nevertheless, future studies are required to elucidate in more detail the mechanisms behind the impairment in BDNF trafficking in humans. Further research is also necessary to unravel the impact of the polymorphism in patient-derived neurons in order to investigate the potential of BDNF treatment for clinical use in neuropsychiatric disorders.

9 References

1. Barde YA, Edgar D, Thoenen H. Purification of a new neurotrophic factor from mammalian brain. EMBO J. 1982 May;1(5):549–53.

2. Hallböök F. Evolution of the vertebrate neurotrophin and Trk receptor gene families. Curr Opin Neurobiol. 1999 Oct;9(5):616–21.

3. Maisonpierre PC, Belluscio L, Friedman B, Alderson RF, Wiegand SJ, Furth ME, et al. NT-3, BDNF, and NGF in the developing rat nervous system: Parallel as well as reciprocal patterns of expression. Neuron. 1990 Oct;5(4):501–9.

4. Friedman WJ, Olson L, Persson H. Cells that Express Brain-Derived Neurotrophic Factor mRNA in the Developing Postnatal Rat Brain. European Journal of Neuroscience. 1991 Jul;3(7):688–97.

5. Webster MJ, Weickert CS, Herman MM, Kleinman JE. BDNF mRNA expression during postnatal development, maturation and aging of the human prefrontal cortex. Developmental Brain Research. 2002 Dec;139(2):139–50.

6. Schmidt-Kastner R, WETMORE C, OLSON L. COMPARATIVE STUDY OF BRAIN-DERIVED NEUROTROPHIC FACTOR MESSENGER RNA AND PROTEIN AT THE CELLULAR LEVEL SUGGESTS MULTIPLE ROLES IN HIPPOCAMPUS, STRIATUM AND CORTEX. Neuroscience. 1996 Sep;74(1):161–83.

7. Mandel AL, Ozdener H, Utermohlen V. Identification of pro- and mature brain-derived neurotrophic factor in human saliva. Arch Oral Biol. 2009 Jul;54(7):689–95.

8. Seki M, Nawa H, Fukuchi T, Abe H, Takei N. BDNF is Upregulated by Postnatal Development and Visual Experience: Quantitative and Immunohistochemical Analyses of BDNF in the Rat Retina. Investigative Opthalmology & Visual Science. 2003 Jul 1;44(7):3211.

9. Friedman WJ, Olson L, Persson H. Cells that Express Brain-Derived Neurotrophic Factor mRNA in the Developing Postnatal Rat Brain. European Journal of Neuroscience. 1991 Jul;3(7):688–97.

10. Altar CA, Cai N, Bliven T, Juhasz M, Conner JM, Acheson AL, et al. Anterograde transport of brain-derived neurotrophic factor and its role in the brain. Nature. 1997 Oct;389(6653):856–60.

11. Altar CA, DiStefano PS. Neurotrophin trafficking by anterograde transport. Trends Neurosci. 1998 Oct;21(10):433–7.

12. Andreska T, Aufmkolk S, Sauer M, Blum R. High abundance of BDNF within glutamatergic presynapses of cultured hippocampal neurons. Front Cell Neurosci. 2014 Apr 11;8(1 APR).

13. Zafra F, Lindholm D, Castren E, Hartikka J, Thoenen H. Regulation of brain-derived neurotrophic factor and nerve growth factor mRNA in primary cultures of hippocampal neurons and astrocytes. The Journal of Neuroscience. 1992 Dec 1;12(12):4793–9.

14. Elkabes S, DiCicco-Bloom E, Black I. Brain microglia/macrophages express neurotrophins that selectively regulate microglial proliferation and function. The Journal of Neuroscience. 1996 Apr 15;16(8):2508–21.

15. Dai X, Lercher LD, Clinton PM, Du Y, Livingston DL, Vieira C, et al. The Trophic Role of Oligodendrocytes in the Basal Forebrain. The Journal of Neuroscience. 2003 Jul 2;23(13):5846–53.

16. Binder DK, Scharfman HE. Brain-derived neurotrophic factor. Vol. 22, Growth Factors. 2004. p. 123–31.

17. Pruunsild P, Kazantseva A, Aid T, Palm K, Timmusk T. Dissecting the human BDNF locus: Bidirectional transcription, complex splicing, and multiple promoters. Genomics. 2007 Sep;90(3):397–406.

18. Timmusk T, Palm K, Metsis M, Reintam T, Paalme V, Saarma M, et al. Multiple promoters direct tissue-specific expression of the rat BDNF gene. Neuron. 1993 Mar;10(3):475–89.

19. An JJ, Gharami K, Liao GY, Woo NH, Lau AG, Vanevski F, et al. Distinct Role of Long 3' UTR BDNF mRNA in Spine Morphology and Synaptic Plasticity in Hippocampal Neurons. Cell. 2008 Jul;134(1):175–87.

20. Brigadski T, Leßmann V. The physiology of regulated BDNF release. Cell Tissue Res. 2020 Oct 18;382(1):15–45.

21. Chen ZY. Sortilin Controls Intracellular Sorting of Brain-Derived Neurotrophic Factor to the Regulated Secretory Pathway. Journal of Neuroscience. 2005 Jun 29;25(26):6156–66.

22. Lou H, Kim SK, Zaitsev E, Snell CR, Lu B, Loh YP. Sorting and Activity-Dependent Secretion of BDNF Require Interaction of a Specific Motif with the Sorting Receptor Carboxypeptidase E. Neuron. 2005 Jan;45(2):245–55.

23. Lessmann V, Gottmann K, Malcangio M. Neurotrophin secretion: current facts and future prospects. Prog Neurobiol. 2003 Apr;69(5):341–74.

24. Brigadski T. Differential Vesicular Targeting and Time Course of Synaptic Secretion of the Mammalian Neurotrophins. Journal of Neuroscience. 2005 Aug 17;25(33):7601–14.

25. Leßmann V, Brigadski T. Mechanisms, locations, and kinetics of synaptic BDNF secretion: An update. Neurosci Res. 2009 Sep;65(1):11–22.

26. Hartmann M. Synaptic secretion of BDNF after high-frequency stimulation of glutamatergic synapses. EMBO J. 2001 Nov 1;20(21):5887–97.

27. Adachi N, Kohara K, Tsumoto T. Difference in trafficking of brain-derived neurotrophic factor between axons and dendrites of cortical neurons, revealed by live-cell imaging. BMC Neurosci. 2005 Dec 21;6(1):42.

28. Kohara K, Kitamura A, Morishima M, Tsumoto T. Activity-Dependent Transfer of Brain-Derived Neurotrophic Factor to Postsynaptic Neurons. Science (1979). 2001 Mar 23;291(5512):2419–23.

29. Kolbeck R, Jungbluth S, Barde YA. Characterisation of Neurotrophin Dimers and Monomers. Eur J Biochem. 1994 Nov;225(3):995–1003.

30. Mowla SJ, Pareek S, Farhadi HF, Petrecca K, Fawcett JP, Seidah NG, et al. Differential Sorting of Nerve Growth Factor and Brain-Derived Neurotrophic Factor in Hippocampal Neurons. The Journal of Neuroscience. 1999 Mar 15;19(6):2069–80.

31. Seidah NG, Benjannet S, Pareek S, Chrétien M, Murphy RA. Cellular processing of the neurotrophin precursors of NT3 and BDNF by the mammalian proprotein convertases. FEBS Lett. 1996 Feb 5;379(3):247–50.

32. Lee R, Kermani P, Teng KK, Hempstead BL. Regulation of Cell Survival by Secreted Proneurotrophins. Science (1979). 2001 Nov 30;294(5548):1945–8.

33. Huang EJ, Reichardt LF. NEUROTROPHINS: Roles in Neuronal Development and Function * [Internet]. 2001. Available from: www.annualreviews.org

34. Reichardt LF. Neurotrophin-regulated signalling pathways. Philosophical Transactions of the Royal Society B: Biological Sciences. 2006 Sep 29;361(1473):1545–64.

35. Huang EJ, Reichardt LF. Trk Receptors: Roles in Neuronal Signal Transduction. Annu Rev Biochem. 2003 Jun;72(1):609–42.

36. Yoshii A, Constantine-Paton M. Postsynaptic BDNF-TrkB signaling in synapse maturation, plasticity, and disease. Dev Neurobiol. 2010;NA-NA.

37. Sarbassov DD, Guertin DA, Ali SM, Sabatini DM. Phosphorylation and Regulation of Akt/PKB by the Rictor-mTOR Complex. Science (1979). 2005 Feb 18;307(5712):1098–101.

38. Mai J, Fok L, Gao H, Zhang X, Poo M m. Axon Initiation and Growth Cone Turning on Bound Protein Gradients. Journal of Neuroscience. 2009 Jun 10;29(23):7450–8.

39. Arancio O, Chao M v. Neurotrophins, synaptic plasticity and dementia. Curr Opin Neurobiol. 2007 Jun;17(3):325–30.

40. Cohen-Cory S, Kidane AH, Shirkey NJ, Marshak S. Brain-derived neurotrophic factor and the development of structural neuronal connectivity. Dev Neurobiol. 2010;NA-NA.

41. Patterson SL, Abel T, Deuel TAS, Martin KC, Rose JC, Kandel ER. Recombinant BDNF Rescues Deficits in Basal Synaptic Transmission and Hippocampal LTP in BDNF Knockout Mice. Neuron. 1996 Jun;16(6):1137–45.

42. Kang H, Schuman E. Neurotrophin-induced modulation of synaptic transmission in the adult hippocampus. Journal of Physiology-Paris. 1995 Jan;89(1):11–22.

43. Lu B, Gottschalk W. Modulation of hippocampal synaptic transmission and plasticity by neurotrophins. In 2000. p. 231–41.

44. Poo M ming. Neurotrophins as synaptic modulators. Nat Rev Neurosci. 2001 Jan;2(1):24–32.

45. Carvalho AL, Caldeira M v, Santos SD, Duarte CB. Role of the brain-derived neurotrophic factor at glutamatergic synapses. Br J Pharmacol. 2008 Mar;153(S1):S310–24.

46. Sala R, Viegi A, Rossi FM, Pizzorusso T, Bonanno G, Raiteri M, et al. Nerve growth factor and brain-derived neurotrophic factor increase neurotransmitter release in the rat visual cortex. European Journal of Neuroscience. 1998 Jun;10(6):2185–91.

47. Jovanovic JN, Czernik AJ, Fienberg AA, Greengard P, Sihra TS. Synapsins as mediators of BDNF-enhanced neurotransmitter release. Nat Neurosci. 2000 Apr;3(4):323–9.

48. Narisawa-Saito M, Iwakura Y, Kawamura M, Araki K, Kozaki S, Takei N, et al. Brain-derived Neurotrophic Factor Regulates Surface Expression of α-Amino-3-hydroxy-5-methyl-4-isoxazoleproprionic Acid Receptors by Enhancing the N-Ethylmaleimide-sensitive Factor/GluR2 Interaction in Developing Neocortical Neurons. Journal of Biological Chemistry. 2002 Oct;277(43):40901–10.

49. Alder J. Early Presynaptic and Late Postsynaptic Components Contribute Independently to Brain-Derived Neurotrophic Factor-Induced Synaptic Plasticity. Journal of Neuroscience. 2005 Mar 23;25(12):3080–5.

50. Nakata H, Nakamura S. Brain-derived neurotrophic factor regulates AMPA receptor trafficking to post-synaptic densities via IP3R and TRPC calcium signaling. FEBS Lett. 2007 May 15;581(10):2047–54.

51. Park H, Poo M ming. Neurotrophin regulation of neural circuit development and function. Nat Rev Neurosci. 2013 Jan 20;14(1):7–23.

52. Gottmann K, Mittmann T, Lessmann V. BDNF signaling in the formation, maturation and plasticity of glutamatergic and GABAergic synapses. Vol. 199, Experimental Brain Research. 2009. p. 203–34.

53. Liepinsh E. NMR structure of the death domain of the p75 neurotrophin receptor. EMBO J. 1997 Aug 15;16(16):4999–5005.

54. Teng HK. ProBDNF Induces Neuronal Apoptosis via Activation of a Receptor Complex of p75NTR and Sortilin. Journal of Neuroscience. 2005 Jun 1;25(22):5455–63.

55. Anastasia A, Deinhardt K, Chao M v., Will NE, Irmady K, Lee FS, et al. Val66Met polymorphism of BDNF alters prodomain structure to induce neuronal growth cone retraction. Nat Commun. 2013 Dec 20;4(1):2490.

56. Bandtlow C, Dechant G. From Cell Death to Neuronal Regeneration, Effects of the p75 Neurotrophin Receptor Depend on Interactions with Partner Subunits. Science's STKE. 2004 Jun;2004(235).

57. Gentry JJ, Barker PA, Carter BD. The p75 neurotrophin receptor: multiple interactors and numerous functions. In 2004. p. 25–39.

58. Knable MB, Barci BM, Webster MJ, Meador-Woodruff J, Torrey EF. Molecular abnormalities of the hippocampus in severe psychiatric illness: postmortem findings from the Stanley Neuropathology Consortium. Mol Psychiatry. 2004 Jun 6;9(6):609–20.

59. Karege F, Vaudan G, Schwald M, Perroud N, la Harpe R. Neurotrophin levels in postmortem brains of suicide victims and the effects of antemortem diagnosis and psychotropic drugs. Molecular Brain Research. 2005 May;136(1–2):29–37.

60. Campbell S, Macqueen G. The role of the hippocampus in the pathophysiology of major depression. J Psychiatry Neurosci. 2004 Nov;29(6):417–26.

61. CASTREN E, VOIKAR V, RANTAMAKI T. Role of neurotrophic factors in depression. Curr Opin Pharmacol. 2007 Feb;7(1):18–21.

62. Thompson Ray M, Weickert CS, Wyatt E, Webster MJ. Decreased BDNF, trkB-TK+ and GAD67 mRNA expression in the hippocampus of individuals with schizophrenia and mood disorders. J Psychiatry Neurosci. 2011 May;36(3):195–203.

63. Yagasaki Y, Numakawa T, Kumamaru E, Hayashi T, Su TP, Kunugi H. Chronic Antidepressants Potentiate via Sigma-1 Receptors the Brain-derived Neurotrophic Factor-induced Signaling for Glutamate Release. Journal of Biological Chemistry. 2006 May;281(18):12941–9.

64. Martínez-Turrillas R, del Río J, Frechilla D. Sequential changes in BDNF mRNA expression and synaptic levels of AMPA receptor subunits in rat hippocampus after chronic antidepressant treatment. Neuropharmacology. 2005 Dec;49(8):1178–88.

65. de Kloet ER, Sibug RM, Helmerhorst FM, Schmidt M. Stress, genes and the mechanism of programming the brain for later life. Neurosci Biobehav Rev. 2005 Apr;29(2):271–81.

66. Schaaf MJM, de Kloet ER, Vreugdenhil E. Corticosterone Effects on BDNF Expression in the Hippocampus Implications for Memory Formation. Stress. 2000 Jan 7;3(3):201–8.

67. Egan MF, Kojima M, Callicott JH, Goldberg TE, Kolachana BS, Bertolino A, et al. The BDNF val66met Polymorphism Affects Activity-Dependent Secretion of BDNF and Human Memory and Hippocampal Function and its val/met polymorphism in human memory and hippocampal function and suggest val/met exerts these effects by impacting intracellular trafficking and activity-dependent secretion of BDNF. Vol. 112, Cell. 2003.

68. Shimizu E, Hashimoto K, Iyo M. Ethnic difference of the BDNF 196G/A (val66met) polymorphism frequencies: The possibility to explain ethnic mental traits. Am J Med Genet. 2004 Apr 1;126B(1):122–3.

69. Itoh K, Hashimoto K, Kumakiri C, Shimizu E, Iyo M. Association between brain-derived neurotrophic factor 196 G/A polymorphism and personality traits in healthy subjects. Am J Med Genet. 2004 Jan 1;124B(1):61–3.

70. Ventriglia M, Bocchio Chiavetto L, Benussi L, Binetti G, Zanetti O, Riva MA, et al. Association between the BDNF 196 A/G polymorphism and sporadic Alzheimer's disease. Mol Psychiatry. 2002 Feb 1;7(2):136–7.

71. Bath KG, Lee FS. Variant BDNF (Val66Met) impact on brain structure and function. Cogn Affect Behav Neurosci. 2006 Mar 1;6(1):79–85.

72. Hong CJ, Liou YJ, Tsai SJ. Effects of BDNF polymorphisms on brain function and behavior in health and disease. Brain Res Bull. 2011 Nov;86(5–6):287–97.

73. Notaras M, Hill R, van den Buuse M. The BDNF gene Val66Met polymorphism as a modifier of psychiatric disorder susceptibility: progress and controversy. Mol Psychiatry. 2015 Aug 31;20(8):916–30.

74. Ventriglia M, Bocchio Chiavetto L, Benussi L, Binetti G, Zanetti O, Riva MA, et al. Association between the BDNF 196 A/G polymorphism and sporadic Alzheimer's disease. Mol Psychiatry. 2002 Feb 18;7(2):136–7.

75. Dincheva I, Glatt CE, Lee FS. Impact of the BDNF Val66Met Polymorphism on Cognition. The Neuroscientist. 2012 Oct 24;18(5):439–51.

76. Chen ZY. Variant Brain-Derived Neurotrophic Factor (BDNF) (Met66) Alters the Intracellular Trafficking and Activity-Dependent Secretion of Wild-Type BDNF in Neurosecretory Cells and Cortical Neurons. Journal of Neuroscience. 2004 May 5;24(18):4401–11.

77. Chiaruttini C, Vicario A, Li Z, Baj G, Braiuca P, Wu Y, et al. Dendritic trafficking of BDNF mRNA is mediated by translin and blocked by the G196A (Val66Met) mutation. Proceedings of the National Academy of Sciences. 2009 Sep 22;106(38):16481–6.

78. del Toro D, Canals JM, Ginés S, Kojima M, Egea G, Alberch J. Mutant huntingtin impairs the post-Golgi trafficking of brain-derived neurotrophic factor but not its Val66Met polymorphism. Journal of Neuroscience. 2006 Dec 6;26(49):12748–57.

79. Bath KG, Jing DQ, Dincheva I, Neeb CC, Pattwell SS, Chao M v, et al. BDNF Val66Met Impairs Fluoxetine-Induced Enhancement of Adult Hippocampus Plasticity. Neuropsychopharmacology. 2012 Apr 4;37(5):1297–304.

80. Jin P, Andiappan AK, Quek JM, Lee B, Au B, Sio YY, et al. A functional brain-derived neurotrophic factor (BDNF) gene variant increases the risk of moderate-to-severe allergic rhinitis. Journal of Allergy and Clinical Immunology. 2015 Jun;135(6):1486-1493.e8.

81. Pezawas L. The Brain-Derived Neurotrophic Factor val66met Polymorphism and Variation in Human Cortical Morphology. Journal of Neuroscience. 2004 Nov 10;24(45):10099–102.

82. Szeszko PR, Lipsky R, Mentschel C, Robinson D, Gunduz-Bruce H, Sevy S, et al. Brain-derived neurotrophic factor Val66met polymorphism and volume of the hippocampal formation. Mol Psychiatry. 2005 Jul 15;10(7):631–6.

83. Chen ZY, Bath K, McEwen B, Hempstead B, Lee F. Impact of genetic variant BDNF (Val66Met) on brain structure and function. Novartis Found Symp. 2008;289:180–8; discussion 188-95.

84. Xu X, Garcia J, Ewalt R, Nason S, Pozzo-Miller L. The BDNF val-66-met polymorphism affects neuronal morphology and synaptic transmission in cultured hippocampal neurons from rett syndrome mice. Front Cell Neurosci. 2017 Jul 13;11.

85. Anastasia A, Deinhardt K, Chao M v., Will NE, Irmady K, Lee FS, et al. Val66Met polymorphism of BDNF alters prodomain structure to induce neuronal growth cone retraction. Nat Commun. 2013 Sep 18;4.

86. Hariri AR, Goldberg TE, Mattay VS, Kolachana BS, Callicott JH, Egan MF, et al. Brain-Derived Neurotrophic Factor val ^{66} met Polymorphism Affects Human Memory-Related Hippocampal Activity and Predicts Memory Performance. The Journal of Neuroscience. 2003 Jul 30;23(17):6690–4.

87. Soliman F, Glatt CE, Bath KG, Levita L, Jones RM, Pattwell SS, et al. A Genetic Variant BDNF Polymorphism Alters Extinction Learning in Both Mouse and Human. Science (1979). 2010 Feb 12;327(5967):863–6.

88. Uegaki K, Kumanogoh H, Mizui T, Hirokawa T, Ishikawa Y, Kojima M. BDNF binds its pro-peptide with high affinity and the common val66met polymorphism attenuates the interaction. Int J Mol Sci. 2017 May 12;18(5).

89. Mizui T, Ishikawa Y, Kumanogoh H, Lume M, Matsumoto T, Hara T, et al. BDNF pro-peptide actions facilitate hippocampal LTD and are altered by the common BDNF polymorphism Val66Met. Proceedings of the National Academy of Sciences. 2015 Jun 9;112(23):E3067–74.

90. Notaras M, Hill R, van den Buuse M. A role for the BDNF gene Val66Met polymorphism in schizophrenia? A comprehensive review. Neurosci Biobehav Rev. 2015 Apr;51:15–30.

91. Neves-Pereira M, Mundo E, Muglia P, King N, Macciardi F, Kennedy JL. The Brain-Derived Neurotrophic Factor Gene Confers Susceptibility to Bipolar Disorder: Evidence from a Family-Based Association Study. The American Journal of Human Genetics. 2002 Sep;71(3):651–5.

92. Sklar P, Gabriel SB, McInnis MG, Bennett P, Lim YM, Tsan G, et al. Family-based association study of 76 candidate genes in bipolar disorder: BDNF is a potential risk locus. Mol Psychiatry. 2002 Jul 30;7(6):579–93.

93. Chepenik LG, Fredericks C, Papademetris X, Spencer L, Lacadie C, Wang F, et al. Effects of the Brain-Derived Neurotrophic Growth Factor Val66Met Variation on Hippocampus Morphology in Bipolar Disorder. Neuropsychopharmacology. 2009 Mar 13;34(4):944–51.

94. McIntosh AM, Moorhead TWJ, McKirdy J, Sussmann JED, Hall J, Johnstone EC, et al. Temporal grey matter reductions in bipolar disorder are associated with the BDNF Val66Met polymorphism. Mol Psychiatry. 2007 Oct 26;12(10):902–3.

95. Li M, Chang H, Xiao X. BDNF Val66Met polymorphism and bipolar disorder in European populations: A risk association in case-control, family-based and GWAS studies. Neurosci Biobehav Rev. 2016 Sep;68:218–33.

96. Borroni B, Grassi M, Archetti S, Costanzi C, Bianchi M, Caimi L, et al. BDNF Genetic Variations Increase the Risk of Alzheimer's Disease-Related Depression. Journal of Alzheimer's Disease. 2009 Nov 12;18(4):867–75.

97. Prats C, Arias B, Ortet G, Ibáñez MI, Moya J, Pomarol-Clotet E, et al. Role of neurotrophins in depressive symptoms and executive function: Association analysis of NRN1 gene and its interaction with BDNF gene in a non-clinical sample. J Affect Disord. 2017 Mar;211:92–8.

98. Tsai SJ, Hong CJ, Liou YJ. Recent molecular genetic studies and methodological issues in suicide research. Prog Neuropsychopharmacol Biol Psychiatry. 2011 Jun;35(4):809–17.

99. González-Castro TB, Salas-Magaña M, Juárez-Rojop IE, López-Narváez ML, Tovilla-Zárate CA, Hernández-Díaz Y. Exploring the association between BDNF Val66Met polymorphism and suicidal behavior: Meta-analysis and systematic review. J Psychiatr Res. 2017 Nov;94:208–17.

100. Cheng CY, Hong CJ, Yu YWY, Chen TJ, Wu HC, Tsai SJ. Brain-derived neurotrophic factor (Val66Met) genetic polymorphism is associated with substance abuse in males. Molecular Brain Research. 2005 Oct;140(1–2):86–90.

101. Andero R, Choi DC, Ressler KJ. BDNF–TrkB Receptor Regulation of Distributed Adult Neural Plasticity, Memory Formation, and Psychiatric Disorders. In 2014. p. 169–92.

102. Tsai SJ. Critical Issues in BDNF Val66Met Genetic Studies of Neuropsychiatric Disorders. Front Mol Neurosci. 2018 May 15;11.

103. Wobus AM, Boheler KR. Embryonic Stem Cells: Prospects for Developmental Biology and Cell Therapy. Physiol Rev. 2005 Apr;85(2):635–78.

104. Thomson JA, Itskovitz-Eldor J, Shapiro SS, Waknitz MA, Swiergiel JJ, Marshall VS, et al. Embryonic Stem Cell Lines Derived from Human Blastocysts. Science (1979). 1998 Nov 6;282(5391):1145–7.

105. Hockemeyer D, Jaenisch R. Induced Pluripotent Stem Cells Meet Genome Editing. Cell Stem Cell. 2016 May;18(5):573–86.

106. Aasen T, Raya A, Barrero MJ, Garreta E, Consiglio A, Gonzalez F, et al. Efficient and rapid generation of induced pluripotent stem cells from human keratinocytes. Nat Biotechnol. 2008 Nov 17;26(11):1276–84.

107. Staerk J, Dawlaty MM, Gao Q, Maetzel D, Hanna J, Sommer CA, et al. Reprogramming of human peripheral blood cells to induced pluripotent stem cells. Cell Stem Cell. 2010 Jul 2;7(1):20–4.

108. Takahashi K, Yamanaka S. Induction of Pluripotent Stem Cells from Mouse Embryonic and Adult Fibroblast Cultures by Defined Factors. Cell. 2006 Aug;126(4):663–76.

109. Yu J, Vodyanik MA, Smuga-Otto K, Antosiewicz-Bourget J, Frane JL, Tian S, et al. Induced Pluripotent Stem Cell Lines Derived from Human Somatic Cells. Science (1979). 2007 Dec 21;318(5858):1917–20.

110. Chen IP, Fukuda K, Fusaki N, Iida A, Hasegawa M, Lichtler A, et al. Induced Pluripotent Stem Cell Reprogramming by Integration-Free Sendai Virus Vectors from Peripheral Blood of Patients with Craniometaphyseal Dysplasia. Cell Reprogram. 2013 Dec;15(6):503–13.

111. Muratore CR, Srikanth P, Callahan DG, Young-Pearse TL. Comparison and Optimization of hiPSC Forebrain Cortical Differentiation Protocols. PLoS One. 2014 Aug 28;9(8):e105807.

112. Musunuru K, Sheikh F, Gupta RM, Houser SR, Maher KO, Milan DJ, et al. Induced Pluripotent Stem Cells for Cardiovascular Disease Modeling and Precision Medicine: A Scientific Statement From the American Heart Association. Circ Genom Precis Med. 2018 Jan;11(1).

113. Lu J, Xia Q, Zhou Q. How to make insulin-producing pancreatic β cells for diabetes treatment. Sci China Life Sci. 2017 Mar 27;60(3):239–48.

114. Rubin LL. Stem Cells and Drug Discovery: The Beginning of a New Era? Cell. 2008 Feb;132(4):549–52.

115. Lin J. Applications and Limitations of Genetically Modified Mouse Models in Drug Discovery and Development. Curr Drug Metab. 2008 Jun 1;9(5):419–38.

116. Grade S, Götz M. Neuronal replacement therapy: previous achievements and challenges ahead. NPJ Regen Med. 2017 Dec 23;2(1):29.

117. Vierbuchen T, Ostermeier A, Pang ZP, Kokubu Y, Südhof TC, Wernig M. Direct conversion of fibroblasts to functional neurons by defined factors. Nature. 2010 Feb 27;463(7284):1035–41.

118. Ladewig J, Koch P, Brüstle O. Leveling Waddington: the emergence of direct programming and the loss of cell fate hierarchies. Nat Rev Mol Cell Biol. 2013 Apr 13;14(4):225–36.

119. Broccoli V, Giannelli SG, Mazzara PG. Modeling physiological and pathological human neurogenesis in the dish. Front Neurosci. 2014 Jul 24;8.

120. Tao Y, Zhang SC. Neural Subtype Specification from Human Pluripotent Stem Cells. Cell Stem Cell. 2016 Nov;19(5):573–86.

121. Chambers SM, Fasano CA, Papapetrou EP, Tomishima M, Sadelain M, Studer L. Highly efficient neural conversion of human ES and iPS cells by dual inhibition of SMAD signaling. Nat Biotechnol. 2009 Mar 1;27(3):275–80.

122. Kirkeby A, Grealish S, Wolf DA, Nelander J, Wood J, Lundblad M, et al. Generation of Regionally Specified Neural Progenitors and Functional Neurons from Human Embryonic Stem Cells under Defined Conditions. Cell Rep. 2012 Jun;1(6):703–14.

123. Lancaster MA, Renner M, Martin CA, Wenzel D, Bicknell LS, Hurles ME, et al. Cerebral organoids model human brain development and microcephaly. Nature. 2013 Sep 19;501(7467):373–9.

124. van Kuppeveld FJ, van der Logt JT, Angulo AF, van Zoest MJ, Quint WG, Niesters HG, et al. Genus- and species-specific identification of mycoplasmas by 16S rRNA amplification. Appl Environ Microbiol. 1992 Aug;58(8):2606–15.

125. Ossewaarde JM, de Vries A, Bestebroer T, Angulo AF. Application of a Mycoplasma group-specific PCR for monitoring decontamination of Mycoplasma-infected Chlamydia sp. strains. Appl Environ Microbiol. 1996 Feb;62(2):328–31.

126. Telezhkin V, Schnell C, Yarova P, Yung S, Cope E, Hughes A, et al. Forced cell cycle exit and modulation of GABA $_{A}$, CREB, and GSK3β signaling promote functional maturation of induced pluripotent stem cell-derived neurons. American Journal of Physiology-Cell Physiology. 2016 Apr 1;310(7):C520–41.

127. Kemp PJ, Rushton DJ, Yarova PL, Schnell C, Geater C, Hancock JM, et al. Improving and accelerating the differentiation and functional maturation of human stem cell-derived neurons: role of extracellular calcium and GABA. J Physiol. 2016 Nov 15;594(22):6583–94.

128. R Core Team. R: A Language and Environment for Statistical Computing. Vienna, Austria; 2020.

129. Love MI, Huber W, Anders S. Moderated estimation of fold change and dispersion for RNA-seq data with DESeq2. Genome Biol. 2014 Dec 5;15(12):550.

130. Yu G, Wang LG, Han Y, He QY. clusterProfiler: an R package for comparing biological themes among gene clusters. OMICS. 2012;16(5):284–7.

131. Carlson M. org.Hs.eg.db: Genome wide annotation for Human. 2020.

132. Walter W, Sánchez-Cabo F, Ricote M. GOplot: an R package for visually combining expression data with functional analysis: Fig. 1. Bioinformatics. 2015 Sep 1;31(17):2912–4.

133. Ran FA, Hsu PD, Wright J, Agarwala V, Scott DA, Zhang F. Genome engineering using the CRISPR-Cas9 system. Nat Protoc. 2013 Nov 24;8(11):2281–308.

134. Kannagi R, Cochran NA, Ishigami F, Hakomori S, Andrews PW, Knowles BB, et al. Stage-specific embryonic antigens (SSEA-3 and -4) are epitopes of a unique globo-series ganglioside isolated from human teratocarcinoma cells. EMBO J. 1983 Dec;2(12):2355–61.

135. PAN GJ, CHANG ZY, SCHÖLER HR, PEI D. Stem cell pluripotency and transcription factor Oct4. Cell Res. 2002 Dec;12(5–6):321–9.

136. Zhang S. Sox2, a key factor in the regulation of pluripotency and neural differentiation. World J Stem Cells. 2014;6(3):305.

137. Lewin GR, Barde YA. Physiology of the Neurotrophins. Annu Rev Neurosci. 1996 Mar;19(1):289–317.

138. Carvalho AL, Caldeira M v., Santos SD, Duarte CB. Role of the brain-derived neurotrophic factor at glutamatergic synapses. In: British Journal of Pharmacology. 2008.

139. Caldeira M v., Melo C v., Pereira DB, Carvalho RF, Carvalho AL, Duarte CB. BDNF regulates the expression and traffic of NMDA receptors in cultured hippocampal neurons. Molecular and Cellular Neuroscience. 2007 Jun;35(2):208–19.

140. Numata S, Ueno S ichi, Iga J ichi, Yamauchi K, Hongwei S, Ohta K, et al. Brain-derived neurotrophic factor (BDNF) Val66Met polymorphism in schizophrenia is associated with age at onset and symptoms. Neurosci Lett. 2006 Jun;401(1–2):1–5.

141. Mallei A, Baj G, Ieraci A, Corna S, Musazzi L, Lee FS, et al. Expression and Dendritic Trafficking of BDNF-6 Splice Variant are Impaired in Knock-In Mice Carrying Human BDNF Val66Met Polymorphism. International Journal of Neuropsychopharmacology. 2015 Nov;18(12):pyv069.

142. Pound P, Ram R. Are researchers moving away from animal models as a result of poor clinical translation in the field of stroke? An analysis of opinion papers. BMJ Open Science. 2020 Jan;4(1):e100041.

143. Leenaars CHC, Kouwenaar C, Stafleu FR, Bleich A, Ritskes-Hoitinga M, de Vries RBM, et al. Animal to human translation: a systematic scoping review of reported concordance rates. J Transl Med. 2019 Dec 15;17(1):223.

144. Ellis J. Silencing and Variegation of Gammaretrovirus and Lentivirus Vectors. Hum Gene Ther. 2005 Nov;16(11):1241–6.

145. Farhy-Tselnicker I, Allen NJ. Astrocytes, neurons, synapses: a tripartite view on cortical circuit development. Neural Dev. 2018 Dec 1;13(1):7.

146. Goodman LJ, Valverde J, Lim F, Geschwind MD, Federoff HJ, Geller AI, et al. Regulated Release and Polarized Localization of Brain-Derived Neurotrophic Factor in Hippocampal Neurons. Molecular and Cellular Neuroscience. 1996 Mar;7(3):222–38.

147. Conner JM, Lauterborn JC, Yan Q, Gall CM, Varon S. Distribution of Brain-Derived Neurotrophic Factor (BDNF) Protein and mRNA in the Normal Adult Rat CNS: Evidence for Anterograde Axonal Transport. The Journal of Neuroscience. 1997 Apr 1;17(7):2295–313.

148. Dieni S, Matsumoto T, Dekkers M, Rauskolb S, Ionescu MS, Deogracias R, et al. BDNF and its pro-peptide are stored in presynaptic dense core vesicles in brain neurons. Journal of Cell Biology. 2012 Mar 19;196(6):775–88.

149. Farhadi HF, Mowla SJ, Petrecca K, Morris SJ, Seidah NG, Murphy RA. Neurotrophin-3 Sorts to the Constitutive Secretory Pathway of Hippocampal Neurons and Is Diverted to the Regulated Secretory Pathway by Coexpression with Brain-Derived Neurotrophic Factor. The Journal of Neuroscience. 2000 Jun 1;20(11):4059–68.

150. Haubensak W, Narz F, Heumann R, Lessmann V. BDNF-GFP containing secretory granules are localized in the vicinity of synaptic junctions of cultured cortical neurons. J Cell Sci. 1998 Jun 1;111(11):1483–93.

151. Klyachko VA, Jackson MB. Capacitance steps and fusion pores of small and large-dense-core vesicles in nerve terminals. Nature. 2002 Jul;418(6893):89–92.

152. Salio C, Averill S, Priestley JV, Merighi A. Costorage of BDNF and neuropeptides within individual dense-core vesicles in central and peripheral neurons. Dev Neurobiol. 2007 Feb 15;67(3):326–38.

153. Horch HW, Katz LC. BDNF release from single cells elicits local dendritic growth in nearby neurons. Nat Neurosci. 2002 Nov 30;5(11):1177–84.

154. Chen Q, Zhou Z, Zhang L, Wang Y, Zhang YW, Zhong M, et al. Tau protein is involved in morphological plasticity in hippocampal neurons in response to BDNF. Neurochem Int. 2012 Feb;60(3):233–42.

155. Wirth MJ, Brün A, Grabert J, Patz S, Wahle P. Accelerated dendritic development of rat cortical pyramidal cells and interneurons after biolistic transfection with BDNF and NT4/5. Development. 2003 Dec 1;130(23):5827–38.

156. McAllister AK, Lo DC, Katz LC. Neurotrophins regulate dendritic growth in developing visual cortex. Neuron. 1995 Oct;15(4):791–803.

157. Cheng PL, Song AH, Wong YH, Wang S, Zhang X, Poo MM. Self-amplifying autocrine actions of BDNF in axon development. Proc Natl Acad Sci U S A. 2011 Nov 8;108(45):18430–5.

158. Kimpinski K, Campenot RB, Mearow K. Effects of the neurotrophins nerve growth factor, neurotrophin-3, and brain-derived neurotrophic factor (BDNF) on neurite growth from adult sensory neurons in compartmented cultures. J Neurobiol. 1997 Oct;33(4):395–410.

159. Gavazzi I, Kumar RDC, McMahon SB, Cohen J. Growth responses of different subpopulations of adult sensory neurons to neurotrophic factors in vitro. European Journal of Neuroscience. 1999 Oct;11(10):3405–14.

160. Lindsay R. Nerve growth factors (NGF, BDNF) enhance axonal regeneration but are not required for survival of adult sensory neurons. The Journal of Neuroscience. 1988 Jul 1;8(7):2394–405.

161. Blesch A, Tuszynski MH. Cellular GDNF delivery promotes growth of motor and dorsal column sensory axons after partial and complete spinal cord transections and induces remyelination. J Comp Neurol. 2003 Dec 15;467(3):403–17.

162. Jones DM, Tucker BA, Rahimtula M, Mearow KM. The synergistic effects of NGF and IGF-1 on neurite growth in adult sensory neurons: convergence on the PI 3-kinase signaling pathway. J Neurochem. 2003 Jul 28;86(5):1116–28.

163. Baj G, Carlino D, Gardossi L, Tongiorgi E. Toward a unified biological hypothesis for the BDNF Val66Met-associated memory deficits in humans: A model of impaired dendritic mRNA trafficking. Vol. 7, Frontiers in Neuroscience. Frontiers Media S.A.; 2013.

164. Wilson Horch H, Krüttgen A, Portbury SD, Katz LC. Destabilization of Cortical Dendrites and Spines by BDNF. Neuron. 1999 Jun;23(2):353–64.

165. Verstraelen P, Pintelon I, Nuydens R, Cornelissen F, Meert T, Timmermans JP. Pharmacological Characterization of Cultivated Neuronal Networks: Relevance to Synaptogenesis and Synaptic Connectivity. Cell Mol Neurobiol. 2014 Jul 19;34(5):757–76.

166. Brewer LD, Dowling ALS, Curran-Rauhut MA, Landfield PW, Porter NM, Blalock EM. Estradiol Reverses a Calcium-Related Biomarker of Brain Aging in Female Rats. Journal of Neuroscience. 2009 May 13;29(19):6058–67.

167. Sun Z, Südhof TC. A simple Ca2+-imaging approach to neural network analyses in cultured neurons. J Neurosci Methods. 2021 Feb;349:109041.

168. Artimovich E, Jackson RK, Kilander MBC, Lin YC, Nestor MW. PeakCaller: an automated graphical interface for the quantification of intracellular calcium obtained by high-content screening. BMC Neurosci. 2017 Dec 16;18(1):72.

169. Li YX, Zhang Y, Lester HA, Schuman EM, Davidson N. Enhancement of Neurotransmitter Release Induced by Brain-Derived Neurotrophic Factor in Cultured Hippocampal Neurons. The Journal of Neuroscience. 1998 Dec 15;18(24):10231–40.

170. Levine ES, Dreyfus CF, Black IB, Plummer MR. Brain-derived neurotrophic factor rapidly enhances synaptic transmission in hippocampal neurons via postsynaptic tyrosine kinase receptors. Proceedings of the National Academy of Sciences. 1995 Aug 15;92(17):8074–7.

171. Pattwell SS, Bath KG, Perez-Castro R, Lee FS, Chao M v., Ninan I. The BDNF Val66Met Polymorphism Impairs Synaptic Transmission and Plasticity in the Infralimbic Medial Prefrontal Cortex. Journal of Neuroscience. 2012 Feb 15;32(7):2410–21.

172. Jing D, Lee FS, Ninan I. The BDNF Val66Met polymorphism enhances glutamatergic transmission but diminishes activity-dependent synaptic plasticity in the dorsolateral striatum. Neuropharmacology. 2017 Jan;112:84–93.

173. Galvin C, Lee FS, Ninan I. Alteration of the Centromedial Amygdala Glutamatergic Synapses by the BDNF Val66Met Polymorphism. Neuropsychopharmacology. 2015 Aug 18;40(9):2269–77.

174. Ninan I, Bath KG, Dagar K, Perez-Castro R, Plummer MR, Lee FS, et al. The BDNF Val66Met Polymorphism Impairs NMDA Receptor-Dependent Synaptic Plasticity in the Hippocampus. Journal of Neuroscience. 2010 Jun 30;30(26):8866–70.

Appendix, Statistic

Table 33: Statistical analysis of the percentage of NeuN⁺ and TBR1⁺ cells using the two-tailed Mann-Whitney U test

Comparison	p-value	sig	Mean + SD	Mean + SD
NeuN Val/Val vs Met/Met	0.0599	ns	77.08 ± 15.42; n = 14	85.36 ± 12.36; n = 33
TBR1 Val/Val vs Met/Met	0.2045	ns	75.88 ± 8.12; n = 7	70.88 ± 11.88; n = 15

Table 34: Statistical analysis of BDNF and NTRK2 expression levels using the two-tailed Mann-Whitney U test

Comparison a vs b	p-value	sig	a: Mean ± SD	b: Mean ± SD
BDNF Progenitors vs Neurons	0.0211	*	0.23 ± 0.10; n = 4	1.00 ± 0.0; n = 4
BDNF Val/Val vs Met/Met	0.2426	ns	1.09 ± 0.50; n = 10	70.88 ± 11.88; n = 20
NTRK2 Progenitors vs Neurons	0.0636	ns	0.37 ± 0.13; n = 3	1.00 ± 0.0; n = 3
NTRK2 Val/Val vs Met/Met	0.0636	ns	1.0 ± 0.0; n = 3	1.22 ± 0.28; n = 3

Table 35: Statistical analysis for BDNF and NTRKB expression levels using the Kruskal-Wallis test

Comparison a vs b	p-value	sig	a: Mean ± SD	b: Mean ± SD
BDNF	0.9329	ns		
Val/Val 1 vs Val/Val 2	> 0.05	ns	1.0 ± 0.0; n = 5	1.173 ± 0.7336; n = 5
Val/Val 1 vs Met/Met 1	> 0.05	ns		1.498 ± 0.7878; n = 6
Val/Val 1 vs Met/Met 2	> 0.05	ns		2.078 ± 1.126; n = 3
Val/Val 1 vs Met/Met 3	> 0.05	ns		1.867 ± 2.256; n = 3
Val/Val 1 vs Met/Met^{Iso} 1	> 0.05	ns		1.68 ± 1.318; n = 3
Val/Val 1 vs Met/Met^{Iso} 2	> 0.05	ns		2.07 ± 2.31; n = 3
Val/Val 2 vs Met/Met 1	> 0.05	ns		
Val/Val 2 vs Met/Met 2	> 0.05	ns		
Val/Val 2 vs Met/Met 3	> 0.05	ns		
Val/Val 2 vs Met/Met^{Iso} 1	> 0.05	ns		
Val/Val 2 vs Met/Met^{Iso} 2	> 0.05	ns		
NTRKB	0.2341	ns		
Val/Val 1 vs Val/Val 2	> 0.05	ns	1.0 ± 0.0; n = 3	0.717 ± 0.327; n = 3
Val/Val 1 vs Met/Met 1	> 0.05	ns		1.088 ± 0.1236; n = 3
Val/Val 1 vs Met/Met 2	> 0.05	ns		0.4793 ± 0.2318; n = 3
Val/Val 1 vs Met/Met 3	> 0.05	ns		0.7875 ± 0.4726; n = 3
Val/Val 1 vs Met/Met^{Iso} 1	> 0.05	ns		1.241 ± 0.7013; n = 3
Val/Val 1 vs Met/Met^{Iso} 2	> 0.05	ns		1.279 ± 0.4156; n = 3
Val/Val 2 vs Met/Met 1	> 0.05	ns		
Val/Val 2 vs Met/Met 2	> 0.05	ns		
Val/Val 2 vs Met/Met 3	> 0.05	ns		
Val/Val 2 vs Met/Met^{Iso} 1	> 0.05	ns		
Val/Val 2 vs Met/Met^{Iso} 2	> 0.05	ns		

Table 36: Statistical analysis for BDNF density and localization using the Kruskal-Wallis test

Comparison a vs b	p-value	sig	a: Mean ± SD	b: Mean ± SD
BDNF density				
Val/Val MAP vs Val/Val TAU	< 0.001	***	108.4 ± 44.77; n = 60	54.33 ± 24.84; n = 30

Val/Val MAP vs Met/Met MAP	> 0.05	ns		87.11 ± 32.40; n = 45
Met/Met MAP vs Met/Met TAU	< 0.05	*		n = 40
Val/Val TAU vs Met/Met TAU	> 0.05	ns		
Val/Val 1 vs Val/Val 2	> 0.05	ns	123.1 ± 51.92; n = 77	130.6 ± 29.71; n = 25
Val/Val 1 vs Val/Val 3	> 0.05	ns		118.6 ± 53.22; n = 72
Val/Val 1 vs Met/Met 1	> 0.05	ns		100.1 ± 23.4; n = 60
Val/Val 1 vs Met/Met 2	> 0.05	ns		105.7 ± 36.81; n = 72
Val/Val 1 vs Met/Met 3	< 0.05	*		91.89 ± 13.63; n = 40
Val/Val 2 vs Val/Val 3	> 0.05	ns		
Val/Val 2 vs Met/Met 1	< 0.01	**		
Val/Val 2 vs Met/Met 2	> 0.05	ns		
Val/Val 2 vs Met/Met 3	< 0.001	***		
Val/Val 3 vs Met/Met 1	> 0.05	ns		
Val/Val 3 vs Met/Met 2	> 0.05	ns		
Val/Val 3 vs Met/Met 3	> 0.05	ns		
Val/Val 1 vs Met/Met^{lso} 1	< 0.001	***		74.69 ± 43.22; n = 78
Val/Val 1 vs Met/Met^{lso} 2	< 0.001	***		68.79 ± 18.64; n = 85
BDNF intensity at soma				
Val/Val 1 vs Val/Val 2	< 0.001	***	1.0 ± 0.60; n = 50	1.89 ± 0.93; n = 61
Val/Val 1 vs Met/Met 2	< 0.001	***		2.85 ± 2.12; n = 68
Val/Val 1 vs Met/Met 3	< 0.001	***		2.95 ± 2.65; n = 70
Val/Val 1 vs Met/Met^{lso} 1	< 0.001	***		3.97 ± 2.57; n = 50
Val/Val 2 vs Met/Met 2	> 0.05	ns		
Val/Val 2 vs Met/Met 3	> 0.05	ns		
Val/Val 2 vs Met/Met^{lso} 1	< 0.01	**		
BDNF SCG2 colocalization	0.7837	ns		
Val/Val 1 vs Val/Val 2	> 0.05	ns	63.25 ± 10.50; n = 19	63.82 ± 14.78; n = 19
Val/Val 1 vs Met/Met1	> 0.05	ns		56.47 ± 28.05; n = 22
Val/Val 1 vs Met/Met 2	> 0.05	ns		56.07 ± 22.36; n = 15
Val/Val 2 vs Met/Met 1	> 0.05	ns		
Val/Val 2 vs Met/Met 2	> 0.05	ns		

Table 37: Statistical analysis of BDNF density and localization using the two-tailed Mann-Whitney U test

Comparison a vs b	**p-value**	**sig**	**a: Mean ± SD**	**b: Mean ± SD**
% MAP2 Val/Val vs Met/Met	0.5608	ns	76.21 ± 31.03; n = 20	67.49 ± 32.51; n = 20
% TAU Val/Val vs Met/Met	0.4359	ns	23.79 ± 13.65; n = 10	32.51 ± 22.31; n = 10
Density Val/Val vs Met/Met	0.0009	***	122.3 ± 49.85; n = 174	100.6 ± 28.68; n = 172
Size Val 1 vs Met^{lso} 1	0.0089	**	0.89 ± 0.51; n = 30	0.62 ± 0.62; n = 30
Soma Val/Val vs Met/Met	< 0.001	***	1.49 ± 0.91; n = 111	3.35 ± 2.99; n = 190
SCG2 Val/Val vs Met/Met	0.4679	ns	63.54 ± 12.65; n = 38	56.31 ± 25.56; n = 37

Table 38: Statistical analysis for neurite length and branching using the Kruskal-Wallis test

Comparison a vs b	**p-value**	**sig**	**a: Mean ± SD**	**b: Mean ± SD**
Length day 1				
Val/Val 1 vs Val/Val 2	> 0.05	ns	108.1 ± 56.89; n = 496	108.4 ± 44.77; n = 542
Val/Val 1 vs Val/Val 3	< 0.001	***		88.36 ± 45.89; n = 441
Val/Val 1 vs Met/Met 1	> 0.05	ns		104.7 ± 48.69; n = 377
Val/Val 1 vs Met/Met 2	< 0.01	**		98.51 ± 60.31; n = 355

Val/Val 1 vs Met/Met 3	< 0.001	***		69.66 ± 32.89; n = 329
Val/Val 2 vs Val/Val 3	< 0.001	***		
Val/Val 2 vs Met/Met 1	< 0.01	ns		
Val/Val 2 vs Met/Met 2	< 0.001	***		
Val/Val 2 vs Met/Met 3	< 0.001	***		
Val/Val 3 vs Met/Met 1	< 0.001	***		
Val/Val 3 vs Met/Met 2	> 0.05	ns		
Val/Val 3 vs Met/Met 3	< 0.001	***		
Val/Val 1 vs Met/Met^{lso} 1	< 0.001	***		93.29 ± 64.97; n = 202
Val/Val 1 vs Met/Met^{lso} 2	< 0.001	***		91.07 ± 49.64; n = 403
Length day 3				
Val/Val 1 vs Met/Met^{lso} 1	< 0.001	***	179.2 ± 97.15; n = 424	135.8 ± 62.40; n = 188
Val/Val 1 vs Met/Met^{lso} 2	< 0.001	***		129.2 ± 59.90; n = 266
Length day 5				
Val/Val 1 vs Val/Val 2	< 0.001	***	344.6 ± 127.9; n = 283	265.0 ± 87.81; n = 374
Val/Val 1 vs Val/Val 3	< 0.001	***		268.2 ± 115.2; n = 376
Val/Val 1 vs Met/Met 1	< 0.001	***		227.7 ± 87.20; n = 355
Val/Val 1 vs Met/Met 2	< 0.001	***		223.3 ± 132.9; n = 311
Val/Val 1 vs Met/Met 3	< 0.001	***		161.0 ± 80.23; n = 263
Val/Val 2 vs Val/Val 3	> 0.05	ns		
Val/Val 2 vs Met/Met 1	< 0.001	***		
Val/Val 2 vs Met/Met 2	< 0.001	***		
Val/Val 2 vs Met/Met 3	< 0.001	***		
Val/Val 3 vs Met/Met 1	< 0.001	***		
Val/Val 3 vs Met/Met 2	< 0.001	***		
Val/Val 3 vs Met/Met 3	< 0.001	***		
Val/Val 1 vs Met/Met^{lso} 1	< 0.001	***		222.2 ± 104.2; n = 186
Val/Val 1 vs Met/Met^{lso} 2	< 0.001	***		248.7 ± 110.4; n = 347
Val/Val 1 vs Val 1 10 ng/µl BDNF	< 0.01	**		316.3 ± 184.6; n = 185
Val/Val 1 vs Val 1 20 ng/µl BDNF	> 0.05	ns		330.2 ± 140.4; n = 242
Met^{lso} vs Met^{lso} 1 10 ng/µl BDNF	< 0.001	***		334.5 ± 258.0; n = 273
Met^{lso} vs Met^{lso} 1 20 ng/µl BDNF	< 0.001	***		353.5 ± 154.8; n = 242
Primary day 1				
Val/Val 1 vs Val/Val 2	> 0.05	ns	2.24 ± 0.90; n = 154	2.31 ± 0.59; n = 179
Val/Val 1 vs Val/Val 3	> 0.05	ns		2.58 ± 1.24; n = 174
Val/Val 1 vs Met/Met 1	> 0.05	ns		2.40 ± 1.27; n = 172
Val/Val 1 vs Met/Met 2	> 0.05	ns		2.09 ± 0.97; n = 177
Val/Val 1 vs Met/Met 3	> 0.05	ns		2.27 ± 1.02; n = 154
Val/Val 2 vs Val/Val 3	> 0.05	ns		
Val/Val 2 vs Met/Met 1	> 0.05	ns		
Val/Val 2 vs Met/Met 2	< 0.05	*		
Val/Val 2 vs Met/Met 3	> 0.05	ns		
Val/Val 3 vs Met/Met 1	> 0.05	ns		
Val/Val 3 vs Met/Met 2	< 0.01	**		
Val/Val 3 vs Met/Met 3	> 0.05	ns		
Val/Val 1 vs Met/Met^{lso} 1	> 0.05	ns		2.32 ± 1.09; n = 202
Val/Val 1 vs Met/Met^{lso} 2	> 0.05	ns		2.31 ± 1.00; n = 403
Primary day 3				
Val/Val 1 vs Val/Val 2	> 0.05	ns	3.10 ± 1.19; n = 160	2.72 ± 0.81; n = 151
Val/Val 1 vs Val/Val 3	< 0.001	***		3.77 ± 1.39; n = 154

Val/Val 1 vs Met/Met 1	> 0.05	ns		2.85 ± 1.32; n = 162
Val/Val 1 vs Met/Met 2	< 0.001	***		1.97 ± 0.85; n = 170
Val/Val 1 vs Met/Met 3	< 0.001	***		2.49 ± 1.09; n = 126
Val/Val 2 vs Val/Val 3	< 0.001	***		
Val/Val 2 vs Met/Met 1	> 0.05	ns		
Val/Val 2 vs Met/Met 2	< 0.001	***		
Val/Val 2 vs Met/Met 3	> 0.05	ns		
Val/Val 3 vs Met/Met 1	< 0.001	***		
Val/Val 3 vs Met/Met 2	< 0.001	***		
Val/Val 3 vs Met/Met 3	< 0.001	***		
Val/Val 1 vs Met/Met^{lso} 1	< 0.05	*		2.73 ± 1.04; n = 188
Val/Val 1 vs Met/Met^{lso} 2	< 0.001	***		2.58 ± 0.97; n = 265
Primary day 5				
Val/Val 1 vs Val/Val 2	> 0.05	ns	3.05 ± 1.15; n = 129	2.92 ± 0.90; n = 155
Val/Val 1 vs Val/Val 3	< 0.001	***		3.84 ± 1.20; n = 163
Val/Val 1 vs Met/Met 1	< 0.001	***		2.53 ± 1.10; n = 163
Val/Val 1 vs Met/Met 2	< 0.001	***		2.06 ± 0.71; n = 161
Val/Val 1 vs Met/Met 3	< 0.001	***		2.37 ± 1.03; n = 137
Val/Val 2 vs Val/Val 3	> 0.05	***		
Val/Val 2 vs Met/Met 1	< 0.01	**		
Val/Val 2 vs Met/Met 2	< 0.001	***		
Val/Val 2 vs Met/Met 3	< 0.001	***		
Val/Val 3 vs Met/Met 1	< 0.001	***		
Val/Val 3 vs Met/Met 2	< 0.001	***		
Val/Val 3 vs Met/Met 3	< 0.001	***		
Val/Val 1 vs Met/Met^{lso} 1	> 0.05	ns		2.91 ± 1.25; n = 186
Val/Val 1 vs Met/Met^{lso} 2	< 0.001	***		2.57 ± 0.88; n = 346
Val/Val 1 vs Val 1 BDNF	> 0.05	ns	2.57 ± 1.11; n = 195	2.39 ± 1.24; n = 183
Val/Val 1 vs Met/Met^{lso} 1	< 0.01	*		
Met^{lso} vs Met^{lso} 1 BDNF	> 0.05	ns	2.28 ± 0.96; n = 269	2.31 ± 0.85; n = 271
Val 1 BDNF vs Met^{lso} 1 BDNF	> 0.05	ns		
Branch points day 1				
Val/Val 1 vs Val/Val 2	< 0.001	***	0.49 ± 0.87; n = 505	0.25 ± 0.47; n = 560
Val/Val 1 vs Val/Val 3	> 0.05	ns		0.37 ± 0.84; n = 357
Val/Val 1 vs Met/Met 1	> 0.05	ns		0.32 ± 0.61; n = 343
Val/Val 1 vs Met/Met 2	> 0.05	ns		0.35 ± 0.69; n = 332
Val/Val 1 vs Met/Met 3	< 0.05	*		0.35 ± 0.78; n = 344
Val/Val 2 vs Val/Val 3	> 0.05	ns		
Val/Val 2 vs Met/Met 1	> 0.05	ns		
Val/Val 2 vs Met/Met 2	< 0.05	ns		
Val/Val 2 vs Met/Met 3	> 0.05	ns		
Val/Val 3 vs Met/Met 1	> 0.05	ns		
Val/Val 3 vs Met/Met 2	> 0.05	ns		
Val/Val 3 vs Met/Met 3	> 0.05	ns		
Val/Val 1 vs Met/Met^{lso} 1	> 0.05	ns		0.56 ± 0.91; n = 202
Val/Val 1 vs Met/Met^{lso} 2	> 0.05	ns		0.37 ± 0.71; n = 403
Branch points day 3				
Val/Val 1 vs Val/Val 2	> 0.05	ns	1.16 ± 1.21; n = 397	0.99 ± 1.00; n = 476
Val/Val 1 vs Val/Val 3	< 0.001	***		2.00 ± 1.59; n = 392
Val/Val 1 vs Met/Met 1	< 0.001	***		0.56 ± 0.90; n = 448

Val/Val 1 vs Met/Met 2	< 0.001	***		0.72 ± 1.15; n = 303
Val/Val 1 vs Met/Met 3	< 0.001	***		0.51 ± 0.82; n = 273
Val/Val 2 vs Val/Val 3	< 0.001	***		
Val/Val 2 vs Met/Met 1	< 0.001	***		
Val/Val 2 vs Met/Met 2	< 0.001	***		
Val/Val 2 vs Met/Met 3	< 0.001	***		
Val/Val 3 vs Met/Met 1	< 0.001	***		
Val/Val 3 vs Met/Met 2	< 0.001	***		
Val/Val 3 vs Met/Met 3	< 0.001	***		
Val/Val 1 vs Met/Met^{lso} 1	< 0.001	***		0.70 ± 0.97; n = 188
Val/Val 1 vs Met/Met^{lso} 2	< 0.001	***		0.63 ± 0.87; n = 265
Branch points day 5				
Val/Val 1 vs Val/Val 2	< 0.001	***	2.16 ± 1.85; n = 281	1.36 ± 1.23; n = 376
Val/Val 1 vs Val/Val 3	> 0.05	ns		1.97 ± 1.42; n = 372
Val/Val 1 vs Met/Met 1	< 0.001	***		0.62 ± 1.06; n = 351
Val/Val 1 vs Met/Met 2	< 0.001	***		0.76 ± 1.12; n = 309
Val/Val 1 vs Met/Met 3	< 0.001	***		0.70 ± 0.94; n = 259
Val/Val 2 vs Val/Val 3	> 0.05	***		
Val/Val 2 vs Met/Met 1	< 0.01	**		
Val/Val 2 vs Met/Met 2	< 0.001	***		
Val/Val 2 vs Met/Met 3	< 0.001	***		
Val/Val 3 vs Met/Met 1	< 0.001	***		
Val/Val 3 vs Met/Met 2	< 0.001	***		
Val/Val 3 vs Met/Met 3	< 0.001	***		
Val/Val 1 vs Met/Met^{lso} 1	< 0.001	***		0.98 ± 1.05; n = 186
Val/Val 1 vs Met/Met^{lso} 2	< 0.001	***		0.88 ± 1.15; n = 347
Val/Val 1 vs Val 1 10 ng/µl BDNF	> 0.05	ns		0.56 ± 0.78; n = 160
Val/Val 1 vs Val 1 20 ng/µl BDNF	> 0.05	ns		1.13 ± 1.35; n = 240
Met^{lso} vs Met^{lso} 1 10 ng/µl BDNF	< 0.001	***		0.73 ± 1.17; n = 271
Met^{lso} vs Met^{lso} 1 20 ng/µl BDNF	< 0.001	***		1.95 ± 1.45; n = 240

Table 39: Statistical analysis of neurite length and branching using the two-tailed Mann-Whitney U test

Comparison a vs b	**p-value**	**sig**	**a: Mean ± SD**	**b: Mean ± SD**
Length				
day 1 Val/Val vs Met/Met	< 0.001	***	102.3 ± 50.3; n = 1479	91.8 ± 51.2; n = 1061
day 3 Val/Val vs Met/Met	0.0070	**	202.0 ± 88.7; n = 1274	194.2 ± 101.7; n = 706
day 5 Val/Val vs Met/Met	< 0.001	***	288.0 ± 115.3; n = 1033	207.5 ± 107.0; n = 928
Primary				
day 1 Val/Val vs Met/Met	0.0034	**	2.38 ± 0.96; n = 507	2.24 ± 1.14; n = 349
day 3 Val/Val vs Met/Met	< 0.001	***	3.20 ± 1.24; n = 465	2.42 ± 1.16; n = 458
day 5 Val/Val vs Met/Met	< 0.001	***	3.29 ± 1.17; n = 447	2.32 ± 0.98; n = 461
Branch points				
day 1 Val/Val vs Met/Met	0.3593	ns	0.34 ± 0.74; n = 1422	0.34 ± 0.70; n = 1019
day 3 Val/Val vs Met/Met	< 0.001	***	1.36 1.34; n = 1265	0.59 0.96; n = 1024
day 5 Val/Val vs Met/Met	< 0.001	***	1.80 ± 1.53; n = 1029	0.69 ± 1.05; n = 919

Table 40: Statistical analysis for Sholl analysis using the Kruskal-Wallis test

Comparison a vs b	p-value	sig	a: Mean ± SD	b: Mean ± SD
Total Length				
Val/Val 1 vs Val/Val 2	< 0.05	*	726.3 ± 332.5; n = 240	881.8 ± 440.6; n = 240
Val/Val 1 vs Met/Met 1	< 0.001	***		402.8 ± 159.1; n = 240
Val/Val 1 vs Met/Met 2	< 0.001	***		451.7 ± 181.3; n = 245
Val/Val 1 vs Met/Met 3	< 0.001	***		406.5 ± 175.7; n = 220
Val/Val 2 vs Met/Met 1	< 0.001	***		
Val/Val 2 vs Met/Met 2	< 0.001	***		
Val/Val 2 vs Met/Met 3	< 0.001	***		
Val/Val 1 vs Met/Met^{lso} 1	< 0.001	***		468.3 ± 250.0; n = 180
Val/Val 1 vs Val/Val 1 BDNF	< 0.001	***		1043 ± 392.1; n = 109
Met/Met^{lso} 1 vs Met^{lso} 1 BDNF	< 0.001	***		1072 ± 409.3; n = 179
Val 1 BDNF vs Met^{lso} 1 BDNF	< 0.05	ns		
Sum of intersections				
Val/Val 1 vs Val/Val 2	< 0.05	*	29.05 ± 13.30; n = 240	35.27 ± 17.62; n = 240
Val/Val 1 vs Met/Met 1	< 0.001	***		16.11 ± 6.365; n = 240
Val/Val 1 vs Met/Met 2	< 0.001	***		18.07 ± 7.250; n = 245
Val/Val 1 vs Met/Met 3	< 0.001	***		16.26 ± 7.028; n = 220
Val/Val 2 vs Met/Met 1	< 0.001	***		
Val/Val 2 vs Met/Met 2	< 0.001	***		
Val/Val 2 vs Met/Met 3	< 0.001	***		
Val/Val 1 vs Met/Met^{lso} 1	< 0.001	***		18.73 ± 9.99; n = 180
Val/Val 1 vs Val/Val 1 BDNF	< 0.001	***		41.73 ± 15.68; n = 109
Met/Met^{lso} 1 vs Met^{lso} 1 BDNF	< 0.001	***		42.88 ± 16.37; n = 179
Val 1 BDNF vs Met^{lso} 1 BDNF	ns			
Processes from soma				
Val/Val 1 vs Val/Val 2	< 0.001	***	6.063 ± 2.547; n = 240	6.583 ± 2.799; n = 240
Val/Val 1 vs Met/Met 1	< 0.001	***		4.504 ± 2.199; n = 240
Val/Val 1 vs Met/Met 2	< 0.001	***		3.763 ± 2.000; n = 245
Val/Val 1 vs Met/Met 3	< 0.001	***		4.774 ± 2.357; n = 220
Val/Val 2 vs Met/Met 1	< 0.001	***		
Val/Val 2 vs Met/Met 2	< 0.001	***		
Val/Val 2 vs Met/Met 3	< 0.001	***		
Val/Val 1 vs Met/Met^{lso} 1	< 0.001	***		5.439 ± 3.118; n = 180
Val/Val 1 vs Val/Val 1 BDNF	< 0.05	*		7.275 ± 2.309; n = 109
Met/Met^{lso} 1 vs Met^{lso} 1 BDNF	< 0.001	***		8.676 ± 3.068; n = 179
Val 1 BDNF vs Met^{lso} 1 BDNF	< 0.05	*		

Table 41: Statistical analysis of Sholl analysis using the two-tailed Mann-Whitney U test

Comparison a vs b	p-value	sig	a: Mean ± SD	b: Mean ± SD
Length Val/Val vs Met/Met	< 0.001	***	804.0 ± 397.6; n = 480	421.0 ± 173.5; n = 705
Sum Val/Val vs Met/Met	< 0.001	***	32.16 ± 15.90; n = 480	16.84 ± 6.94; n = 705
Processes Val/Val vs Met/Met	< 0.001	***	6.353 ± 2.686; n = 480	4.330 ± 2.223; n = 705

Table 42: Statistical analysis of synaptic proteins using the Kruskal-Wallis test

Comparison a vs b	p-value	sig	a: Mean ± SD	b: Mean ± SD
SYN				

Val/Val 1 vs Val/Val 2	< 0.001	***	65.72 ± 29.46; n = 150	91.35 ± 34.11; n = 150
Val/Val 1 vs Met/Met 2	> 0.05	ns		61.56 ± 30.37; n = 120
Val/Val 1 vs Met/Met 3	< 0.001	***		28.30 ± 20.55; n = 130
Val/Val 2 vs Met/Met 2	< 0.001	***		
Val/Val 2 vs Met/Met 3	< 0.001	***		
Val/Val 1 vs Met/Met^{lso} 1	< 0.001	***		42.59 ± 17.36; n = 150
Val/Val 1 vs Val/Val 1 BDNF	< 0.001	***		89.06 ± 46.94; n = 200
Met/Met^{lso} 1 vs Met^{lso} 1 BDNF	< 0.001	***		88.87± 52.96; n = 150
Val 1 BDNF vs Met^{lso} 1 BDNF	> 0.05	ns		
PSD95				
Val/Val 1 vs Val/Val 2	< 0.001	***	52.79 ± 38.73; n = 150	82.00 ± 38.15; n = 150
Val/Val 1 vs Met/Met 2	< 0.001	***		25.96 ± 20.16; n = 120
Val/Val 1 vs Met/Met 3	< 0.001	***		28.30 ± 20.55; n = 130
Val/Val 2 vs Met/Met 2	< 0.001	***		
Val/Val 2 vs Met/Met 3	< 0.001	***		
Val/Val 1 vs Met/Met^{lso} 1	< 0.001	***		31.08 ± 21.78; n = 150
Val/Val 1 vs Val/Val 1 BDNF	< 0.001	***		85.37 ± 48.30; n = 200
Met/Met^{lso} 1 vs Met^{lso} 1 BDNF	< 0.001	***		55.04 ± 33.38; n = 150
Val 1 BDNF vs Met^{lso} 1 BDNF	< 0.001	***		
SYN/PSD95				
Val/Val 1 vs Val/Val 2	> 0.05	ns	23.33 ± 28.82; n = 150	13.15 ± 8.56; n = 150
Val/Val 1 vs Met/Met 2	> 0.05	ns		13.14 ± 12.94; n = 120
Val/Val 1 vs Met/Met 3	< 0.001	***		3.62 ± 4.53; n = 130
Val/Val 2 vs Met/Met 2	> 0.05	ns		
Val/Val 2 vs Met/Met 3	< 0.001	***		73.07 ± 41.06; n = 106
Val/Val 1 vs Met/Met^{lso} 1	< 0.001	***		12.66 ± 14.35; n = 150
Val/Val 1 vs Val/Val 1 BDNF	< 0.001	***		33.94 ± 24.98; n = 200
Met/Met^{lso} 1 vs Met^{lso} 1 BDNF	< 0.001	***		19.37 ± 14.93; n = 150
Val 1 BDNF vs Met^{lso} 1 BDNF	< 0.001	***		

Table 43: Statistical analysis of synaptic proteins using the two-tailed Mann-Whitney U test

Comparison a vs b	**p-value**	**sig**	**a: Mean ± SD**	**b: Mean ± SD**
SYN Val/Val vs Met/Met	< 0.001	***	78.54 ± 34.31; n = 300	54.51 ± 28.08; n = 250
PSD95 Val/Val vs Met/Met	< 0.001	***	67.40 ± 41.07; n = 300	27.18 ± 30.36; n = 250
SYN/PSD Val/Val vs Met/Met	< 0.001	***	18.24 ± 21.50; n = 300	8.19 ± 10.64; n = 250
SYN WB Val/Val vs Met/Met	0.0148	*		
PSD95 Val 1 vs Met^{lso} 1	< 0.001	***	57.74 ± 20.15; n = 75	39.41 ± 20.33; n = 70
HOMER Val 1 vs Met^{lso} 1	< 0.001	***	64.52 ± 20.12; n = 75	41.07 ± 17.10; n = 70
PSD/HOMER Val 1 vs Met^{lso} 1	< 0.001	***	31.85 ± 11.82; n = 75	15.24 ± 9.51; n = 70

Table 44: Statistical analysis for calcium imaging using the Kruskal-Wallis test

Comparison a vs b	**p-value**	**sig**	**a: Mean ± SD**	**b: Mean ± SD**
Single neurons Frequency	0.0028	**		
Val 1 low vs Val 1 high	> 0.05	ns	1.02 ± 0.18; n = 15	0.99 ± 0.28; n = 9
Val 1 high vs Met^{lso} 1 high	> 0.05	ns		
Met^{lso} 1 low vs Met^{lso} 1 high	> 0.05	ns	0.79 ± 0.21; n = 15	0.79 ± 0.17; n = 9
Single neurons Amplitude	0.0021	**		

Val 1 low vs Val 1 high	> 0.05	ns	0.34 ± 0.10; n = 15	0.24 ± 0.06; n = 9
Val 1 high vs Met^{Iso} 1 high	> 0.05	ns		
Met^{Iso} 1 low vs Met^{Iso} 1 high	> 0.05	ns	0.23 ± 0.06; n = 15	0.19 ± 0.05; n = 9
Network activity Frequency	0.2800	ns		
Val 1 low vs Val 1 high	> 0.05	ns	0.56 ± 0.54; n = 15	1.26 ± 1.02; n = 9
Val 1 high vs Met^{Iso} 1 high	> 0.05	ns		
Met^{Iso} 1 low vs Met^{Iso} 1 high	> 0.05	ns	0.47 ± 0.39; n = 15	0.74 ± 0.60; n = 9
Network activity Amplitude	0.0016	**		
Val 1 low vs Val 1 high	< 0.01	**	0.24 ± 0.12; n = 10	0.08 ± 0.04; n = 9
Val 1 high vs Met^{Iso} 1 high	> 0.05	ns		
Met^{Iso} 1 low vs Met^{Iso} 1 high	> 0.05	ns	0.13 ± 0.06; n = 13	0.08 ± 0.05; n = 8

Table 45: Statistical analysis of calcium imaging using the two-tailed Mann-Whitney U test

Comparison a vs b	**p-value**	**sig**	**a: Mean ± SD**	**b: Mean ± SD**
Single neurons dynamics				
Frequency Val 1 vs Met^{Iso} 1	0.0008	***	1.02 ± 0.18; n = 15	0.79 ± 0.21; n = 15
Amplitude Val 1 vs Met^{Iso} 1	0.0037	**	0.34 ± 0.10; n = 15	0.23 ± 0.06; n = 15
Network activity				
Frequency Val 1 vs Met^{Iso} 1	0.8493	ns	0.56 ± 0.54; n = 15	0.47 ± 0.39; n = 15
Amplitude Val 1 vs Met^{Iso} 1	0.0255	*	0.24 ± 0.12; n = 10	0.13 ± 0.06; n = 13
Synchronization Val 1 vs Met^{Iso} 1	0.4698	ns	0.10 ± 0.09; n = 7	0.06 ± 0.06; n = 9

Table 46: Statistical analysis of electrophysiological measurements using the two-tailed Mann-Whitney U test

Comparison a vs b	**p-value**	**sig**	**a: Mean ± SD**	**b: Mean ± SD**
Na^{2+} Val 1 vs Met^{Iso} 1	0.3080	ns	-2078 ± 1263; n = 17	-1641 ± 606.8; n = 8
K^{+} Val 1 vs Met^{Iso} 1	0.8384	ns	1894 ± 1000; n = 17	1941 ± 685.1; n = 8
#AP Val 1 vs Met^{Iso} 1	0.7962	ns	33.80 ± 14.93; n = 17	36.25 ± 15.95; n = 8
AP amplitude Val 1 vs Met^{Iso} 1	0.7712	ns	94.64 ± 19.18; n = 17	91.99 ± 20.76; n = 8
Resistance Val 1 vs Met^{Iso} 1	0.0432	*	-1.89 ± 0.65; n = 17	-2.46 ± 0.46; n = 8
Capacitance Val 1 vs Met^{Iso} 1	0.8384	ns	-128.8 ± 87.97; n = 17	-145.9 ± 34.26; n = 8
sEPSCs + astrocytes				
Frequency Val 1 vs Met^{Iso} 1	0.0025	**	1.08 ± 1.30; n = 19	0.37 ± 0.37; n = 15
Amplitude Val 1 vs Met^{Iso} 1	0.0611	ns	18.90 ± 6.90; n = 19	23.45 ± 8.11; n = 15
sEPSCs - astrocytes				
Frequency Val 1 vs Met^{Iso} 1	0.1097	ns	1.71 ± 2.37; n = 17	0.92 ± 1.35; n = 11
Amplitude Val 1 vs Met^{Iso} 1	0.3715	ns	18.71 ± 6.99; n = 17	21.58 ± 8.83; n = 11
mEPSC				
Frequency Val 1 vs Met^{Iso} 1	0.0721	ns	1.12 ± 0.76; n = 20	0.68 ± 0.55; n = 16
Amplitude Val 1 vs Met^{Iso} 1	0.4738	ns	14.88 ± 4.73; n = 20	15.09 ± 2.38; n = 16
Frequency Val 1 vs Met^{Iso} 2	< 0.001	***	1.05 ± 0.7692; n = 21	0.25 ± 0.21; n = 47
Amplitude Val 1 vs Met^{Iso} 2	< 0.001	***	23.24 ± 4.27; n = 21	19.32 ± 3.69; n =47

Table 47: Statistical analysis for NMDA receptors using the Kruskal-Wallis test

Comparison a vs b	p-value	sig	a: Mean ± SD	b: Mean ± SD
GRIN1	0.0443	*		
Val/Val 1 vs Val/Val 2	> 0.05	ns	1.0 ± 0.0; n = 8	1.9 ± 2.3; n = 6
Val/Val 1 vs Met/Met 1	> 0.05	ns		0.9 ± 0.5; n = 6
Val/Val 1 vs Met/Met 2	< 0.05	*		0.3 ± 0.3; n = 8
Val/Val 1 vs Met/Met 3	> 0.05	ns		1.3 ± 1.6; n = 4
Val/Val 2 vs Met/Met 1	> 0.05	ns		
Val/Val 2 vs Met/Met 2	> 0.05	ns		
Val/Val 2 vs Met/Met 3	> 0.05	ns		
GRIN2	< 0.0001	***		
Val/Val 1 vs Val/Val 2	> 0.05	ns	1.0 ± 0.0; n = 14	0.8 ± 0.6; n = 6
Val/Val 1 vs Met/Met 1	> 0.05	ns		0.3 ± 0.2; n = 5
Val/Val 1 vs Met/Met 2	< 0.001	***		0.1 ± 0.1; n = 6
Val/Val 1 vs Met/Met 3	> 0.05	ns		0.4 ± 0.4; n = 4
Val/Val 2 vs Met/Met 1	> 0.05	ns		
Val/Val 2 vs Met/Met 2	> 0.05	ns		
Val/Val 2 vs Met/Met 3	> 0.05	ns		
NMDAR2B	< 0.0001	***		
Val/Val 1 vs Val/Val 2	> 0.05	ns	94.78 ± 50.79; n = 112	104.1 ± 47.70; n = 106
Val/Val 1 vs Met/Met 1	> 0.05	ns		95.00 ± 38.62; n = 106
Val/Val 1 vs Met/Met 2	< 0.05	*		73.07 ± 41.06; n = 106
Val/Val 1 vs Met/Met 3	> 0.05	ns		77.37 ± 29.06; n = 72
Val/Val 2 vs Met/Met 1	> 0.05	ns		
Val/Val 2 vs Met/Met 2	< 0.001	***		
Val/Val 2 vs Met/Met 3	< 0.001	***		

Table 48: Statistical analysis of NMDA receptors using the two-tailed Mann-Whitney U test

Comparison a vs b	p-value	sig	a: Mean ± SD	b: Mean ± SD
GRIN1 Val/Val vs Met/Met	0.0123	*	1.0 ± 1.1; n = 14	0.4 ± 0.3; n = 17
GRIN2 Val/Val vs Met/Met	0.0002	***	1.0 ± 0.5; n = 14	0.3 ± 0.1; n = 15
NMDAR2B Val/Val vs Met/Met	0.0003	***	99.29 ± 49.42; n = 218	82.35 ± 38.59; n = 284
NMDAR2B Val 1 vs Met^{lso} 1	0.0168	*	94.78 ± 50.79; n = 112	75.41 ± 44.30; n = 110

Appendix II, Plasmid Sequence

>pX459-BDNF gRNA-Cas9-Puro

U6 promotor gRNA gRNA scaffold CMV enhancer hSpCas9 T2A PuromycinR AmpicillinR

gagggcctatttcccatgattccttcatatttgcatatacgatacaaggctgttagagagataattggaattaatttgactgtaaacacaaagatattagtacaaa
atacgtgacgtagaaagtaataatttcttgggtagtttgcagttttaaaattatgttttaaaatggactatcatatgcttaccgtaacttgaaagtatttcgatttctt
ggctttatatatcttgtggaaaggacCACCGACACGTGATAGAAGAGCTGTgttttagagctagaaatagcaagttaaaataaggctagtccgttatc
aacttgaaaaagtggcaccgagtcggtgcttttttgttttagagctagaaatagcaagttaaaataaggctagtccgtttttagcgcgtgcgccaattctgcagac
aaatggctctagaggtacccgttacataacttacggtaaatggcccgcctggctgaccgcccaacgacccccgcccattgacgtcaatagtaacgccaataggg
actttccattgacgtcaatgggtggagtatttacggtaaactgcccacttggcagtacatcaagtgtatcatatgccaagtacgccccctattgacgtcaatgacg
gtaaatggcccgcctggcattgtgcccagtacatgaccttatgggactttcctacttggcagtacatctacgtattagtcatcgctattaccatggtcgaggtgagc
cccacgttctgcttcactctcccatctccccccctcccaccccaattttgtatttatttatttttttaattattttgtgcagcgatgggggcgggggggggggggg
ggcgcgcgccaggcggggcggggcggggcgaggggcggggcggggcgaggcggagaggtgcggcggcagccaatcagagcggcgcgctccgaaagtttcc
ttttatggcgaggcggcggcggcggccctataaaaagcgaagcgcgcggcgggcgggagtcgctgcgcgctgccttcgccccgtgccccgctccgccgccg
cctcgcgccgcccgccccggctctgactgaccgcgttactcccacaggtgagcgggcgggacggcccttctcctccgggctgtaattagctgagcaagaggtaag
ggtttaagggatggttggttggtggggtattaatgtttaattacctggagcacctgcctgaaatcacttttttcaggttggaccggtgccaccatggactataagg
accacgacggagactacaaggatcatgatattgattacaaagacgatgacgataagatggccccaaagaagaagcggaaggtcggtatccacggagtcccag
cagccgacaagaagtacagcatcggcctggacatcggcaccaactctgtgggctgggccgtgatcaccgacgagtacaaggtgcccagcaagaaattcaaggt
gctgggcaacaccgaccggcacagcatcaagaagaacctgatcggagccctgctgttcgacagcggcgaaacagccgaggccacccggctgaagagaaccg
ccagaagaagatacaccagacggaagaaccggatctgctatctgcaagagatcttcagcaacgagatggccaaggtggacgacagcttcttccacagactgga
agagtccttcctggtggaagaggataagaagcacgagcggcaccccatcttcggcaacatcgtggacgaggtggcctaccacgagaagtaccccaccatctac
cacctgagaaagaaactggtggacagcaccgacaaggccgacctgcggctgatctatctggccctggcccacatgatcaagttccggggccacttcctgatcga
gggcgacctgaaccccgacaacagcgacgtggacaagctgttcatccagctggtgcagacctacaaccagctgttcgaggaaaaccccatcaacgccagcggc
gtggacgccaaggccatcctgtctgccagactgagcaagagcagacggctggaaaatctgatcgcccagctgcccggcgagaagaagaatggcctgttcggaa
acctgattgccctgagcctgggcctgacccccaacttcaagagcaacttcgacctggccgaggatgccaaactgcagctgagcaaggacacctacgacgacga
cctggacaacctgctggcccagatcggcgaccagtacgccgacctgtttctggccgccaagaacctgtccgacgccatcctgctgagcgacatcctgagagtga
acaccgagatcaccaaggcccccctgagcgcctctatgatcaagagatacgacgagcaccaccaggacctgaccctgctgaaagctctcgtgcggcagcagct
gcctgagaagtacaaagagattttcttcgaccagagcaagaacggctacgccggctacattgacggcggagccagccaggaagagttctacaagttcatcaag
cccatcctggaaaagatggacggcaccgaggaactgctcgtgaagctgaacagagaggacctgctgcggaagcagcggaccttcgacaacggcagcatcccc
caccagatccacctgggagagctgcacgccattctgcggcggcaggaagatttttacccattcctgaaggacaaccgggaaaagatcgagaagatcctgacctt
ccgcatcccctactacgtgggccctctggccaggggaaacagcagattcgcctggatgaccagaaagagcgaggaaaccatcacccccctggaacttcgaggaa
gtggtggacaagggcgcttccgcccagagcttcatcgagcggatgaccaacttcgataagaacctgcccaacgagaaggtgctgcccaagcacagcctgctgt
acgagtacttcaccgtgtataacgagctgaccaaagtgaaatacgtgaccgagggaatgagaaagcccgccttcctgagcggcgagcagaaaaaggccatcg
tggacctgctgttcaagaccaaccggaaagtgaccgtgaagcagctgaaagaggactacttcaagaaaatcgagtgcttcgactccgtggaaatctccggcgtg
gaagatcggttcaacgcctccctgggcacataccacgatctgctgaaaattatcaaggacaaggacttcctggacaatgaggaaaacgaggacattctggaag
atatcgtgctgaccctgacactgtttgaggacagagagatgatcgaggaacggctgaaaacctatgcccacctgttcgacgacaaagtgatgaagcagctgaa
gcggcggagatacaccggctggggcaggctgagccggaagctgatcaacggcatccgggacaagcagtccggcaagacaatcctggatttcctgaagtccga
cggcttcgccaacagaaacttcatgcagctgatccacgacgacagcctgaccttaaagaggacatccagaaagcccaggtgtccggccagggcgatagcctg
cacgagcacattgccaatctggccggcagccccgccattaagaagggcatcctgcagacagtgaaggtggtggacgagctcgtgaaagtgatgggccggcaca
agcccgagaacatcgtgatcgaaatggccagagagaaccagaccacccagaagggacagaagaacagccgcgagagaatgaagcggatcgaagagggcat
caaagagctgggcagccagatcctgaaagaacaccccgtggaaaacacccagctgcagaacgagaagctgtacctgtactacctgcagaatgggcgggatat
gtacgtggaccaggaactggacatcaaccggctgtccgactacgatgtggaccatatcgtgcctcagagctttctgaaggacgactccatcgacaacaaggtgc
tgaccagaagcgacaagaaccggggcaagagcgacaacgtgccctccgaagaggtcgtgaagaagatgaagaactactggcggcagctgctgaacgccaag
ctgattacccagagaaagttcgacaatctgaccaaggccgagagaggcggcctgagcgaactggataaggccggcttcatcaagagacagctggtggaaacc
cggcagatcacaaagcacgtggcacagatcctggactcccggatgaacactaagtacgacgagaatgacaagctgatccgggaagtgaaagtgatcaccctg
aagtccaagctggtgtccgatttccggaaggatttccagttttacaaagtgcgcgagatcaacaactaccaccacgcccacgacgcctacctgaacgccgtcgtg

ggaaccgccctgatcaaaaagtaccctaagctggaaagcgagttcgtgtacggcgactacaaggtgtacgacgtgcggaagatgatcgccaagagcgagcag
gaaatcggcaaggctaccgccaagtacttcttctacagcaacatcatgaacttttcaagaccgagattaccctggccaacggcgagatccggaagcggcctctg
atcgagacaaacggcgaaaccggggagatcgtgtgggataagggccgggattttgccaccgtgcggaaagtgctgagcatgccccaagtgaatatcgtgaaa
aagaccgaggtgcagacaggcggcttcagcaaagagtctatcctgcccaagaggaacagcgataagctgatcgccagaaagaaggactgggaccctaagaa
gtacggcggcttcgacagccccaccgtggcctattctgtgctggtggtggccaaagtggaaaagggcaagtccaagaaactgaagagtgtgaaagagctgctg
gggatcaccatcatggaaagaagcagcttcgagaagaatcccatcgactttctggaagccaagggctacaaagaagtgaaaaaggacctgatcatcaagctg
cctaagtactccctgttcgagctggaaaacggccggaagagaatgctggcctctgccggcgaactgcagaagggaaacgaactggccctgccctccaaatatgt
gaacttcctgtacctggccagccactatgagaagctgaagggctccccgaggataatgagcagaaacagctgtttgtggaacagcacaagcactacctggac
gagatcatcgagcagatcagcgagttctccaagagagtgatcctggccgacgctaatctggacaaagtgctgtccgcctacaacaagcaccgggataagccca
tcagagagcaggccgagaatatcatccacctgtttaccctgaccaatctgggagcccctgccgccttcaagtactttgacaccaccatcgaccggaagaggtaca
ccagcaccaaagaggtgctggacgccaccctgatccaccagagcatcaccggcctgtacgagacacggatcgacctgtctcagctgggaggcgacaaaaggc
cggcggccacgaaaaaggccggccaggcaaaaaagaaaaaggaattcggcagtggagagggcagaggaagtctgctaacatgcggtgacgtcgaggagaa
tcctggcccaatgaccgagtacaagcccacggtgcgcctcgccacccgcgacgacgtccccagggccgtacgcaccctcgccgccgcgttcgccgactaccccg
ccacgcgccacaccgtcgatccggaccgccacatcgagcgggtcaccgagctgcaagaactcttcctcacgcgcgtcgggctcgacatcggcaaggtgtgggtc
gcggacgacggcgccgcggtggcggtctggaccacgccggagagcgtcgaagcgggggcggtgttcgccgagatcggcccgcgcatggccgagttgagcggt
tcccggctggccgcgcagcaacagatggaaggcctcctggcgccgcaccggcccaaggagcccgcgtggttcctggccaccgtcggagtctcgcccgaccacc
agggcaagggtctgggcagcgccgtcgtgctccccggagtggaggcggccgagcgcgccggggtgcccgccttcctggagacctccgcgccccgcaacctccc
cttctacgagcggctcggcttcaccgtcaccgccgacgtcgaggtgcccgaaggaccgcgcacctggtgcatgacccgcaagcccggtgcctgagaattctaact
agagctcgctgatcagcctcgactgtgccttctagttgccagccatctgttgtttgcccctcccccgtgccttccttgaccctggaaggtgccactcccactgtccttt
cctaataaaatgaggaaattgcatcgcattgtctgagtaggtgtcattctattctgggggggtggggtggggcaggacagcaagggggaggattgggaagagaat
agcaggcatgctggggagcggccgcaggaacccctagtgatggagttggccactccctctctgcgcgctcgctcgctcactgaggccgggcgaccaaaggtcgc
ccgacgcccgggctttgcccgggcggcctcagtgagcgagcgagcgcgcagctgcctgcaggggcgcctgatgcggtattttctccttacgcatctgtgcggtatt
tcacaccgcatacgtcaaagcaaccatagtacgcgccctgtagcggcgcattaagcgcggcgggtgtggtggttacgcgcagcgtgaccgctacacttgccagc
gccttagcgcccgctcctttcgctttcttcccttcctttctcgccacgttcgccggctttccccgtcaagctctaaatcgggggctccctttagggttccgatttagtgct
ttacggcacctcgaccccaaaaaacttgatttgggtgatggttcacgtagtgggccatcgccctgatagacggtttttcgccctttgacgttggagtccacgttcttt
aatagtggactcttgttccaaactggaacaacactcaactctatctcgggctattcttttgatttataagggattttgccgatttcggtctattggttaaaaaatgag
ctgatttaacaaaaatttaacgcgaattttaacaaaatattaacgtttacaattttatggtgcactctcagtacaatctgctctgatgccgcatagttaagccagcc
ccgacacccgccaacacccgctgacgcgccctgacgggcttgtctgctcccggcatccgcttacagacaagctgtgaccgtctccgggagctgcatgtgtcagag
gttttcaccgtcatcaccgaaacgcgcgagacgaaagggcctcgtgatacgcctatttttataggttaatgtcatgataataatggtttcttagacgtcaggtggca
cttttcggggaaatgtgcgcggaacccctatttgtttatttttctaaatacattcaaatatgtatccgctcatgagacaataaccctgataaatgcttcaataatatt
gaaaaaggaagagtatgagtattcaacatttccgtgtcgcccttattcccttttttgcggcattttgccttcctgtttttgctcacccagaaacgctggtgaaagtaa
aagatgctgaagatcagttgggtgcacgagtgggttacatcgaactggatctcaacagcggtaagatccttgagagttttcgccccgaagaacgttttccaatga
tgagcacttttaaagttctgctatgtggcgcggtattatcccgtattgacgccgggcaagagcaactcggtcgccgcatacactattctcagaatgacttggttgag
tactcaccagtcacagaaaagcatcttacggatggcatgacagtaagagaattatgcagtgctgccataaccatgagtgataacactgcggccaacttacttctg
acaacgatcggaggaccgaaggagctaaccgcttttttgcacaacatgggggatcatgtaactcgccttgatcgttgggaaccggagctgaatgaagccatacc
aaacgacgagcgtgacaccacgatgcctgtagcaatggcaacaacgttgcgcaaactattaactggcgaactacttactctagcttcccggcaacaattaatag
actggatggaggcggataaagttgcaggaccacttctgcgctcggcccttccggctggctggtttattgctgataaatctggagccggtgagcgtggaagccgcg
gtatcattgcagcactggggccagatggtaagccctcccgtatcgtagttatctacacgacggggagtcaggcaactatggatgaacgaaatagacagatcgct
gagataggtgcctcactgattaagcattggtaactgtcagaccaagtttactcatatatactttagattgatttaaaacttcatttttaatttaaaaggatctaggtg
aagatccttttgataatctcatgaccaaaatcccttaacgtgagttttcgttccactgagcgtcagaccccgtagaaaagatcaaaggatcttcttgagatccttttt
tttctgcgcgtaatctgctgcttgcaaacaaaaaaaccaccgctaccagcggtggtttgtttgccggatcaagagctaccaactctttttccgaaggtaactggctt
cagcagagcgcagataccaaatactgttcttctagtgtagccgtagttaggccaccacttcaagaactctgtagcaccgcctacatacctcgctctgctaatcctgt
taccagtggctgctgccagtggcgataagtcgtgtcttaccgggttggactcaagacgatagttaccggataaggcgcagcggtcgggctgaacgggggttcg
tgcacacagcccagcttggagcgaacgacctacaccgaactgagatacctacagcgtgagctatgagaaagcgccacgcttcccgaagggagaaaggcggac
aggtatccggtaagcggcagggtcggaacaggagagcgcacgagggagcttccagggggaaacgcctggtatctttatagtcctgtcgggtttcgccacctctg
acttgagcgtcgatttttgtgatgctcgtcaggggggcggagcctatggaaaaacgccagcaacgcggcctttttacggttcctggccttttgctggccttttgctca
catgt

Contributions

I would like to highlight two particularly important contributions for which I am very thankful:

Dr. Anne Hoffrichter performed quality control, processing and visualization of RNAseq data. She provided custom-made R applications allowing me to spend my time on detailed data analysis.

Dr. Mahnaz Davoudi performed the electrophysiological measurements on neuronal cultures that I differentiated.

Eidesstattliche Erklärung

Eidesstattliche Versicherung gemäß § 8 der Promotionsordnung der Gesamtfakultät für Mathematik, Ingenieur- und Naturwissenschaften der Universität Heidelberg

1. Bei der eingereichten Dissertation mit dem Titel „Implications of the Val66Met polymorphism of the *BDNF* gene on neuronal morphology and function using human iPSC-derived neuronal cultures“ handelt es sich um meine eigenständig erbrachte Leistung.

2. Ich habe nur die angegebenen Quellen und Hilfsmittel benutzt und mich keiner unzulässigen Hilfe Dritter bedient. Insbesondere habe ich wörtlich oder sinngemäß aus anderen Werken übernommene Inhalte als solche kenntlich gemacht.

3. Die Arbeit oder Teile davon habe bislang nicht an einer Hochschule des In- oder Auslands als Bestandteil einer Prüfungs- oder Qualifikationsleistung vorgelegt.

4. Die Richtigkeit der vorstehenden Erklärungen bestätige ich.

5. Die Bedeutung der eidesstattlichen Versicherung und die strafrechtlichen Folgen einer unrichtigen oder unvollständigen eidesstattlichen Versicherung sind mir bekannt.

Ich versichere an Eides statt, dass ich nach bestem Wissen die reine Wahrheit erklärt und nichts verschwiegen habe.

Die Hauptveröffentlichung meiner Dissertation befindet sich in finaler Vorbereitung.

_____ _____

Ort und Datum Unterschrift

Danksagung

Als Erstes danke ich Prof. Dr. med. Philipp Koch dafür, dass ich die Möglichkeit hatte meine Promotion am Hector Institut für Translationale Hirnforschung (HITBR) durchzuführen. Insbesondere vielen Dank für die fachliche Betreuung, das Vertrauen und die Gelegenheit innovative Methoden während meiner Zeit hier im Labor zu erlernen.

Ein großer Dank geht an Prof. Dr. Christoph Schuster, der sich bereiterklärte mein Erstgutachter zu werden und mir während der TAC-Meetings an der Seite von Prof. Dr. Wolfgang Kelsch viele konstruktive Ideen für mein Projekt mitgegeben hat.

PD Dr. Georg Köhr und Dr. Francesca Ciccolini danke ich dafür, dass sie sich die Zeit und das Interesse genommen haben mein Prüfungskomitee zu vervollständigen.

Darüber hinaus möchte ich dem Interdisziplinären Zentrum für Neurowissenschaften dafür danken, dass sie mir die Möglichkeit gegeben haben, Teil dieser großartigen Graduiertenschule zu sein.

I was fortunate to have wonderful colleagues. Thanks to all of you for the great group cohesion, the warm working atmosphere, the many pieces of advice and the delicious cakes.

Danke an PD Dr. Thorsten Lau für die Unterstützung während meiner Anfangszeit als PhD.

Many thanks also to Fabio Marsoner and Karen Schmitt for your help and friendship, even after you were no longer in our lab. Ein besonderer Dank geht natürlich an Julia Wangemann, Klara Rehder und Malin Schmidt, die mich von Anfang bis Ende begleitet und immer unterstützt haben, egal ob es sich um arbeitsbezogene Themen oder um Privates gehandelt hat. Es tut mir leid, dass ihr nicht nur meine Frustration an den gescheiterten Versuchen, sondern auch die an der Deutschen Bahn miterleben musstet. Wir waren ein tolles Team und ich weiß nicht, was ich ohne euch gemacht hätte. Ich weiß nur, dass ich euch vermissen werde.

Muchisimas gracias gehen natürlich an meine Eltern, meine Schwester Daniela und meinem Verlobten Tobias für die Unterstützung und die Geduld in den letzten Jahren. Ihr habt immer an mich geglaubt und wart stets an meiner Seite, das weiß ich sehr zu schätzen.

Als aller letztes möchte ich auch allen anderen danken, die immer an meiner Forschung interessiert waren und es amüsant fanden, wenn ich über meine Zellen erzählt habe.

Thanks, Dankeschön und Muchas Gracias